ΕΘΝΙΚΟ ΜΕΤΣΟΒΙΟ ΠΟΛΥΤΕΧΝΕΙΟ

Εργαστήριο Ατμοκινητήρων & Λεβήτων

Τομέας Θερμότητας της Σχολής Μηχανολόγων Μηχανικών

ΔΙΠΛΩΜΑΤΙΚΗ ΕΡΓΑΣΙΑ

Techno-economic comparison of subcritical and transcritical Organic Rankine Cycle systems

Τεχνο-οικονομική σύγκριση συστημάτων υποκρισίμου και υπερκρισίμου Οργανικού Κύκλου Rankine

Του Φοιτητή

Παραδεισιάδη Δημητρίου

Επιβλέπων

Καρέλλας Σωτήριος, Αναπληρωτής Καθηγητής,
Σχολή Μηχανολόγων Μηχανικών, ΕΜΠ

Αθήνα, Ιούλιος 2019

Περίληψη

Η παγκόσμια ζήτηση ενέργειας αυξάνεται ραγδαία, εξαιτίας της συνεχούς αύξησης του πληθυσμού και της αυξανόμενης κατά κεφαλήν κατανάλωσης ενέργειας σε παγκόσμιο επίπεδο. Καθώς η συντριπτική πλειοψηφία της πρωτογενούς ενέργειας προέρχεται από ορυκτά καύσιμα, έχουν εγερθεί σοβαρές περιβαλλοντικές ανησυχίες και αμφιβολίες για τη βιωσιμότητα του πλανήτη. Πέραν των διαφόρων Ανανεωσίμων Πηγών Ενέργειας, είναι απαραίτητη η αξιολόγηση Συστημάτων Ανάκτησης Θερμότητας, λόγω της ικανότητάς τους να αξιοποιούν αποβαλλόμενη θερμότητα αποδοτικά, χωρίς περαιτέρω ανάγκη σε καύσιμο.

Ο Οργανικός Κύκλος Rankine αποτελεί μια αξιόπιστη και βιώσιμη τεχνολογία για αποκεντρωμένα συστήματα μικρής κλίμακας, ιδιαίτερα για πηγές θερμότητας χαμηλής θερμοκρασίας. Τα τελευταία χρόνια το επιστημονικό ενδιαφέρον έχει επικεντρωθεί στον Υπερκρίσιμο Οργανικό Κύκλο Rankine ως μια εναλλακτική για περαιτέρω αύξηση του βαθμού απόδοσης. Ο Υπερκρίσιμος Κύκλος, ωστόσο, παρουσιάζει διάφορες δυσκολίες, όπως οι υψηλές απαιτήσεις κεφαλαίου ή οι αυξημένες απαιτήσεις των υλικών σε αντοχή.

Εξ’ αυτού, η παρούσα μελέτη αποσκοπεί στο να συγκρίνει άμεσα έναν Υποκρίσιμο και έναν Υπερκρίσιμο Οργανικό Κύκλο Rankine για 6 εργαζόμενα μέσα, με σταθερή πηγή θερμότητας θερμικού ελαίου μέγιστης θερμοκρασίας 200°C. Η μελέτη εμπεριέχει βιβλιογραφική διερεύνηση ενός Οργανικού Κύκλου και μία αρχική μελέτη, η οποία εξετάζει την επίδραση ορισμένων παραμέτρων στη συνολική απόδοση του κύκλου και στη συνέχεια μια αναλυτική προσέγγιση για τα διάφορα εξαρτήματα της εγκατάστασης, προκειμένου να μοντελοποιηθούν.

Τα δύο τελευταία κεφάλαια παρουσιάζουν τα αποτελέσματα που προέκυψαν από τη μελέτη, τόσο θερμοδυναμικά, όσο και από οικονομικής απόψεως. Προκειμένου να εξαχθούν συμπεράσματα και να αξιολογηθεί το πλέον κατάλληλο εργαζόμενο μέσο και ο πλέον κατάλληλος κύκλος, εισήχθησαν 3 βασικοί οικονομικοί δείκτες, οι οποίοι σχετίζονται με το κόστος παραγωγής ενέργειας και την αποπληρωμή της επένδυσης. Όπως προέκυψε, υπό τις πλέον ευνοϊκές συνθήκες (5120 ώρες λειτουργίας ανά έτος για υποκρίσιμο σύστημα που βρίσκεται στη Γερμανία) ο Χρόνος Αποπληρωμής της επένδυσης υπολογίζεται σε λιγότερο από 5 έτη, με εργαζόμενο μέσο το R-134a.

Abstract

The global energy demand is rapidly increasing, due to the growing world population, as well as the increasing consumption of energy per capita, on a worldwide scale. As the vast majority of primary energy stems from fossil fuels, environmental concerns and questions over the planet's sustainability have arisen. Besides the various Renewable Energy Sources, it is important to assess the feasibility of Waste Heat Recovery Systems due to their potential to efficiently utilize energy, without further needs of fuel.

The Organic Rankine Cycle presents a proven and viable technology for small scale, decentralized systems with high efficiency, especially for low temperature sources. Lately, the scientific focus has shifted on the transcritical ORC, as an alternative to further increase the efficiency of such systems. There are various difficulties related to the transcritical cycle, however, such as higher investment costs or higher material durability requirements.

For this reason, the current study aims to directly compare a subcritical and a transcritical Organic Rankine Cycle for 6 working fluids, under a constant heat source of a 200°C thermal oil. The study includes a literature review of the Organic Rankine Cycle, a preliminary analysis of an ORC, which examines the effect of various parameters on the overall efficiency of the cycle and subsequently a detailed approach of the various components of the installation that is required for their modelling.

The final two chapters present the results obtained from the study both thermodynamically and financially. In order to draw conclusions and assess the most appropriate working fluid and cycle, 3 important economic indexes were introduced, which are related to energy production costs and investment payback. It was concluded, that under the most favorable conditions (5120 working hours per year for a subcritical system operating in Germany) a Payback Period of less than 5 years can be achieved for R-134a as a working fluid.

Preface

By submitting my Undergraduate Thesis and therefore completing my studies at the National Technical University of Athens, I would like to thank the people that helped me during the period of my studies.

Firstly, I would like to thank my Thesis Supervisor, Associate Professor Sotirios Karellas, for the cooperation we had during the final semester and also for his valuable help during my exchange studies at the Technical University of Munich. Secondly, I would like to thank PhD candidate Tryfon Roumpedakis for guiding me throughout the semester and offering quality feedback, despite his very busy schedule.

At this point, I would also like to acknowledge the people who were close to me during these years and mostly I would like to thank my family for supporting me and providing me with everything necessary, throughout my studies and during my lifetime in general.

Table of contents

List of figures

List of Tables

Nomenclature

A	*Surface*	$[m^2]$
a	*Year*	$[-]$
b	*Plate Amplitude*	$[m]$
Bo	*Boiling Number*	$[-]$
c	*Cost*	[€]
c_p	*Specific Heat Capacity*	$[J\ kg^{-1}K^{-1}]$
D	*Diameter*	$[m]$
E	*Energy*	$[J]$
$\dot{E}x$	*Exergy*	$[W]$
f	*Friction Factor*	$[-]$
ff	*Filling Factor*	$[-]$
G	*Mass Velocity*	$[kg\ m^{-2}s^{-1}]$
h	*Specific Enthalpy*	$[J\ kg^{-1}]$
hr	*Hours*	$[-]$
i	*Discount Rate*	$[-]$
k	*Thermal Conductivity*	$[W\ m^{-1}K^{-1}]$
L	*Length*	$[m]$
$\dot{m}$	*Mass Flow Rate*	$[kg\ s^{-1}]$
N	*Rotational Speed*	$[rpm]$
Nm	*Number*	$[-]$
n	*Year Number*	$[-]$
Nu	*Nusselt Number*	$[-]$
P	*Pressure*	$[Pa]$
p	*Pitch*	$[m]$
PR	*Pressure Ratio*	$[-]$
Pr	*Prandtl Number*	$[-]$
Q	*Vapor Quality*	$[-]$
$\dot{q}$	*Heat*	$[W]$
R	*Resistance*	$[m^2K\ W^{-1}]$
Re	*Reynolds Number*	$[-]$
s	*Specific Entropy*	$[J\ kg^{-1}K^{-1}]$
T	*Temperature*	$[K]$
t	*Plate Thickness*	$[m]$
U	*Overall Heat Transfer Coefficient*	$[W\ m^{-2}K^{-1}]$
V	*Volume*	$[m^3]$
$\dot{V}$	*Volumetric Flowrate*	$[m^3\ s^{-1}]$
W	*Mechanical Work*	$[J]$
x	*Dryness*	$[-]$

Greek Symbols

α	*Convection Heat Transfer Coefficient*	$[W\ m^{-2}K^{-1}]$
β	*Chevron Angle*	$[rad]$
Δp	*Pressure Drop*	$[Pa]$
η	*Efficiency*	$[-]$
μ	*Dynamic Viscosity*	$[kg\ m^{-1}s^{-1}]$
ξ	*Darcy Friction Coefficient*	$[-]$
ρ	*Density*	$[kg\ m^{-3}]$
τ	*Torque*	$[Nm]$
φ	*Enlargement Factor*	$[-]$

Subscripts

amb	*Ambient*
b	*Bulk*
c	*Cold*
ch	*Channel*
cond	*Condensation*
conde	*Condensing Part of Condenser*
crit	*Critical*
ct	*Cents*
D12	*Thermal Oil D12*
des	*Desuperheater*
dp	*Design Point*
el	*Electric*
eq	*Equivalent*
ev	*Evaporating Part of Evaporator*
evap	*Evaporator*
exp	*Expander*
f	*Fouling*
G	*Gas*
gen	*Generator*
h	*Hydraulic*
heatex	*Heat Exchanger*
in	*Inlet*
inv	*Inverter*
is	*Isentropic*
iso	*isothermal*
iter	*Iterative*
L	*Liquid*
lm	*Logarithmic*
ltm	*Liters per Minute*
mech	*Mechanical*

nom	*Nominal*
oil	*Thermal Oil D12*
out	*Outlet*
p	*Port*
pc	*Pseudocritical*
preh	*Preheater*
ref	*Reference*
req	*Required*
sh	*Superheater*
subc	*Subcooler*
t	*Year t*
th	*Thermal*
tot	*Total*
w	*Wall*
wat	*Water*

Abbreviations

ASHRAE	*American Society for Heating, Refrigerating and Air Conditioning of Engineers*
CHP	*Combined Heat and Power*
CRF	*Capital Recovery Factor*
DORC	*Dual-Loop Organic Rankine Cycle*
EU	*European Union*
GWP	*Global Warming Potential*
HCFCs	*Hydrochlorofluorocarbons*
HCs	*Hydrocarbons*
HFCs	*Hydrofluorocarbons*
IC	*Investment Cost*
kWh	*Kilowatt hour*
LCOE	*Levelized Cost of Energy*
LFR	*Linear Fresnel Reactor*
MWh	*Megawatt hour*
NCF	*Net Cash Flow*
NIST	*National Institute of Standards and Technology*
NN	*Node Number*
NPV	*Net Present Value*
ODP	*Ozone Depletion Potential*
OM	*Operation and Maintenance*
ORC	*Organic Rankine Cycle*
PBP	*Payback Period*
REV	*Revenue*
SORC	*Supercritical Organic Rankine Cycle*
WHR	*Waste Heat Recovery*

Chapter 1. Introduction

1.1 Water- Steam Rankine Cycle

The Rankine cycle (also known as water-steam cycle) is a thermodynamic cycle used for power generation in conventional power plants. A simplified design and the corresponding T-s diagram of a Rankine cycle are presented in Figure 1.1.

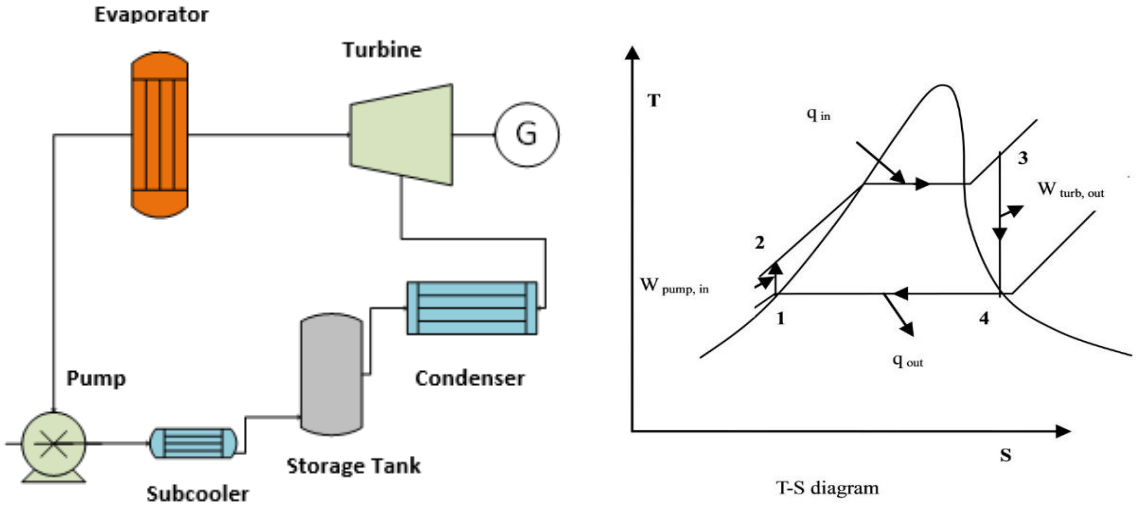

(a) *(b)*

Figure 1.1: (a) Schematic and (b) T-s diagram for a conventional water-steam Rankine cycle

The temperature- entropy diagram of Figure 1.1 presents an ideal Rankine cycle, consisting of reversible processes, which are not possible during actual operation. A non-ideal Rankine cycle would generate entropy, due to the irreversibilities in the operation of the boiler, the turbine, the condenser and the pump, as well as the pipeline losses [1]. Therefore, the shape of the actual T-s diagram would be dictated from the turbine's and the pump's efficiencies, as well as the pressure losses that mostly occur in the combustion chamber and the heat exchangers.

The conventional Rankine cycle has four main components, which are the following [2]:

1) Circulation pump:

   Compresses the saturated liquid that exits the condenser, up to the design high pressure. It is able to significantly increase the liquid's pressure with relatively low power, due to the liquid's low specific volume.

2) Steam generator (Boiler):

   The steam generator is responsible for producing steam of high energy content and consists of 3 parts:

- The economizer, which preheats the water until it reaches boiling temperature for the design pressure.
- The evaporator, which allows the water's complete phase change from liquid to steam.
- The superheater, which produces superheated steam of high enthalpy, in order to achieve higher mechanical work at the turbine [3].

The required power for this process is supplied by the fuel that is combusted in the combustion chamber.

3) Turbine

The steam turbine produces power by converting the steam's kinetic and thermal energy to mechanical work. The turbine is coupled with a generator, producing eventually power. The steam exits the turbine with significantly lower pressure and energy content, either as saturated steam but more commonly as a gas- liquid mixture of low moisture content.

4) Condenser

The condenser rejects heat to the environment, therefore allowing the isobaric cooling of the water- steam mixture, until it reaches the saturated liquid state. As the saturated liquid exits the condenser, it enters the circulation pump and the cycle restarts.

Power production from a conventional Rankine cycle is the most commonly used method and is applied at most thermal and nuclear power plants [2]. The cycle's efficiency is a very crucial aspect, especially on large scale applications, due to significant financial benefits and reduction of emissions. For this reason, there are various alternatives used to enhance the plant's efficiency [3]. The most common ones include:

1) Cycle design optimization: According to Carnot's law, a thermodynamic cycle's theoretical efficiency is a function of the mean temperature of heat addition. By increasing the gas generator's exit temperature, or the system's high pressure, this value can be increased and therefore, higher efficiency can be realized. Another possibility is the reduction of the condenser's pressure. As the Rankine cycle is a closed loop, pressures much lower than the atmospheric can be achieved. The lower the condenser's temperature, the higher the mechanical work produced at the turbine and therefore the efficiency of the cycle.
2) Reheating: Another method that increases the mean temperature of heat addition is reheating. The steam expands at the turbine's high-pressure stages, is later reheated to the maximum temperature and then expands fully before it enters the condenser. An added advantage of the method is achieving higher steam dryness, thus protecting the turbine's low-pressure units from erosion [4].
3) Water preheating: It is also possible to preheat the liquid by using superheated steam that has partially expanded at the turbine. The cycle would then specifically be described as Regenerative Rankine Cycle, as it decreases the need for fuel and despite reducing the plant's power output, it increases its overall efficiency.

Nowadays, thermal power plants display efficiencies of around 30-40%, with modern technologies reaching values up to 43.5%, as they employ one or various of the aforementioned modifications [5]. Water has various advantages as a working fluid, including abundancy, high heat capacity and low cost; however, it has also some disadvantages, mainly due to its high boiling temperature, which creates the necessity for high operating temperatures and pressures (extra costs related to materials, power consumption and complexity of the plant) . For this reason, power production can be realized only with fuels with a high heating value which are mostly not environmentally friendly (e.g. oil, natural gas, coal, nuclear fuel).

1.2 Organic Rankine Cycle

The Organic Rankine Cycle (ORC) has a similar technical concept to the Water-Steam cycle, but instead of using water, it makes use of organic fluids, such as hydrocarbons (HCs), hydrofluorocarbons (HFCs), hydrochlorofluorocarbons (HCFCs) and other organic media that will be presented in more detail in the following sections [6].

The main advantage of the ORC is its ability to produce power driven by low temperature heat sources, at which the water steam Rankine cycle is not technologically feasible. A significant advantage is the flexibility it displays in terms of utilizing various heat sources on a wide temperature range [7]. The main prime movers associated with the ORC are biomass, geothermal energy, solar energy and waste heat recovery [8].

The main layout of the ORC for waste heat or biomass applications is presented below [8].

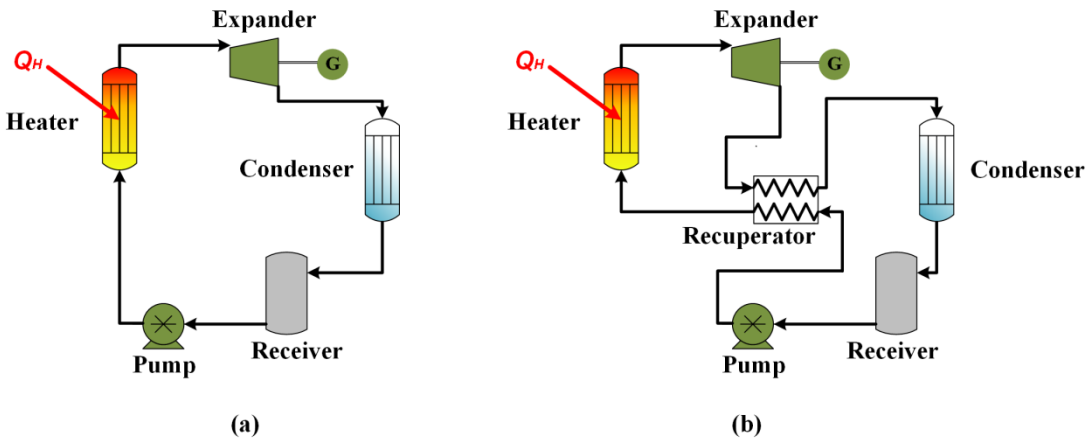

Figure 1.2. Schematic of (a) a conventional ORC and (b) a recuperated ORC

As Figure 1.2 shows, the cycle works under the same principle as the Rankine cycle, but with few important differences. The ORC uses a single heat exchanger for the fluid's preheating, evaporation and superheating. The ORC can be powered by low grade heat sources, mainly thanks to the working fluids' properties which allow for adequate pressures at significantly lower temperatures compared to water. An obvious advantage, except the lower power consumption is the simplification of the system's design, as lower pressures and temperatures decrease the need for expensive materials. In addition, as Figure 1.2 (b) shows, the use of a recuperator is possible in order to preheat the organic fluid and reduce even further the heat

supply at the evaporator. The recuperator's influence heavily relies on the heat source that is available and with its use final thermal efficiencies over 20% can be achieved [9].

Waste heat recovery is a very attractive option, since the need for reducing energy consumption is a worldwide priority for financial, as well as environmental reasons. It has been noted that over 50% of industrial waste heat is categorized as "low temperature" (meaning less than 230℃) [10]. For this reason, the ORC can be a viable and extremely useful technology as its main advantage lies on the utilization of low and medium temperature heat.

Solar power generated from parabolic troughs or concentrated solar power systems can also be used as a heat source for a conventional Water-Steam cycle, as high temperatures can be achieved [8]. The Organic Rankine cycle, however, can be easily combined with solar energy applications and it is currently the most commonly used technology for power generation from solar thermal power due to the low temperature input required [9]. The concept is known as Solar Organic Rankine Cycle.

1.2.1 Working fluid selection

One of the most important aspects of the Organic Rankine Cycle is the selection of the working fluid, as it affects the plant's efficiency, but also its operational range in terms of pressure and temperature. For this reason, one of the main factors related to working fluid selection is the available heat source, which mainly determines the pressures and temperatures the cycle will operate at.

Fluids are most commonly categorized according to the saturation curve of their T-s diagram. Fluids that display a positive vapor curve are referred to as dry, fluids with a nearly vertical curve are called isentropic and lastly fluids with a negative vapor curve are described as wet. Water belongs in the last category, which mostly includes fluids of low molecular mass, while the highest is present at dry fluids [6].

Wet fluids that operate at high pressures without being superheated lead to an increase of the percentage of the liquid state at the turbine's last stages. When the mixture contains a large percentage of liquid, the blades are greatly endangered with erosion and mechanical wear [11]. Hence, the practice of using a wet fluid without superheating is not recommended.

A typical T-s diagram including all 3 types is presented below (Figure 1.3).

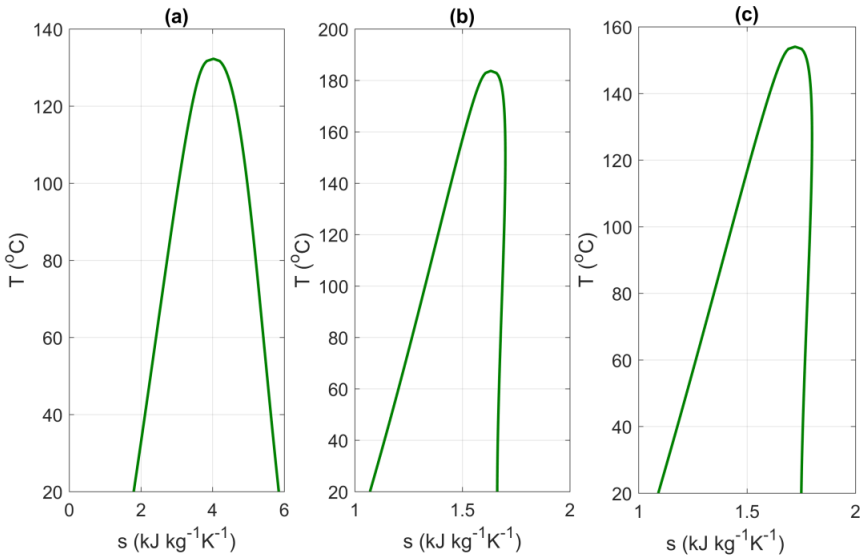

Figure 1.3. T-s diagrams for (a) wet, (b) isentropic and (c) dry fluids

Most organic fluids demonstrate negative environmental effects and therefore two main indexes have been introduced that quantify their impact. The first one is called ODP (Ozone Depletion Potential) and is related to the destruction of the Ozone's layer and the second one is called GWP (Global Warming Potential) and is related to the atmosphere's temperature increase, due to their use. According to the Montreal Protocol that was signed in 1987, fluids that displayed high ODP values would not be permitted for use and thus, their replacement was deemed mandatory [12].

Besides their impact on the environment, organic fluids often present dangers for humans and the plant's overall safety, due to their toxicity, flammability and corrosivity. Toxic fluids must be avoided, because they are harmful to the plant's personnel when leakage occurs. Their flammability is also a crucial factor in case of an accident, as it can lead to fire and possibly to deadly consequences. The fluid's corrosivity is related to the mechanical equipment of the installation, which is gradually worn out and is considered improper for use. The American Society for Heating, Refrigerating and Air Conditioning of Engineers (ASHRAE) classifies fluids to groups according to the dangers they present for humans and the environment. (Table 1-1)

Table 1-1. ASHRAE Safety group classification limits [9]

	Flammability	**Chemical Formula**	**Molecular Mass [kg/kmol]**
Increasing flammability→	Higher flammability	**A3**	**B3**
	Lower flammability	A2	B2
		A2L	B2L
	No flame propagation	A1	B1
		Lower toxicity	**Higher toxicity**

As previously stated, the selection of a working fluid is strongly influenced by the application and the heat source available for the installation. Therefore, there is no optimal solution for all cases, but there are various parameters that need to be considered and have clear advantages for all or almost all of the fluids. Some of them are:

1) Density: For a given mass flow, the higher the fluid's density, the lower the volume of the fluid. High density is advantageous for operating purposes, as it reduces the piping's dimensions and the pump's work and therefore energy consumption.
2) Viscosity: the lower the viscosity of a fluid, the more favorable for the installation, due to less corrosion and mechanical wear of the equipment.
3) Conductivity: High conductivity leads to more efficient heat transfer and in turn smaller heat exchanger surface, allowing cost reduction.
4) Melting temperature: The melting temperature of the fluid should be considerably lower than ambient temperature, because in case the fluid solidifies, the operation and installation will be endangered.

Except the fluid's physical properties, the operational range of the cycle is equally important. A high pressure ratio leads in principle to higher thermal efficiency, but limitations are established due to material durability and legislation, as very high pressures endanger the system's safety. The plant's location also influences the cycle's efficiency, due to the limitation the respective ambient temperature creates. The condenser's low temperature has to be higher than the ambient temperature and the more it increases, the less the potential for power production and therefore, the lower the thermal efficiency [13].

Research has shown that the thermal efficiency of an ORC cycle increases when the system's high pressure and temperature are close to the fluid's critical point. Therefore, it is crucial to select a working fluid that according to the available heat source can operate near its critical parameters. For example, working fluids whose critical temperature is high are better suited for high temperature heat sources and their efficiency on lower temperatures is lower than other fluids with lower critical temperature [6].

Despite the plethora of research that exists upon working fluids, only few of them have been commercially successful and are in operation. Fluids such as toluene and silicone oil have high critical temperatures and boiling point and are often associated with heat sources whose temperature reaches 300℃. In contrast, hydrocarbons and conventional refrigerants present lower critical values and thus are often combined with moderate/low temperature heat sources that do not exceed 200℃ [14].

1.2.2 Supercritical Cycle

A variation of the Organic Rankine Cycle is the supercritical cycle. During supercritical operation, the pump compresses the liquid to very high pressures and is then heated, bypassing the two-phase state. As the temperature increases, it exceeds the fluid's critical point and changes its state from liquid to supercritical. The supercritical state is neither gaseous nor liquid but its properties lie between the two phases [15]. In most occasions, the fluid's density is similar to its liquid state, while its diffusivity resembles its gaseous state.

In principle, a supercritical cycle will display higher thermal efficiency than a subcritical Organic Rankine Cycle [16]. As the fluid is heated above the saturated liquid curve and the critical point, higher temperatures are achieved during operation and as stated on Chapter 1.1, an increased main temperature of heat addition leads to higher theoretical efficiency. The high operating pressure of the cycle, however, requires higher pump work and material durability, which are factors that increase the plant's cost [17].

Another advantage of the supercritical process is the higher exergy efficiency it displays. This operation allows for better thermal match between the heat source's cooling curve and the working fluid's heating curve and thus the process' irreversibility is decreased [18].

Although the supercritical cycle concept exists also on the conventional Rankine cycle, due to water's very high critical pressure and temperature, its employment is an expensive and complicated task. For this reason, the Supercritical Organic Rankine Cycle (SORC) is advantageous, as the organic fluids can reach the supercritical state with lower compression work. A challenge of the cycle, however, is the behavior of most organic fluids at this condition. Often at supercritical pressure operation the fluids display low stability, high flammability and corrosiveness and thus are unsuitable for operation [19]. Therefore, the selection of the working fluid for a supercritical cycle must also adress these issues.

It is important to distinguish a supercritical and a transcritical cycle, despite them often being interchanged in literature. A supercritical cycle would operate completely above the liquid-vapor curve of the fluid, whereas in a transcritical cycle, condensation would take place in the liquid-gas mixture area [14]. Therefore, the cycle presented below is one of a transcritical cycle, which is the focus of this study (Figure 1.4). For simplicity purposes, however, the cycle will be referred as supercritical for the particular study.

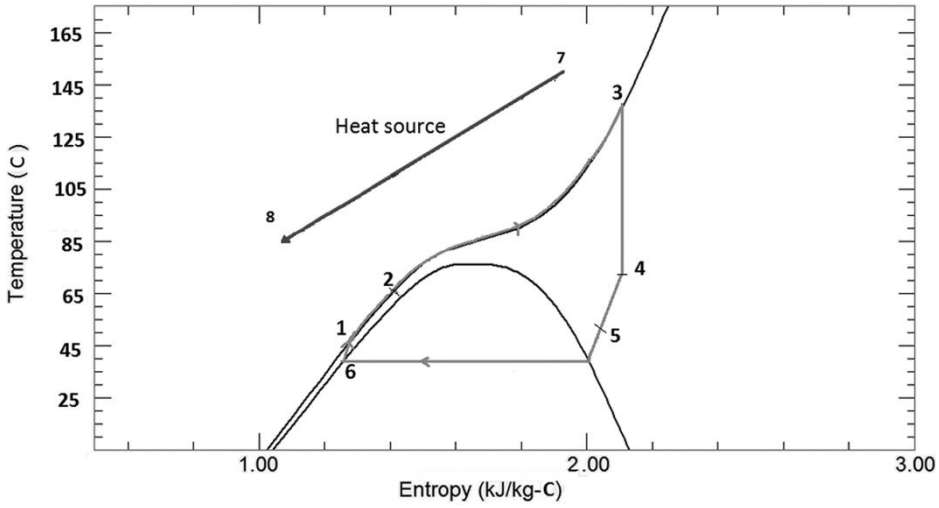

Figure 1.4. Transcritical Organic Rankine Cycle [20]

1.3 Literature Review on the Organic Rankine Cycle

Various studies have been conducted regarding the efficiency, power output and potential of the Organic Rankine Cycle.

An important parameter on the performance of an ORC system that has been thoroughly examined is the working fluid's critical temperature, the role of which is especially important for supercritical operation. Xu et al. [21] analyzed the performance of 3 working fluids for an ORC system with the system's heat source being a flue gas with an initial temperature of 150℃ and a fixed exit temperature of 70℃. The fluids were R236fa, R134a and R218, whose critical pressures and temperatures differ significantly. The results showed that R236fa and R134a, that have higher critical temperatures, display higher thermal and exergy efficiency than R218. This is caused due to the smaller temperature difference at the T-q diagram between the heat source and the working fluid in the evaporator, which leads to higher exergy efficiency, since the study also proved that the evaporator is responsible for the bulk of the system's exergy losses. The maximum thermal efficiency is evident for R134a and is equal to 13.4%, while the same fluid displayed the higher exergy efficiency, with a value around 64.3%, with the cycle operating at maximum temperature equal to 132℃.

Pan et al. [22] investigated the behavior of organic fluids in near- critical conditions of an ORC and compared subcritical and transcritical operation. The study's heat source was not defined, but its temperature was 90℃ and the fluids HFC125, HFC143a and HF218 were considered, due to their ability to operate in both subcritical and supercritical conditions. The study proved that the efficiency of the supercritical cycle is higher compared to subcritical operation and also that the efficiency is a continuous function in near- critical conditions, despite the vast differences between the two cycles. The maximum efficiency of the cycle is evident for the fluid HFC143a and is equal to 7%. In terms of power production, however, the study found the efficiency when operating at near- critical conditions (subcritical) to be higher for HFC125 and HFC143a in comparison to supercritical operation. Therefore, the study concludes that near-critical subcritical ORC might obtain better performances than even a supercritical cycle.

Schuster, Karellas and Aumann [16] analyzed the potential for efficiency optimization in supercritical ORC. The study considered pump and turbine efficiencies of 85% and 80% respectively, constant condensation temperature of 20℃ and 10K pinch point temperatures of recuperator and primary heat exchanger. The fluids that were selected were required to display dryness over 90% after expansion, in order to avoid blade erosion. The study showed that the subcritical system's thermal efficiency was higher than a supercritical system's, but system efficiency is a more important value and is higher for a supercritical cycle. Notably, for initial heat source temperature of 210℃ and maximum cycle temperature of 180℃, the maximum system efficiency of a supercritical cycle is equal to 14.4%, which is considerably higher than the value of 13.3%, that represents maximum subcritical system efficiency. The thermal efficiency reported was around 24%. The authors also reached the conclusion that fluids that present the highest thermal efficiencies do not display equally high system efficiencies, as their heat transfer capacity highly decreases at high vapor temperatures.

Uusitalo et al. [23] analyzed the potential of the Organic Rankine Cycle to utilize waste heat from piston engines. The paper studies a combined cycle, which utilizes exhaust gas at 395℃ and also charge air heat of 210℃, in order to produce electricity and increase the plant's overall efficiency. The cycle that was examined was subcritical, with the evaporator's pressure equal to 95% of each fluid's critical pressure and the fluids considered were toluene, n-pentane, R245fa and cyclohexane. The results showed that working fluids with high critical temperature lead to high power outputs in exhaust gas heat recovery, while the ones with low critical temperature performed best in charge air heat recovery. The authors concluded that the efficiency of a 16.6 MW gas-fired diesel engine can be increased by 11.4% with exhaust gas heat and 2.4% by charge air heat utilization. Toluene was accepted as the most suitable fluid for exhaust gas heat utilization, with a cycle efficiency of 23.9%, while R245fa was chosen for charge air heat utilization, with a thermal efficiency equal to 11.8%. However, the installation's economics should also be considered, as these values can only be achieved with very large heat exchanger area, which might not be economically feasible.

Glover et al. [24] examined the performance of a supercritical ORC for vehicle waste heat recovery (WHR). The authors determined that heat should be supplied both from exhaust gases and coolant, otherwise significant loss of potential waste heat energy would occur. The study considered 18 working fluids from the 105 existing in the NIST database that were deemed most appropriate in terms of critical pressure and temperature, legal issues and maximum cycle temperature. The model developed illustrated that the cycle's two pressures greatly affect its efficiency, whereas the working fluid selected should have a critical temperature slightly lower than the coolant temperature. Regarding the ORC efficiency, the study indicates that a maximum net efficiency of 19.1% is possible, when the working fluid is propyne.

Gao et al. [25] conducted a performance analysis for a supercritical ORC for low grade WHR, evaluating various working fluids. A conventional ORC was considered, with a heat exchanger between the working fluid and the waste heat source. In addition to thermodynamic parameters, the authors also considered technical and economic factors, such as the total heat transfer area and the expander size. Therefore, the results were not only related to optimal thermal or exergy efficiency, but also considered the working fluid with the minimum heat transfer requirements and minimum expander size. For the heat source being air of 320℃, the optimal exergy efficiency was obtained with the use of R245ca and was equal to 57.5% for maximum cycle temperature equal to 227℃.

Boz and Diez [26] compared the power and efficiency of a subcritical and a supercritical cycle for various working fluids on a combined diesel engine-ORC system. For the subcritical system, the evaporator's pressure accounted to 90% of each fluid's critical pressure, whereas for the supercritical system the high pressure was fixed at 70 bar. Results showed that the thermal efficiency is higher for the supercritical cycle, being as high as 41% in the case of cyclohexane, mostly because higher turbine inlet temperature can be achieved. The heat source's temperature was 455℃ and the cycle's maximum operating temperature 425℃. Regarding the fluids, it was concluded that the maximum power was produced by fluids with high heat capacity, such as ethanol. In addition, the authors concluded that the exergy destruction on

subcritical conditions is higher than in the case of supercritical and thus the second law efficiency of the supercritical cycle is also higher.

A dual-loop Organic Rankine Cycle (DORC) was studied by Shu et al. [27] for WHR applications (Figure 1.5). Specifically, the dual loop cycle consists of a high temperature and a low temperature cycle, that aim to recover waste heat from an engine (both exhaust gas and engine coolant). The study compared a subcritical-subcritical cycle and a subcritical-transcritical system (meaning a transcritical low temperature cycle). For the high temperature cycle water was used, as the exhaust gas temperature on full load was very high (519℃). For the low temperature application (engine coolant temperature 83.3℃ on full load) different refrigerants were used for each concept. For the transcritical cycle it was crucial to select fluids with low critical temperature, whereas for the subcritical cycle the focus was to attain high thermal efficiencies. The study's results show that the greatest efficiency was evident under the operation of R143a in a subcritical- transcritical cycle. The recorded ORC efficiency for the low temperature cycle was equal to 12.02% and the system's exergy efficiency 48.42%. An important conclusion was related to the operating load of the application. For low operating loads the exhaust and coolant's temperature and mass flow significantly decrease, therefore damaging the feasibility of a transcritical system. Thus, it is recommended to employ a purely subcritical cycle for loads up to 50% of the maximum, while loads closer to the full would be better utilized by a transcritical cycle.

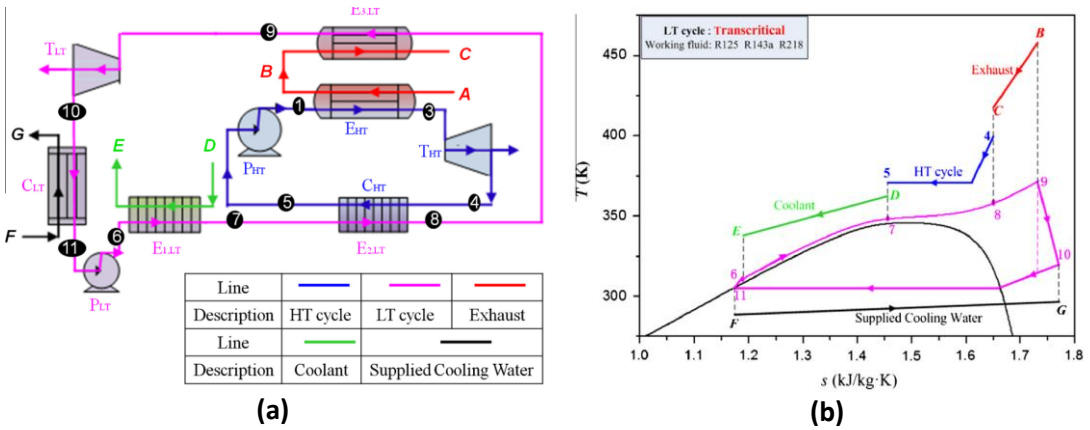

Figure 1.5. (a) Schematic and (b) respective T-s diagram of the dual ORC system investigated by Shu et al. [27]

Braimakis et al. [28] studied the potential of various working fluids, including zeotropic mixtures for low temperature WHR, in comparison with the benchmark fluid R245fa. The study's heat source was assumed to be dry atmospheric air between 150 and 300℃, while five working fluids and their binary mixtures were considered. The results demonstrate that the efficiency of the cycle is positively affected in case the heat source's temperature and working fluid's temperature do not differ greatly. In terms of exergy efficiency, the supercritical ORC leads to higher values, especially for propane which presents 18% increased exergy efficiency compared to its subcritical operation. A conclusion of the analysis was the potential of zeotropic mixtures to significantly improve the cycle's performance on both sub- and supercritical operation. For higher temperatures of the heat source (above 170℃), mixtures operating on supercritical conditions present the greatest thermodynamic performance. In comparison to R245fa, the natural refrigerants and their mixtures presented greater exergy

efficiency and lower turbine size requirements, but demanded larger heat transfer area and higher turbine rotational speed. The highest exergy efficiency that was realized in the study was equal to 39.77% for a mixture with a ratio 0.3 butane/0.7 cyclopentane.

The advantages of a supercritical ORC with a zeotropic mixture as a working fluid were also observed by Chen et al. [29] The study considered 22 mixtures of refrigerants which utilized pressurized hot water at 137℃ and were deemed suitable in terms of thermophysical properties, environmental impact and their critical temperature. The thermal efficiency of a conventional ORC using R134a was calculated in the range of 10%, whereas the zeotropic mixture 0.3 R32/0.7 R134a enhanced system's performance, having an efficiency equal to 11.5% for a maximum cycle temperature equal to 127℃. The supercritical cycle also displayed better exergy results, having an overall exergy efficiency of 38.57% that is significantly higher than the respective value of a subcritical cycle (24.10%). The study also stated that similarly to pure fluids, the zeotropic mixtures selected are advantageous for specific operating conditions. For example, the mixture of 0.7R134a/0.3R32, would not provide equally good results for high temperatures and therefore, would have to be substituted by others. The proposed configuration is presented below (Figure 1.6).

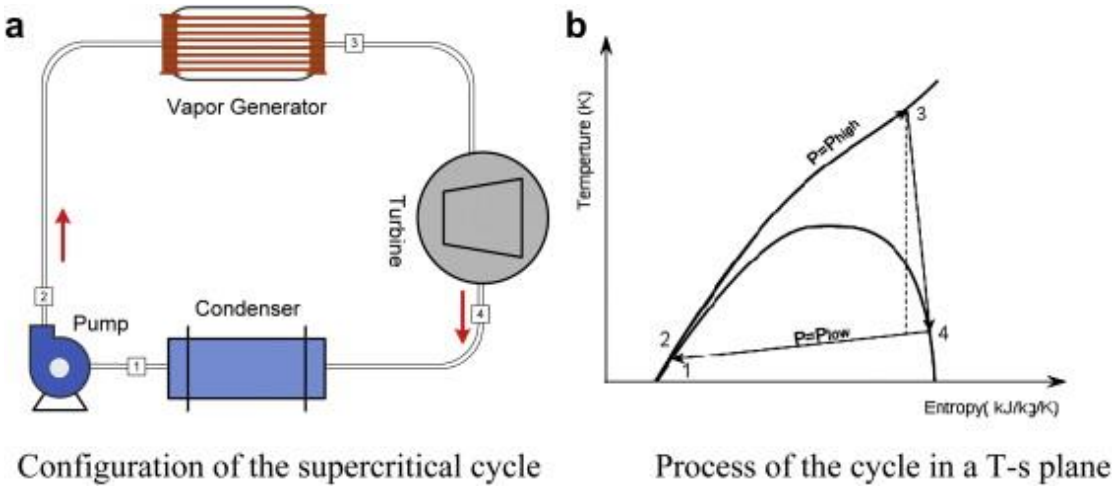

Figure 1.6 (a) Configuration and (b) processes of a zeotropic mixture supercritical Rankine cycle.

Maraver et al. [30] focused on optimizing sub- and transcritical ORCs, while taking into consideration key technical limitations. The fluids in consideration were commercially used refrigerants in large-scale applications and various heat sources were examined, such as thermal oils from CHP applications and exhaust gases. The exergy efficiency of a transcritical cycle is higher, due to the lower temperature differences between the heat source and the working fluid during evaporation, which in turn leads to lower system irreversibilities. The study showed that the temperature profile of the heat source is very crucial in selecting a sub- or transcritical cycle. For high temperature exhaust gases, a subcritical cycle would be optimal, whereas for lower exhaust heat temperature the transcritical cycle would be favorable. An important result of the study was related to the use of a recuperator, which was not deemed necessary, unless a limit had been set on the heat source's outlet temperature. Furthermore, according to the authors, the heat source's temperature should be similar to the working fluid's, in order to avoid systems with poor efficiency or limited economic feasibility. The

results showed that for waste heat of 300℃, the operation of n-Pentane obtained thermal efficiency equal to 22.7% and exergy efficiency of 58.7%, with the fluid's maximum temperature reaching 250℃.

Astolfi et.al. [31],[32] investigated the potential of the ORC to utilize medium and low temperature heat (120-180℃) from geothermal sources, while also considering economic aspects. The study examined various configurations, such as supercritical/subcritical and regenerative or non-regenerative ORCs. The working fluids were selected from the Refprop database and after their environmental impact was assessed, the most harmful ones were excluded. The results indicated that the optimal efficiency is evident for fluids whose critical temperature is around 90% of the heat source temperature. Therefore, for geothermal brine at 150℃ as a heat source, RC318 achieved a thermal efficiency equal to 12.83%, exergy efficiency of 52.17% and the overall system efficiency was calculated as 12.79% for a supercritical cycle. Furthermore, as other studies have shown, the supercritical cycle displayed higher efficiency but also requires higher heat exchange area, which translates to an increase of costs. The economic analysis carried out concludes that for high temperature geothermal brine the supercritical cycle is advantageous. Lastly, the study showed that fluids with critical temperature very close to the heat source's temperature would require more expensive turbines and therefore their use is not economically viable.

Shengjun et al. [33] compared the sub- and transcritical cycles for geothermal power generation, by optimizing the various components of the ORC system. Per Carnot's law, the efficiency of a cycle is increased for high turbine inlet and low condensation temperatures and the study indicates that the maximum efficiency occurred for 84 ℃ and 26 ℃ evaporation and condensation temperatures respectively. For a heat source with a temperature of 90 ℃, R143a achieved a thermal efficiency of 8.11% and an exergy efficiency of 45.9%. An interesting result was that the thermal efficiency of a transcritical cycle was lower than the subcritical's, which is contradicting to most results in previous works. This phenomenon is explained by the very low boiling temperature of the working fluids, which leads to non-isothermal heating in the supercritical area and thus to low mean temperature of heat addition. The transcritical cycle, however, displayed favorable values of vapor expansion ratio and suction specific volume, therefore allowing smaller sized turbines and avoiding problems related to supersonic flow.

Another study related to low temperature geothermal energy utilization by means of an ORC cycle was conducted by Vetter et al. [34] The study showed that the highest net power output is achieved with the use of propane in a supercritical cycle at high pressure and temperature 4.6 MPa and 104℃ respectively, with a thermal efficiency of 10.1%, when the heat source's temperature is 150℃. The model's results indicate that almost all working fluids increase their power output in supercritical application, but their efficiency did not significantly improve, compared to a subcritical cycle. An important conclusion is the importance of the relation between the geothermal fluid's temperature and the working fluid's critical temperature. The study illustrates that fluids whose critical temperature is around 80% of the geothermal fluid's temperature performed best and hence, this ratio should be a criterion in selecting a suitable working fluid for operation.

In terms of low- temperature solar power, Wang et al. [35] compared the performances of pure and zeotropic mixtures for an ORC. The experimental prototype consisted of flat plate collectors, a storage tank after condensation and due to the very low power produced, a throttling valve that simulates the behavior of an expander (Figure 1.7). The fluids considered were pure R245fa and two mixtures of R245fa and R152a with 0.9/0.1 and 0.7/0.3 ratios respectively. The aforementioned fluids were selected due to their zero ODP and low GWP. As expected, the fluid's outlet temperature from the solar collectors is heavily influenced by the absorbed solar irradiation at a given time. The 0.7/0.3 mixture displayed the highest power output and efficiency of the cycle. Due to the lower density of R152a, for constant solar radiation this mixture has the potential for higher heat absorption and therefore ability to increase the system's efficiency. With the fluid's temperature at the collector's outlet reaching a maximum of around 100℃, the 0.7/0.3 mixture achieved the highest Rankine cycle efficiency (5.59%) at a collector efficiency equal to 22.93%, leading to an overall system efficiency of 1.28%. The study concluded that zeotropic mixtures have great potential to improve system efficiency by incorporating an external heat exchanger.

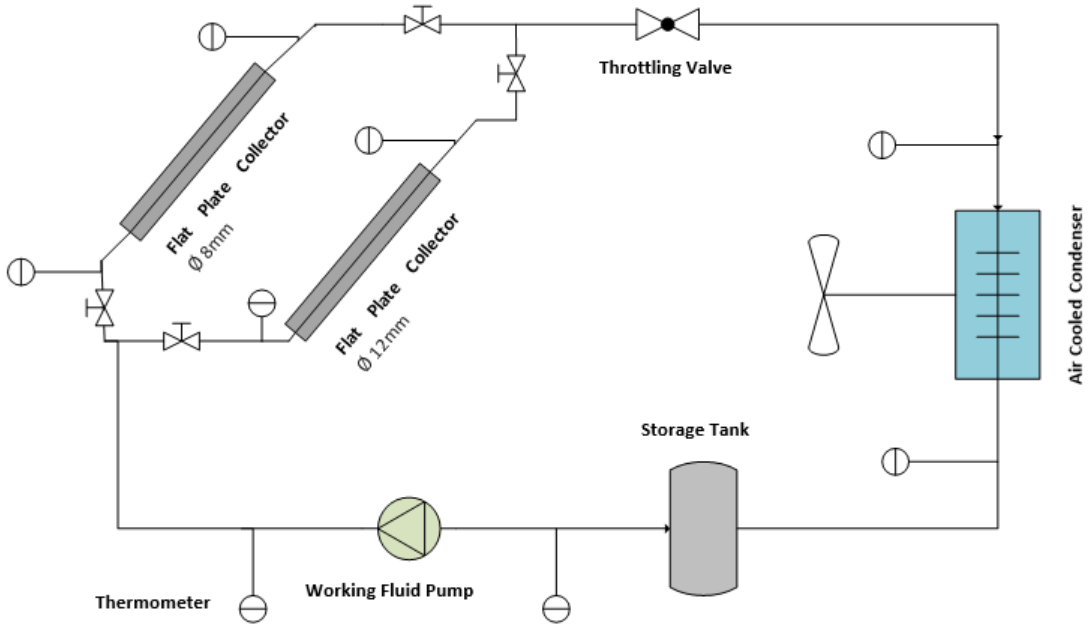

Figure 1.7 The experimental apparatus of Wang et al. [35]

Ferrara et al. [36] studied an ORC with a 20 kW parabolic trough solar power plant as the heat source for different working fluids. The solar circuit's working fluid was a synthetic oil, where various fluids for the ORC system were examined. The use of R-134a displayed very low efficiency, as even with regeneration step, a maximum value of 5.5% was achieved for a cycle's maximum temperature of 200℃ and maximum pressure of 30 bar. The fluid that demonstrated the best results was acetone that allowed efficiency up to 17.8% when a superheated, regenerative cycle was studied (at a maximum temperature 390℃ and maximum pressure of 30 bar). Lastly, the supercritical ORC for acetone was studied and lead to even better results. Specifically, for a high pressure of 100 bar and reheating pressure of 25 bar, the efficiency of the system reached 19.9%. From a thermodynamic standpoint, therefore, acetone clearly performed better than other fluids; however, its flammability is an important factor that needs to be considered under its operation. Another crucial aspect of

the system is the type of the expander. Despite screw type expanders being the most common solution, they are often employed in plants of high power output and the use of micro-screw expanders is not common.

Xu et al. [37] analyzed a direct vapor generation supercritical ORC system by using linear Fresnel reflector (LFR) solar concentrator (Figure 1.8). The LFR concentrator superheats the fluid, which then reaches a supercritical condition. The study considers a radial inflow turbine as the optimal selection, due to its effective operation under high pressure ratios, which are typical for a supercritical cycle and its light weight. The authors considered six potential working fluids, whose critical temperature ranged between 180 and 320℃. Furthermore, the pressure at the expander's inlet was set to be 20% higher than each fluid's critical pressure and a fixed pressure drop was calculated for each heat exchanger. As Carnot's law indicates, higher temperature at the turbine's inlet increases the cycle's efficiency, but the higher the temperature at the turbine's inlet (and therefore at the LFR's outlet), the lower the collector efficiency. Thus, an optimization of the plant's overall efficiency was necessary. It was concluded that cyclohexane displayed the greatest overall efficiency of 16.34% for a subcritical and 19.65% for a supercritical cycle, respectively. The ORC cycle's thermal efficiency was measured 27.95%, with a maximum cycle temperature equal to 350℃. The supercritical cycle is superior not only in terms of thermal efficiency, but also in terms of decreasing the ORC system's irreversibility and therefore improving the exergy efficiency of the system.

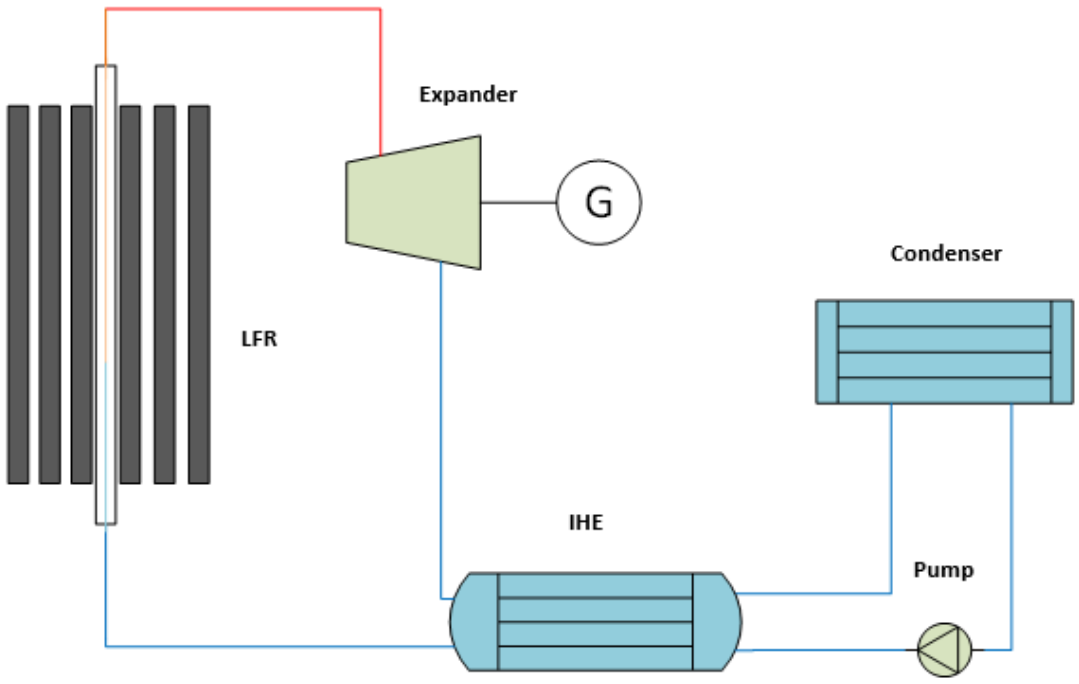

Figure 1.8 The direct vapor generation ORC investigated by Xu et al. [37]

Zhou [38] examined a hybrid solar- geothermal supercritical ORC system in order to assess its thermodynamic and economic feasibility compared to subcritical hybrid systems or to exclusively solar and geothermal systems (Figure 1.9). The working fluid selected for the analysis was isopentane, due to its high critical temperature that allows better energy

utilization at higher operating temperatures. The system utilizes a geothermal system for preheating and evaporation and a solar system to superheat the working fluid, under supercritical conditions. The results showed that the solar collector area plays a crucial role in the system's efficiency and viability. For low solar collector area, the supercritical system's thermal efficiency is greater than the subcritical's, but its exergy efficiency is lower. According to the study, the exact opposite phenomenon is realized for high solar collector area s and therefore the selection should be met according to the owner's priorities. From an economic standpoint, when the solar aperture area is large (greater than 12000 m^2), the supercritical hybrid plant performs better than the respective subcritical and both function more favorably than standalone geothermal or solar systems. The utilization of isopentane ORC with a solar aperture area of 24000 m^2 lead to an exergy efficiency of 14.68% and an overall plant efficiency of 10.8%.

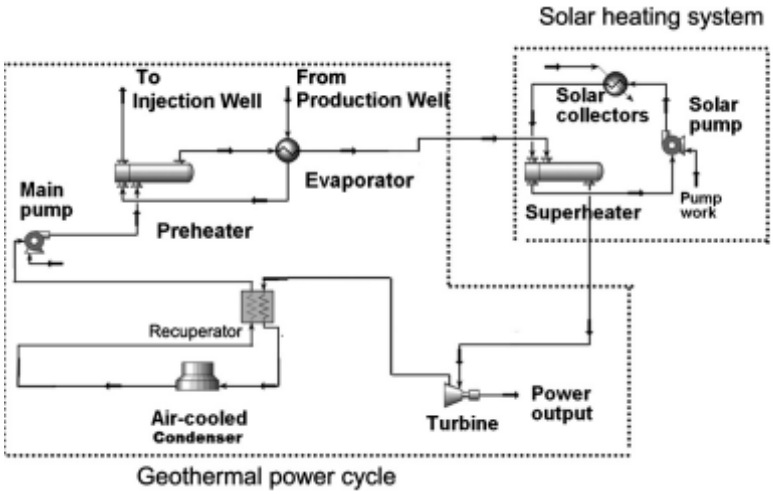

Figure 1.9. The hybrid solar-geothermal power plant evaluated by Zhou [38]

Drescher and Brüggemann [39] assessed various working fluids for an ORC system in biomass power and heat plants. The study focused on identifying the optimal fluid, by calculating the thermal efficiency yielded by 700 substances existing in a fluid database. The study demonstrated the importance of a recuperator in the cycle, as it considerably increases the cycle's efficiency. The results further showed that the optimal performance was achieved using Butylbenzene as working fluid, which operated at a vaporization temperature and pressure equal to 300℃ and 9.2 bar respectively and a condensation temperature of 91℃. The corresponding maximum thermal efficiency was equal to 25.3%.

An analysis carried out by Algieri et al. [40] investigated the performances of high temperature subcritical and transcritical ORCs powered by biomass. For the study, cyclohexane, decane and toluene were used as working fluids in saturated and superheated conditions at the turbine's inlet. The fluids were selected due to their high operating temperatures, which are suitable for high temperature heat sources. The study found the presence of an internal heat exchanger to be extremely crucial, especially for the use of decane as working fluid. The fluid displayed an efficiency of less than 15% at 337℃ without an internal heat exchanger, whereas it fared better than the other two fluids under the presence of a heat exchanger, with a cycle efficiency of 25.1%. Decane at transcritical operation, coupled with the use of an internal heat

exchanger displayed the highest value of thermal efficiency (28.38%). It is important to note, however, that not all working fluids would be suitable for transcritical operation, due to their critical pressure. Fluids with high critical pressure would require substantial compression and also more durable materials to withstand these conditions. For this reason, the study only considers decane for a transcritical cycle, due to its relatively low critical pressure.

A table that summarizes the authors' findings can be seen below (Table 1-2)

Table 1-2. Literature review on the Organic Rankine Cycle

Maximum Cycle Temperature (°C)	Heat Source	Working Fluid	Thermal Efficiency (%)	Exergy Efficiency (%)	System Efficiency (%)	Reference
132	Flue gas (150°C)	R134a	13.4	64.3	-	Xu et al. (2013)
84	N/A (90°C)	HFC143a	7	-	-	Pan et al. (2012)
180	N/A (210°C)	R365mfc	24	-	14.4	Schuster, Karellas, Aumann (2014)
N/A	Waste Heat (Reciprocating Engine) Ex. Gas (395°C) Charge Air (210°C)	Toluene R245fa	23.9 11.8	-	-	Uusitalo et al. (2014)
190	Waste Heat	Propyne	19.1	-	-	Glover et al. (2015)
227	Waste Heat (Air 320°C)	R245ca	-	57.5	-	Gao, Liu et al. (2012)
425	Diesel Engine (455°C)	Cyclohexane	41	-	-	Boz, Diez (2018)
N/A	Waste Heat (Engine) Ex. Gas (519°C) Coolant (83.3°C)	Water R143a	12.02	48.42	-	Shu et al. (2013)
N/A	Waste Heat Air (300°C)	0.3 butane/0.7 cyclopentane	-	39.77	-	Braimakis et al. (2015)
127	Pressurized hot water (137°C)	0.3R32/0.7R134a	11.5	38.57	-	Chen et al. (2011)
250	Waste Heat (Gas 300°C)	n-Pentane	22.7	58.7	-	Maraver et al. (2014)
N/A (Optimized)	Geothermal brine (150°C)	RC318	12.83	52.17	12.79	Astolfi et al. (2014)
84	Geothermal (90°C)	R143a	8.11	45.9	-	Shengjun et al. (2011)
104	Geothermal (150°C)	Propane	10.1	-	-	Vetter et al. (2013)
100	Solar Collectors	(0.7R245fa/0.3R152a)	5.59	-	1.28	Wang et al. (2010)

390	Solar (Parabolic Trough)	Acetone	-	-	19.9	Ferrara et al. (2014)
350	Solar Concentrator (Linear Fresnel Reflector)	Cyclohexane	27.95	-	19.65	Xu et al. (2015)
390	Geothermal/Solar Hybrid (Thermal Oil Temperature 400°C)	Isopentane		14.68	10.8	Zhou (2014)
300	Biomass	Butylbenzene	25.3	-	-	Drescher, Brüggemann (2007)
337	Biomass	Decane	28.38	-	21.81	Algieri et al. (2012)

1.4 Thesis scope

As already discussed in the previous sections, the supercritical ORC is a topic of sufficient interest, however, the competitiveness of this configuration is still vague. The scope of this study is to address the following:

- Which are the differences in the sizing of a subcritical and a supercritical ORC?
- How can a supercritical ORC be designed?
- Which are the energetic and exergetic benefits/drawbacks of the realization of a supercritical ORC with comparison to the respective subcritical cycle?
- Is the supercritical ORC techno-economically feasible?
- Which is the optimal working fluid for a supercritical ORC and a given heat source profile?
- How is the economic feasibility of a supercritical ORC varying in different countries?

Chapter 2. Thermodynamic Cycle Optimization

2.1 Cycle Calculation

The study includes a preliminary analysis of an Organic Rankine Cycle and calculations of its thermal and net electric efficiencies for various parameters. The following design was considered. (Figure 2.1)

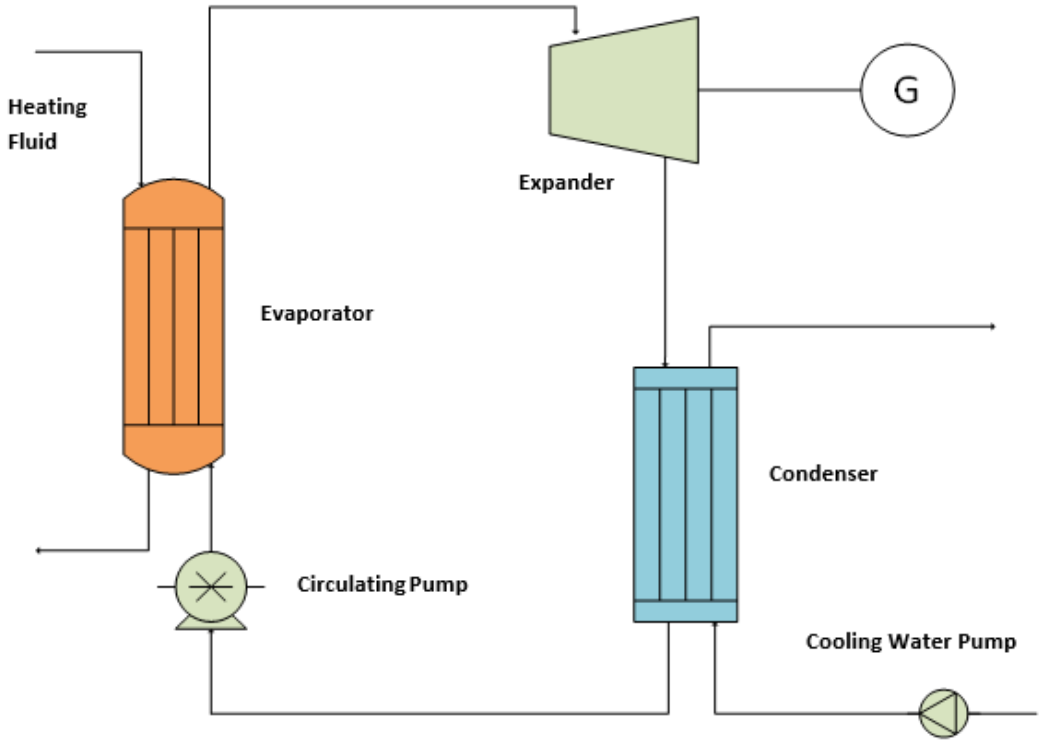

Figure 2.1 Organic Rankine Cycle Design

For the current study, the heating medium will be a thermal oil (D12) that has been heated either by geothermal brine, solar power or waste heat and transfers heat to the working fluid at the evaporator. The power supply to the ORC is assumed to be equal to 65 kW. Exiting the evaporator, it produces power, due to the rotational force applied to the expander.

The study examines various working fluids with a wide spectrum of critical temperatures and pressures, in order to examine which presents the highest thermal efficiency and furthermore which conditions are the optimal from a thermodynamic standpoint. The working fluids considered and their characteristics are presented below (Table 2-1)

Table 2-1 Organic Fluids Properties [41], [42], [43], [44]

Working Fluid	Life Duration (years)	Critical Temperature (°C)	Critical Pressure (bar)	GWP	ODP
R-134a	14	101.06	40.59	1430	0
R-245fa	7.6	154.01	36.51	1030	0
R-227ea	34.2	101.75	29.25	3220	0
R-1234yf	0.03	94.70	33.82	4	0
R-1234ze	0.045	109.37	36.36	6	0
R-410A	16.95	71.34	49.01	2088	0

The analysis includes various scenarios, aiming to demonstrate the effect of each parameter, such as pump efficiency or fluid high pressure. The constant values for the cycle were the generator efficiency, motor efficiency, shaft efficiency, subcooling at the pump's inlet, and a constant condensation temperature. The following values were set:

- Generator Efficiency: $\eta_{gen} = 0.85$
- Motor Efficiency: $\eta_{motor} = 0.85$
- Shaft Mechanical Efficiency: $\eta_m = 0.98$
- Condensation Temperature: $T_{cond} = 25℃$
- Subcooling: $T_{subcool} = T_{cond} - 5$

Each scenario examines a range of values for the following parameters individually, as the others remain constant:

- Turbine Pressure Ratio
- Working Fluid Mass Flow
- Turbine Isentropic Efficiency
- Pump Isentropic Efficiency

The cycle is calculated by using the following methodology.

Point 5: Condenser Outlet/ Storage Tank Inlet

Having set the condensation temperature of the cycle, the fluid's low pressure can be calculated with the Refprop software, considering that condensation takes place inside the working fluid's T-s curve.

$$P_{low} = f(T_{cond}, x = 0) \quad (2.1)$$

Having set the pressure ratio, or examining a range of it, the cycle's high pressure can also be calculated, using the equation:

$$P_{high} = PR \cdot P_{low} \quad (2.2)$$

Point 1: Storage Tank Outlet/ Pump Inlet

According to the problem, the storage tank outlet temperature is lower than the condenser outlet temperature by 5 °C and has the same pressure. The reason for this design is to ensure

that the fluid will be in an exclusively liquid state when entering the pump, as the presence of a two-phase state endangers the pump's safety [45].

Therefore, the pump inlet temperature is calculated as following:

$$T_{subcool} = T_{cond} - 5 \tag{2.3}$$

Since Point 1 is fully defined, its enthalpy and entropy will be calculated using the Refprop software [46] and will be equal to h_1 and s_1 respectively.

Point 2: Pump Outlet/ Evaporator Inlet

The working fluid enters the pump with the pressure and temperature calculated at the equations (2.1) and (2.3) respectively. Assuming no pressure losses for this initial analysis, the compression ratio of the pump will be equal to the PR value initially set.

$$P_2 = P_{high} \tag{2.4}$$

With the help of the pressure and entropy of point 1, the isentropic point 2 can be defined and thus its enthalpy is known (h_{2is}).

The enthalpy of Point 2 will be calculated by using the correlation of the pump's isentropic efficiency:

$$\eta_{is,pump} = \frac{h_{2is} - h_1}{h_2 - h_1} \tag{2.5}$$

which calculates the value h_2, which in turn allows the identification of the temperature of point 2.

Point 3: Evaporator Outlet/ Turbine Inlet

In order to calculate the evaporator outlet conditions, it is necessary to consider the heat source, as the evaporator is the system's component at which power is supplied.

By using an energy balance at the evaporator:

$$\dot{q}_{in} - \dot{q}_{orc} = 0 \Rightarrow \dot{m}_{orc} \cdot (h_3 - h_2) = \dot{q}_{in} \Rightarrow$$

$$h_3 = h_2 + \frac{\dot{q}_{in}}{\dot{m}_{orc}} \tag{2.6}$$

Point 4: Expander Outlet/ Condenser Inlet

The working fluid enters the expander having a high pressure and enthalpy equal to h_3. Thus, its temperature T_3 and entropy s_3 are calculated with the same software. After the expansion the fluid will have low pressure, equal to the condenser's exit, as it has been assumed for this preliminary investigation that no pressure losses occur.

The isentropic point 4 will have low pressure and equal entropy to the previous point. Its enthalpy h_{4is} is therefore calculated:

$$h_{4is} = h(P_{4is} = P_{low}, s_{4is} = s_3) \tag{2.7}$$

The expander's isentropic efficiency is defined as following:

$$\eta_{is,exp} = \frac{h_3 - h_4}{h_3 - h_{4is}} \tag{2.8}$$

Point 4 is then fully defined, as it has known pressure and enthalpy and eventually all cycle's points are identified.

Cycle Efficiencies

The power consumed by the pump can be calculated by the formula:

$$P_{pump} = \dot{m}_{orc} \cdot (h_2 - h_1) \tag{2.9}$$

while the electric power necessary will be equal to:

$$P_{el,pump} = \frac{P_{pump}}{\eta_{motor}} \tag{2.10}$$

The power produced by the expander is calculated as

$$P_{exp} = \dot{m}_{orc} \cdot (h_3 - h_4) \tag{2.11}$$

and the electrical power produced is equal to:

$$P_{el,exp} = P_{exp} \cdot \eta_{mech} \cdot \eta_{gen} \tag{2.12}$$

Therefore, the net power output of the installation is the difference between the power produced by the turbine and the pump and is calculated as

$$P_{el,net} = P_{el,exp} - P_{el,pump} \tag{2.13}$$

Thermal Efficiency:

$$\eta_{th,ORC} = \frac{P_{exp} - P_{pump}}{\dot{q}_{in}} = \frac{(h_3 - h_4) - (h_2 - h_1)}{h_3 - h_2} = 1 - \frac{(h_4 - h_1)}{h_3 - h_2} \tag{2.14}$$

Net Electric Efficiency:

$$\eta_{el,net} = \frac{P_{el,net}}{\dot{q}_{in}} \tag{2.15}$$

2.2 Operational Conditions Selection

SCENARIO 1: Various Fluid Mass Flows

For this scenario, the following values were considered

- Fluid High Pressure: $P_{high} = 1.1 \cdot P_{crit}$
- Expander Pressure Ratio: $PR = 5$
- Expander Isentropic Efficiency: $\eta_{is,exp} = 0.68$
- Pump Isentropic Efficiency: $\eta_{is,pump} = 0.55$

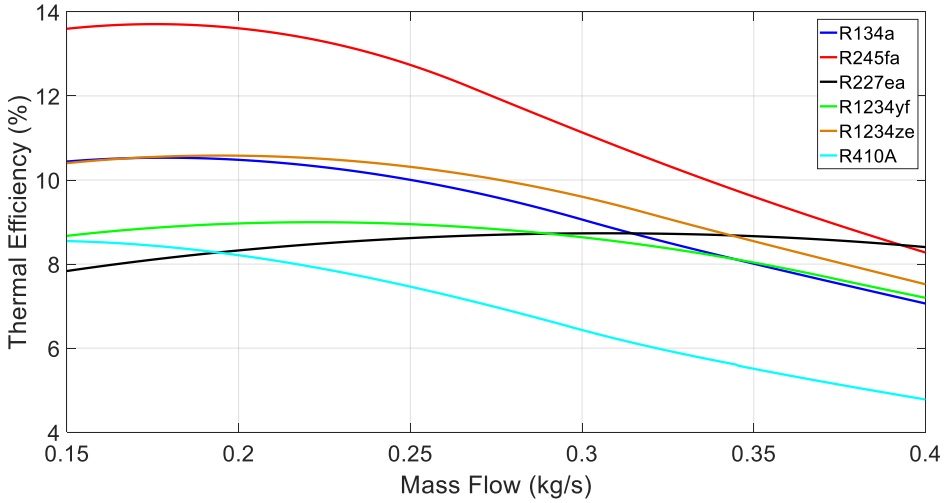

Figure 2.2 Thermal Efficiency of various working fluids for varying Mass Flow

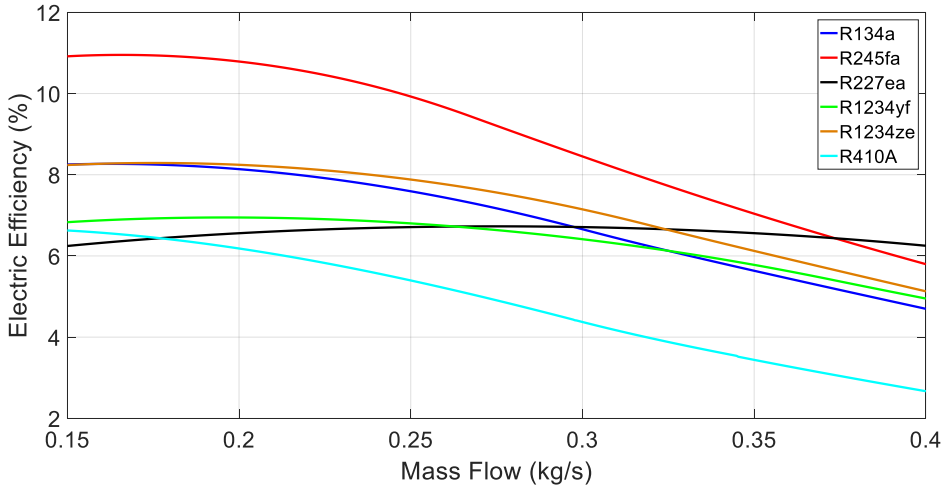

Figure 2.3 Electric Efficiency of various working fluids for varying Mass Flow

As the study concerns a constant heat source, the lower the mass flow of the cycle, the higher the enthalpy difference of the working fluid at the evaporator. In principle, high enthalpies at the turbine inlet lead to higher thermal efficiencies of the system. Thus, it is expected that most fluids display higher efficiencies for low mass flows.

SCENARIO 2: Various Pressure Ratios

For this scenario, the following values were considered

- Working Fluid Mass Flow: $\dot{m}_{orc} = 0.25\ kg/s$
- *Expander Pressure Ratio:* $PR = (5 - 10)$
- Expander Isentropic Efficiency: $\eta_{is,exp} = 0.68$
- Pump Isentropic Efficiency: $\eta_{is,pump} = 0.55$

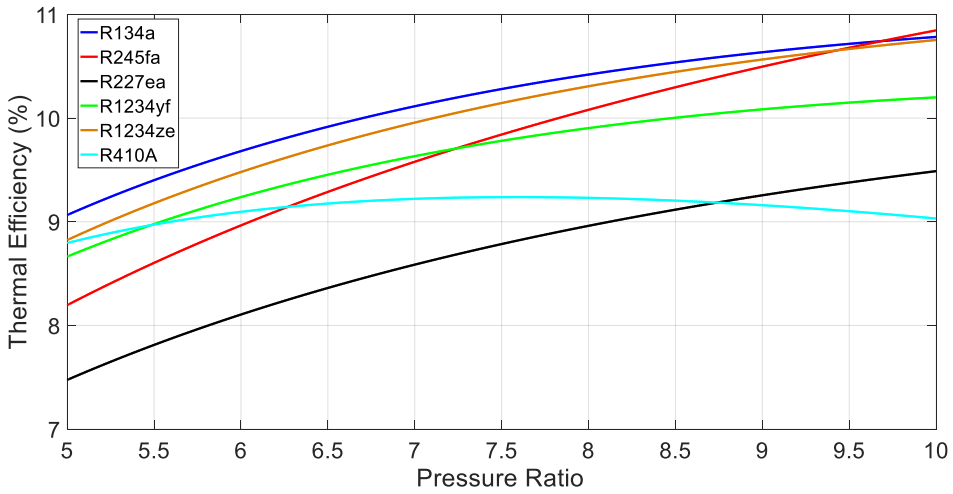

Figure 2.4 Thermal Efficiency of various working fluids for varying Pressure Ratio

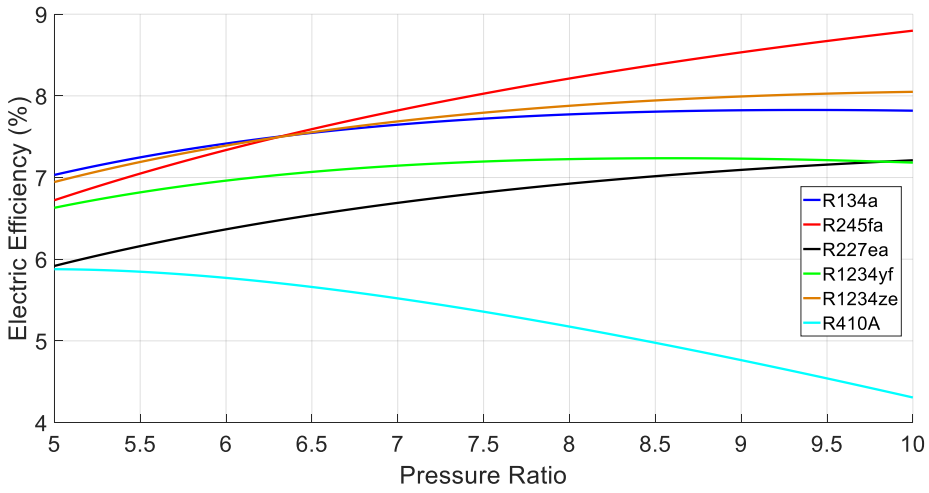

Figure 2.5 Electric Efficiency of various working fluids for varying Pressure Ratio

For a constant condensation temperature, the higher the pressure ratio, the higher the maximum operating pressure of the cycle. In principle, the highest thermal efficiencies of the cycle occur for higher pressures. All the fluids present an increase of efficiency for higher pressure ratios, with the only exception being R410A. The temperature- entropy diagram of this fluid indicates that the condensation temperature of 25℃ corresponds to a low pressure of 16 bars. Thus, a pressure ratio in the range of 5-10 would greatly exceed the critical pressure of the fluid, that is 49 bars. For this reason, it is expected that the efficiency of the fluid would decrease for increasing pressure ratios.

SCENARIO 3: Various Expander Efficiencies

For this scenario, the following values were considered

- Working Fluid Mass Flow: $\dot{m}_{orc} = 0.25\ kg/s$
- Fluid High Pressure: $P_{high} = 1.1 \cdot P_{crit}$
- *Expander Isentropic Efficiency:* $\eta_{is,exp} = 0.5 - 0.85$
- Pump Isentropic Efficiency: $\eta_{is,pump} = 0.55$

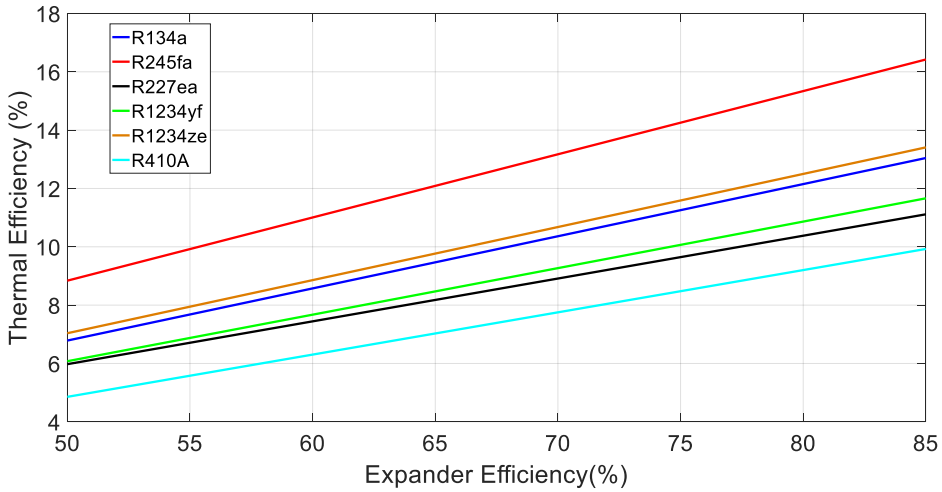

Figure 2.6 Thermal Efficiency of various working fluids for varying Expander Efficiency

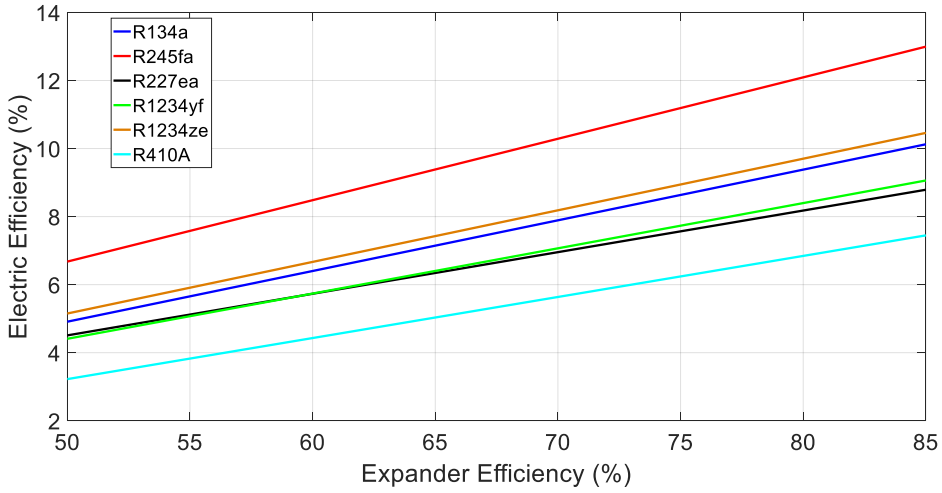

Figure 2.7 Electric Efficiency of various working fluids for varying Expander Efficiency

The figures indicate that the efficiency of the expander significantly affects the thermal and electric efficiency of the cycle. This conclusion is expected, as the turbine is the system's component related to power production and therefore its isentropic efficiency is a crucial indicator of the cycle's performance. The results further indicate that in principle, the higher the fluid's critical temperature, the higher the cycle's efficiency. The only exception is R-227ea, which displays lower efficiencies than R-1234yf and R-1234ze, despite its higher critical temperature. A possible explanation would be that it has the lowest critical pressure of the fluids and since a constant condensation temperature is assumed, the potential for power generation is decreased.

SCENARIO 4: Various Pump Efficiencies

For this scenario, the following values were considered

- Working Fluid Mass Flow: $\dot{m}_{orc} = 0.25\ kg/s$
- Fluid High Pressure: $P_{high} = 1.1 \cdot P_{crit}$
- Expander Isentropic Efficiency: $\eta_{is,exp} = 0.68$
- *Pump Isentropic Efficiency:* $\eta_{is,pump} = 0.4 - 0.7$

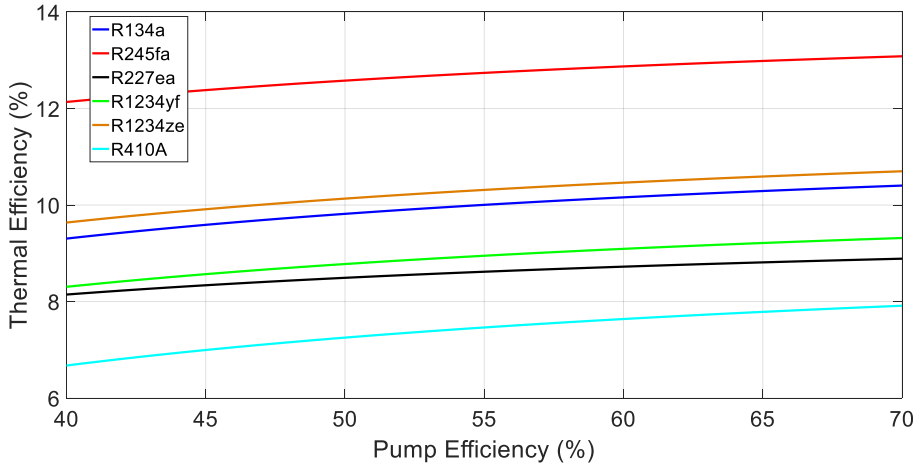

Figure 2.8 Thermal Efficiency of various working fluids for varying Pump Efficiency

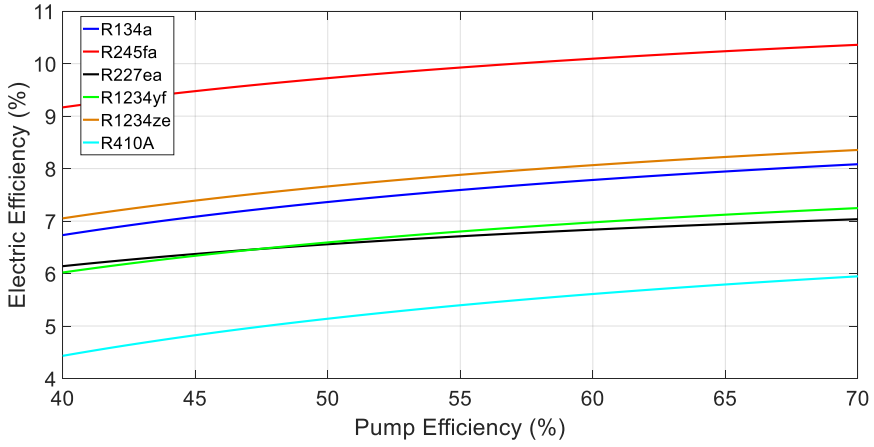

Figure 2.9 Electric Efficiency of various working fluids for varying Pump Efficiency

Similar conclusions can be derived from the figures related to pump efficiency. An important observation is the contribution of the pump's efficiency to the cycle's electrical efficiency. As the pump is the system's component that requires electricity, its efficiency is directly related to the power it consumes and therefore, the lower it is, the less net power is available to the system.

2.3 Pseudocritical State

The supercritical cycle presents various differences and particularities in comparison with the subcritical cycle. An important difference is related to its thermophysical properties, such as specific heat capacity or density. Studies have shown that fluids have a specific temperature, called "pseudocritical temperature", at which a radical increase of some properties is evident. This phenomenon is also the reason why different heat transfer equations have to be examined for the supercritical cycle, in order to attenuate the effect of these peaks.

For each fluid this temperature is different; however, on all cases is located at the affinity of the critical temperature. In addition, this temperature is a function of the high pressure applied to the cycle. The determination of this value for each fluid and pressure is crucial for the study of the supercritical cycle, as cycles that operate near this temperature are usually most efficient [22]. A model was developed in order to calculate the pseudocritical value for conditions set by the user, while also a mathematical formula with sufficient accuracy (R^2 value greater than 0.99) is presented.

In order to determine the pseudocritical temperature of a fluid the following procedure was followed:

It is known that the pseudocritical temperature of the fluid is present near its critical temperature [47]. Therefore, for each fluid the range between 90 and 110% of its critical temperature was examined. Furthermore, for the purposes of this analysis pressures between 1% and 30% higher than the supercritical pressure were studied.

For each high pressure and fluid, a specific profile of the heat capacity as a function of the temperature can be depicted. If the X axis (temperatures axis) is iterated to a number of nodes (100 in this case), *Matlab* is able to calculate the maximum value of the Y axis (heat capacity) and also the node at which it occurs. In order to calculate the temperature from the node number the following simple method is used:

The X axis ranges from points $x_1 = 0.9 \cdot T_{crit}$ and $x_2 = 1.1 \cdot T_{crit}$ and therefore the axis range is equal to $\Delta x = x_2 - x_1 = 0.2 \cdot T_{crit}$. For 100 nodes used, the distance between 2 nodes will be equal to $dx = \frac{\Delta x}{iter} = \frac{0.2 \cdot T_{crit}}{100} = T_{crit} \cdot 2 \cdot 10^{-3}$.

Thus, when *Matlab* presents the result as a node number (NN), the temperature value, which is equal to the pseudocritical temperature, is calculated with the formula $x_{nn} = x_1 + dx \cdot NN$ $\Rightarrow T_{pc} = 0.9 \cdot T_{crit} + 2 \cdot 10^{-3} \cdot T_{crit} \cdot NN$. (With the temperatures calculated in K).

The same number of iterations (100) are used for pressure discretization and therefore a $100x100$ table is formed, which displays the values for the specific heat as a function of pressure for each node. By isolating the maximum values of each column and the number of the node at which it is evident, it is possible to create a chart of pseudocritical temperature and cycle high pressure. The figure obtained is presented below, for each fluid that has been studied (Figure 2.10).

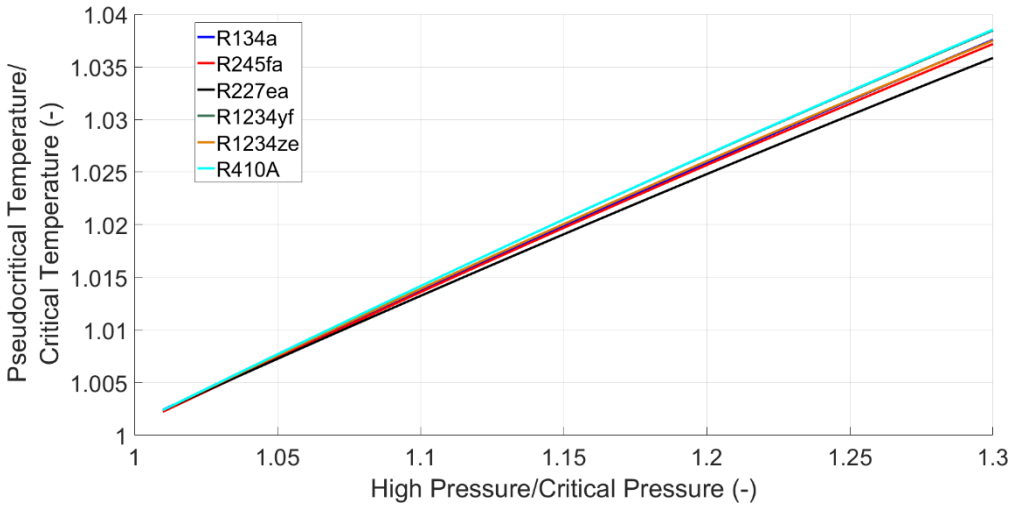

Figure 2.10 Pseudocritical Temperature of various working fluids as a function of Cycle High Pressure

As the fluids have different critical temperatures and pressures, in order to extract general conclusions, the pseudocritical temperature and high pressure of the cycle were divided by the fluid's critical temperature and pressure respectively. Therefore, the variables T_{ratio}, P_{ratio} were created, for which:

$$T_{ratio} = \frac{T_{pc}}{T_{crit}} \tag{2.16}$$

$$P_{ratio} = \frac{P_{high}}{P_{crit}} \tag{2.17}$$

The correlation is almost linear, but for higher accuracy, a second order polynomial correlation for each one was extracted and they are presented below (Table 2-2).

Table 2-2 'Pseudocritical Temperature Correlations for various working fluids'

Fluid	**Correlation**
R-134a	$T_{ratio} = -0.0235 \cdot {P_{ratio}}^2 + 0.1754 \cdot P_{ratio} + 0.8492$
R-245fa	$T_{ratio} = -0.0286 \cdot {P_{ratio}}^2 + 0.1865 \cdot P_{ratio} + 0.843$
R-227ea	$T_{ratio} = -0.0265 \cdot {P_{ratio}}^2 + 0.1766 \cdot P_{ratio} + 0.851$

R-1234yf	$T_{ratio} = -0.0327 \cdot {P_{ratio}}^2 + 0.1999 \cdot P_{ratio} + 0.8339$
R-1234ze	$T_{ratio} = -0.0348 \cdot {P_{ratio}}^2 + 0.2015 \cdot P_{ratio} + 0.8344$
R-410A	$T_{ratio} = -0.0315 \cdot {P_{ratio}}^2 + 0.1973 \cdot P_{ratio} + 0.8352$

Chapter 3. System Components

3.1 Evaporator

3.1.1 Heat Exchanger Design and Characteristics

One of the most crucial components of the installation is the evaporator. As stated before, power is supplied to the circuit at the evaporator, in the form of a hot fluid which allows the working fluid to be heated and therefore increase its energy content before entering the expander.

The flow principle of a plate heat exchanger is presented at the figure below (Figure 3.1)

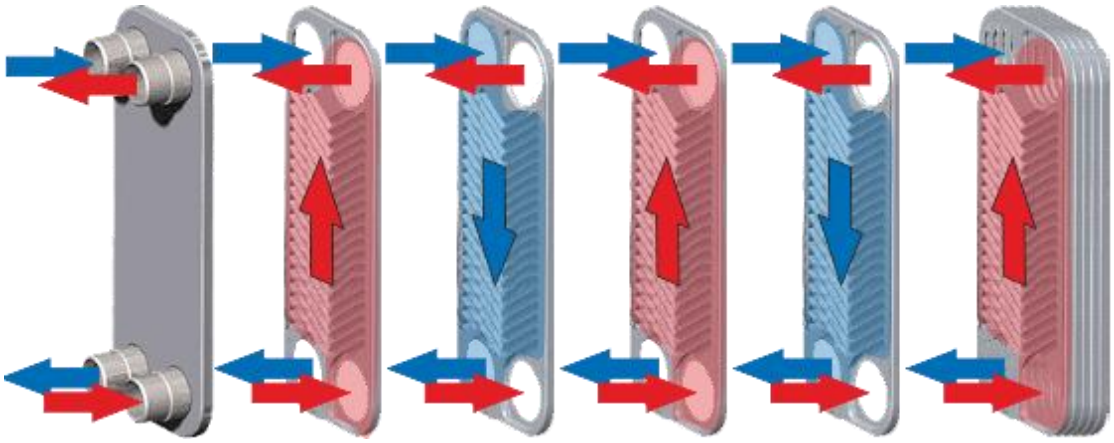

Figure 3.1 Plate Heat Exchanger Flow Principle [48]

The design of the plates and its main dimensions are important factors related to heat transfer and pressure drop and are presented below (Figure 3.2).

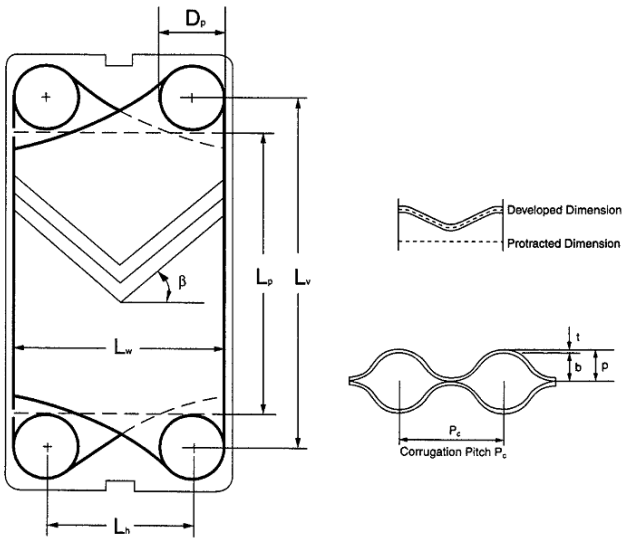

Figure 3.2 Plates design and dimensions [49]

The most important design characteristics of the heat exchangers are presented below (Table 3-1):

Table 3-1 Heat exchangers design characteristics [50]

Number of Passes	$\boldsymbol{Nm_p = 1}$
Plate Thickness	$t = 0.7\ mm$
Chevron Angle	$\beta = 60°$
Enlargement Factor	$\varphi = 1.18$
Thermal Conductivity of the Plate Material for SS304	$k_w = 16.2\ \frac{W}{m \cdot K}$
Pitch	$p = 2.5\ mm$
Plate Amplitude	$b = pitch - t = 1.8\ mm$
Corrugation Pitch	$P_c = 7\ mm$
Horizontal Distance Between Nozzles	$L_w = L_h + D_p$
Vertical Plate Length	$L_p = L_v + D_p$
Channel Surface	$A_{ch} = b \cdot L_w$
Heat Transfer Surface Without Corrugation	$A_{lp} = L_w \cdot L_p$
Single Plate Heat Transfer Area (with Corrugation)	$A_l = \varphi \cdot A_{lp}$
Port Surface	$A_p = \pi \frac{{D_p}^2}{4}$
Hydraulic Diameter	$D_h = \frac{4bL_w}{2(b+L_w\varphi)} \cong 2\frac{b}{\varphi}$
Number of Channels per Pass	$N_{cp} = \frac{N_t - 1}{2}$
Mass Flow of Fluid per Channel	$\dot{m}_{ch} = \frac{\dot{m}}{N_{cp}}$
Mass Velocity of Fluid per Channel	$G_{ch} = \frac{\dot{m}_{ch}}{A_{ch}}$
Mass Velocity of Fluid at the Port	$G_p = \frac{\dot{m}}{A_p}$

The evaporator models that will be examined are products of the company Alfa Laval.

3.1.2 Subcritical Cycle

Heat Transfer Coefficients Calculation

For the calculations, the model's inputs are the working fluid and the thermal oil ("orc" and "oil" indexes respectively), their mass flowrates $\dot{m}_{oil}$ and $\dot{m}_{orc}$, their inlet pressures ${P_{oil}}^{in}$ and ${P_{orc}}^{in}$ and their inlet temperatures ${T_{oil}}^{in}$ and ${T_{orc}}^{in}$. Furthermore, for the application there is a constant heat source of $\dot{q}_{in} = 65\ kW$. The reference thermal oil will be Therminol D12 and the 6 working fluids presented at Table 2-1 will be examined.

As the inlet temperatures of the fluids and their pressure are input values, the enthalpies ${h_{oil,ev}}^{in}$, ${h_{orc,ev}}^{in}$ can be calculated by using the software Refprop, by providing these values and also the fluid that is examined.

The energy balance equation at the heat exchanger as a total is expressed:

$$\dot{q}_{hot} - \dot{q}_{cold} = 0 \Rightarrow$$

$$\dot{m}_{orc} \cdot \left({h_{orc,ev}}^{out} - {h_{orc,ev}}^{in}\right) = \dot{m}_{oil} \cdot \left({h_{oil,ev}}^{in} - {h_{oil,ev}}^{out}\right) = \dot{q}_{in} \tag{3.1}$$

The outlet enthalpy of the hot fluid is therefore calculated as

$${h_{oil,ev}}^{out} = {h_{oil,ev}}^{in} - \frac{\dot{q}_{in}}{\dot{m}_{oil}} \tag{3.2}$$

And the outlet enthalpy of the cold working fluid will be:

$${h_{orc,ev}}^{out} = {h_{orc,ev}}^{in} + \frac{\dot{q}_{in}}{\dot{m}_{orc}} \tag{3.3}$$

For the subcritical application, the heat exchanger will be discretized to 3 main parts. The economizer, which preheats the liquid until it reaches boiling temperature for the design high pressure, the evaporator, which will lead to the working fluid's phase change from liquid to gas, under constant pressure and temperature and lastly the superheater, which will increase the energy content of the fluid under constant pressure.

It is important to note that the heat transfer during preheating and superheating takes place under a single phase of the working fluid (liquid and gas respectively), whereas the fluid change its phase during evaporation. For this reason, different heat transfer equations have to be used to properly describe the phenomenon.

In order to calculate the heat transfer coefficients for both fluids it is necessary to assume a mean temperature of each fluid for each finite element (which will be the average of the inlet and outlet temperature at the element), a mean temperature of the plate and also a mean temperature of the wall for both the hot and the cold fluid. Lastly, the film temperature for the cold fluid will be calculated, as it will be used in a further section. These values are used as reference temperatures for calculating the fluid's properties.

The following are expressed below (From now on the indexes will be neglected for simplicity reasons).

$$\bar{T}_{oil} = \frac{{T_{oil}}^{in} + {T_{oil}}^{out}}{2} \tag{3.4}$$

$$\bar{T}_{orc} = \frac{{T_{orc}}^{in} + {T_{orc}}^{out}}{2} \tag{3.5}$$

$$\bar{T}_{plate} = \frac{\bar{T}_{oil} + \bar{T}_{orc}}{2} \tag{3.6}$$

$$\bar{T}_{wall,oil} = \frac{\bar{T}_{oil} + \bar{T}_{plate}}{2} \tag{3.7}$$

$$\bar{T}_{wall,orc} = \frac{\bar{T}_{orc} + \bar{T}_{plate}}{2} \tag{3.8}$$

$$\bar{T}_{film,orc} = \frac{\bar{T}_{wall,orc} + \bar{T}_{orc}}{2} \tag{3.9}$$

Preheater:

At the preheater there is no significant need for discretization, due to the single phase heat transfer that occurs.

At the evaporator's inlet, where the fluid enters at saturated liquid state, the pressure is set and the quality of the fluid will be equal to zero and therefore

$$h_{orc,evap}{}^{in} = f\left(P_{evap}, x = 0\right) \tag{3.10}$$

For the cold fluid, its outlet enthalpy from the preheater will correspond to its inlet enthalpy at the evaporator. Hence

$$h_{orc,preh}{}^{out} = h_{orc,evap}{}^{in} \tag{3.11}$$

Following the same procedure as for equation (3.1), the following relation for the hot fluid's input can be derived

$$h_{oil,ev}{}^{in} = h_{oil,preh}{}^{out} + \frac{\dot{m}_{orc}}{\dot{m}_{oil}} \cdot \left(h_{orc,preh}{}^{out} - h_{orc,ev}{}^{in}\right) \tag{3.12}$$

It is possible to calculate the Logarithmic Mean Temperature Difference, which is an important value for heat exchanger calculations. It is equal to:

$$\Delta T_{lm} = \frac{\left(T_{oil}{}^{in} - T_{orc}{}^{out}\right) - \left(T_{oil}{}^{out} - T_{orc}{}^{in}\right)}{\ln\left(\frac{T_{oil}{}^{in} - T_{orc}{}^{out}}{T_{oil}{}^{out} - T_{orc}{}^{in}}\right)} \tag{3.13}$$

The first step of the calculations is to determine the Nusselt number. The most appropriate correlation for subcritical, single phase heat transfer at a plate heat exchanger was the Donowski equation, according to which [51]:

$$Nu_{orc} = 0.2875 \cdot Pr_{orc}{}^{\frac{1}{3}} \cdot Re_{orc}{}^{0.78} \tag{3.14}$$

$$Pr_{orc} = \frac{\mu_{orc} \cdot C_{p,orc}}{k_{orc}} \tag{3.15}$$

which are properties calculated with the help of Refprop for each mean cold temperature of the fluid, as calculated by equation (3.5), which is also known as "bulk" temperature and for this reason the index "b" also refers to this temperature.

On the other hand, the Reynolds number can be calculated by the following expression:

$$Re_{orc} = \frac{G_{orc\_ch} \cdot D_h}{\mu_{orc}} \tag{3.16}$$

Combining equations (3.14)-(3.16) and the thermophysical properties of the fluid for the specific conditions of the cycle, the Nusselt number of each part can be calculated.

Lastly, the heat transfer coefficient for the cold fluid is calculated as:

$$a_{orc} = \frac{Nu_{orc} \cdot k_{orc}}{D_h} \tag{3.17}$$

For the hot fluid also the Donowski equation will be used and similarly to the cold fluid it will be:

$$Nu_{oil} = 0.2875 \cdot {Pr_{oil}}^{\frac{1}{3}} \cdot {Re_{oil}}^{0.78} \tag{3.18}$$

$$Pr_{oil} = \frac{\mu_{oil} \cdot C_{p,oil}}{k_{oil}} \tag{3.19}$$

which are properties calculated with the help of Refprop for each mean temperature of the heating fluid, as calculated by equation (3.4).

Similarly to the working fluid, the Reynolds number can be calculated by the following expression:

$$Re_{oil} = \frac{G_{oil\_ch} \cdot D_h}{\mu_{oil}} \tag{3.20}$$

Combining equations (3.18)-(3.20) and the thermophysical properties of the fluid for the specific conditions of the cycle, the Nusselt number of each part can be calculated.

Lastly, the heat transfer coefficient for the hot fluid is calculated as

$$a_{oil} = \frac{Nu_{oil} \cdot k_{oil}}{D_h} \tag{3.21}$$

It is therefore possible to calculate the overall heat transfer coefficient for the preheater, by using the following correlation:

$$U = \frac{1}{\frac{1}{a_{oil}} + \frac{1}{a_{orc}} + \frac{t}{k_w} + R_{forc} + R_{foil}} \tag{3.22}$$

with the values of t and k_w calculated from Table 3-1 and R_{forc}, R_{foil} the fouling resistances of the cold and hot fluid, with the value of $R_{forc} = R_{foil} = 0.00017\ \frac{m^2 \cdot K}{W}$

Lastly, the heat transferred at the preheater will be equal to

$$\dot{q}_{preh} = \dot{m}_{orc} \cdot \left({h_{orc,preh}}^{out} - {h_{orc,ev}}^{in}\right) \tag{3.23}$$

and the required surface for the preheater:

$$A_{preh} = \frac{\dot{q}_{preh}}{\Delta T_{lm,preh} \cdot U} \tag{3.24}$$

Evaporator:

As previously stated, the inlet conditions of the evaporator correspond to the outlet of the preheater and the cold fluid enters the evaporator as saturated liquid and exits as saturated steam.

$${h_{orc,ev}}^{out} = f\left(P_{evap}, x = 1\right) \tag{3.25}$$

The hot fluid calculations will be identical to the preheater part, as the hot fluid remains in liquid phase and thus the equations (3.18)-(3.21) will apply.

The energy balance equations at the evaporator are identical to the ones presented at the preheater, but the main difference between them is the phase change of the cold fluid, which creates the need for different expressions that refer to heat transfer. For this purpose, the Nusselt number for the cold fluid will be calculated by the Yan and Lin correlation, according to which: [52]

$$Nu_{orc} = 19.26 \cdot Re_{orc,eq} \cdot {Re_{orc,L}}^{-0.5} \cdot {Bo_{eq}}^{0.3} \cdot {Pr_{orc}}^{\frac{1}{3}} \tag{3.26}$$

Where the Prandtl number is calculated by equation (3.15)

The equivalent Reynolds number is:

$$Re_{orc,eq} = \frac{G_{c_{cheq}} \cdot D_h}{\mu_{orc}} \tag{3.27}$$

and the equivalent mass flux:

$$G_{orc_{ch},eq} = G_{orc\_ch} \cdot \left(1 - {Q_{orc}}^{out} + {Q_{orc}}^{out} \sqrt{\frac{\rho_{orc,L}}{\rho_{orc,G}}}\right) \tag{3.28}$$

The equivalent Reynolds number for the liquid phase:

$$Re_{orc,L} = \frac{G_{orc\_ch} \cdot D_h}{\mu_{orc,L}} \tag{3.29}$$

And the Boiling number:

$$Bo_{eq} = \frac{\dot{q}}{G_{orc_{ch},eq} \cdot \left({h_{orc}}^{out} - {h_{orc}}^{in}\right)} \tag{3.30}$$

q is the heat flux at the evaporator and will be equal to:

$$\dot{q} = \Delta T_{lm} \cdot U \tag{3.31}$$

For the evaporator, the logarithmic temperature difference will be:

Where U is calculated by equation (3.22).

It is clear that a random value for the overall heat transfer coefficient has to be assigned, which will lead to the heat flux calculation, through equation (3.31), then the boiling number with equation (3.30) and therefore the Nusselt number can be calculated through equation (3.14).

The Nusselt number will lead to the calculation of the cold fluid's heat transfer coefficient through equation (3.17) and lastly a new value of U will be calculated by equation (3.22), until the error becomes small.

Once the correct value of U is calculated, the heat transferred at the evaporator is calculated by

$$\dot{q}_{evap} = \dot{m}_c \cdot \left({h_{orc,evap}}^{out} - {h_{orc,evap}}^{in} \right) \tag{3.32}$$

and the required surface of the evaporator

$$A_{ev} = \frac{\dot{q}_{evap}}{\Delta T_{lm,evap} \cdot U} \tag{3.33}$$

Superheater:

The outlet of the evaporator will correspond to the inlet of the superheater, as the cold working fluid will enter it as saturated steam and the outlet refers to equation (3.3).

$${h_{orc,sh}}^{in} = f\left(P_{evap}, x = 1\right) \tag{3.34}$$

$${h_{orc,sh}}^{out} = {h_{orc,ev}}^{out} \tag{3.35}$$

The equations at the superheater will be identical to the ones of the preheater, as single phase heat transfer occurs. Thus, equations (3.12-3.22) will be used for the heat transfer and for the surface:

$$\dot{q}_{sh} = \dot{m}_{orc} \cdot \left({h_{orc,sh}}^{out} - {h_{orc,sh}}^{in} \right) \tag{3.36}$$

and the required surface of the evaporator

$$A_{sh} = \frac{\dot{q}_{sh}}{\Delta T_{lm,sh} \cdot U} \tag{3.37}$$

The total heat exchanger area required for the subcritical cycle will be equal to the sum of the surface of the three parts and therefore

$$A_{tot,req} = A_{preh} + A_{evap} + A_{sh} \tag{3.38}$$

Pressure Drop Calculation

Besides the heat transfer surface calculations, it is important to identify the pressure drop that occurs at a heat exchanger, as it has the potential to reduce the system's efficiency and lead to higher pump compression requirements.

The pressure drop of a fluid also presents differences regarding two-phase or single phase heat transfer and thus, similarly to before, the evaporator will require different equations to properly assess the cold fluid's pressure drop.

The total pressure drop of a fluid at a plate heat exchanger is equal to:

$$\Delta p_{tot} = \Delta p_{ch} + \Delta p_p \tag{3.39}$$

This value will be calculated for the 3 parts of the heat exchanger and for the full pressure drop it will be:

$$\Delta p_{tot,evap} = \Delta p_{tot(preh)} + \Delta p_{tot(evap)} + \Delta p_{tot(sh)} \tag{3.40}$$

The pressure drop of the channel is equal to [53]:

$$\Delta p_{ch} = \frac{\xi \cdot L_p \cdot {G_{ch}}^2}{D_h \cdot \rho} \tag{3.41}$$

For single phase heat transfer, the ξ parameter refers to the Darcy friction coefficient, which will be calculated with the following equations, according to Martin's equation [54]:

$$\frac{1}{\sqrt{\xi}} = \frac{\cos(\beta)}{\sqrt{0.18 \cdot \tan(\beta) + 0.36 \cdot sin(\beta) + \frac{\xi_o}{\cos(\beta)}}} + \frac{1 - \cos(\beta)}{\sqrt{\xi_1}} \tag{3.42}$$

Where

$$\xi_o = \begin{cases} \frac{64}{Re}, & for\ Re < 2000 \\ (1.8 \cdot \log_{10} Re - 1.5)^{-2}, & for\ Re > 2000 \end{cases} \tag{3.43}$$

And

$$\xi_1 = \begin{cases} \frac{597}{Re} + 3.85, & for\ Re < 2000 \\ \frac{39}{Re^{0.289}}, & for\ Re > 2000 \end{cases} \tag{3.44}$$

Besides the channel pressure drop of the plate heat exchanger, losses occur also due to the port. Therefore, another equation that calculates pressure drop will be applied.

And the pressure drop of the port is equal to:

$$\Delta p_p = 0.7 \cdot \frac{{G_p}^2}{\rho} \tag{3.45}$$

As the heating fluid transfers heat at a single phase, the equations (3.41)-(3.45) can be used for all three parts of the evaporator and therefore the total pressure drop of the thermal oil is calculated.

As it has been previously mentioned, the cold fluid undergoes single phase heat transfer at the preheater and the superheater and therefore the aforementioned equations are applicable. However, during evaporation there is phase change and thus, the Darcy coefficient is not appropriate for pressure drop calculation.

For the cold fluid at the evaporator

$$\Delta p_{ch} = \frac{f \cdot L_p \cdot {G_{c,ch}}^2}{D_h \cdot \rho_{c,L}} \tag{3.46}$$

The Yan and Lin friction factor will be used for low Reynolds numbers and therefore f is equal to:

for $Re_{c,L} < 750$

$$f = 6.1 \cdot 10^4 \cdot {Re_{c,eq}}^{-1.25} \tag{3.47}$$

Whereas for $Re_{c,L} \geq 750$ and $Re_{c,eq} < 6000$ the Hsieh and Lin correlations apply [55]:

$$f = 6.947 \cdot 10^5 \cdot {Re_{c,L}}^{-0.5} \cdot {Re_{c,eq}}^{-1.109} \tag{3.48}$$

In all other instances

$$f = 31.21 \cdot {Re_{c,L}}^{-0.5} \cdot {Re_{c,eq}}^{0.04557} \tag{3.49}$$

Thus, by calculating the pressure drop at the preheater and superheater by equations (3.41)-(3.45) and the pressure drop at the evaporator through (3.41), (3.45), (3.46)-(3.49), the total pressure drop of the working fluid will be given by equation (3.40).

3.1.3 Supercritical Cycle

This case that is examined has one additional complexity, which is the supercritical pressure under which the working fluid operates. The conventional equations for energy calculations are inadequate for the supercritical fluid and therefore have to be replaced by correlations specifically designed for this application, as at the pseudocritical temperature many thermophysical properties of the fluid display a sharp peak. For this reason, there is a danger that the conventional heat transfer correlations will lead to extreme and unrealistic values of required heat transfer area and pressure drop.

In order to properly assess the heat transfer and pressure drop at the evaporator and hence select the most appropriate model, the optimal supercritical correlation has to be used. For

this reason, a preliminary study of the evaporator will follow, which will compare various correlations from the bibliography and the most appropriate one will be selected. Furthermore, as this particularity refers to the working fluid, there is no need for pressure drop and heat transfer calculations of the hot fluid, since they follow exactly the procedure described at section 3.1.2.

For the supercritical cycle, no phase change occurs as the heating of the working fluid takes place above the T-s curve of the fluid. Therefore, there is no significant need to discretize the heat exchanger to various parts and instead the heat exchanger will be examined as one part.

It is important to clarify that this model operates with a reference heat exchanger and a reference working fluid and does not entirely correspond to the cycle's real conditions, but aims to lead to the selection of the most proper equations, which will be further used for calculations at the more precise model. This model, therefore, should not be fully taken into consideration quantitively, but aims to qualitatively compare the proposed equations.

The heat exchanger selected for the equations comparison is the model AC112 from Alfa Laval, with the following characteristics (in addition to the ones presented at Table 3-1) [56]

- Port Diameter: $D_p = 20\ mm$
- Horizontal Distance Between Nozzles: $L_w = 191\ mm$
- Vertical Plate Length: $L_p = 519\ mm$

Table 3-2 Input Conditions of Evaporator Correlations Evaluation Model

	Hot Fluid (Therminol D12)	**Cold Fluid (R134a)**
Inlet Pressure (bar)	4	44.65
Mass Flow (kg/s)	0.75	0.25
Inlet Temperature (℃)	210	25

Heat Transfer Coefficients Calculation:

As the working fluid undergoes a supercritical, single phase heat transfer, specific Nusselt number correlations from the bibliography that apply to supercritical relations will be utilized and are presented below (*Table 3-3).*

Table 3-3 Nusselt Number Correlations for Supercritical Conditions

Authors	**Nusselt Number**	**Comments**
Jackson- Hall [57]	$Nu_b = 0.023 \cdot {Re_b}^{0.82} \cdot \overline{Pr}^{0.5} \cdot \left(\frac{\rho_w}{\rho_b}\right)^{0.3} \cdot \left(\frac{\overline{C_p}}{C_{p,b}}\right)^n$	$\overline{C_p} = \frac{h_b - h_w}{T_b - T_w}$ $n = 0.4 + 0.2 \cdot \left(\frac{T_w}{T_{pc}} - 1\right), T_b < T_{pc} < T_w$ $n = 0.4 + 0.2 \cdot \left(\frac{T_w}{T_{pc}} - 1\right)\left(1 - 5\left(\frac{T_b}{T_{pc}} - 1\right)\right),$ $T_{pc} < T_b < 1.2T_{pc}$ and $T_b < T_w$
Dittus, Boelter [58]	$Nu_b = 0.023 \cdot {Re_b}^{0.8} \cdot {Pr_b}^n$	$n = 0.4$ for heating

Krasnochekov, Protopopov [59]	$Nu_b = Nu_{0,b} \cdot \left(\frac{\overline{C_p}}{C_{p,b}}\right)^{0.35} \cdot \left(\frac{k_b}{k_w}\right)^{-0.33} \cdot \left(\frac{\mu_b}{\mu_w}\right)^{0.11}$	$Nu_{0,b} = \left(\frac{\frac{f_b}{8} \cdot Re_b \cdot \overline{Pr}}{12.7 \cdot \left(\frac{f_b}{8}\right)^{0.5} \cdot \left(\overline{Pr}^{\frac{2}{3}} - 1\right) + 1.07}\right)$ $f = (1.82 \log_{10}(Re_b) - 1.64)^{-2}$
Petukhov et al. [60]	$Nu_b = \left(\frac{\frac{f}{8} \cdot Re_b \cdot \overline{Pr}}{1 + \frac{900}{Re_b} + 12.7 \cdot \left(\frac{f}{8}\right)^{0.5} \cdot \left(\overline{Pr}^{\frac{2}{3}} - 1\right)}\right)$	
Mokry et al. [47]	$Nu_b = 0.0061 \cdot {Re_b}^{0.904} \cdot \overline{Pr}^{0.833} \cdot \left(\frac{\rho_w}{\rho_b}\right)^{0.564}$	
Kang, Chang [61]	$Nu_b = 0.0244 \cdot {Re_b}^{0.762} \cdot \overline{Pr}^{0.552} \cdot \left(\frac{\rho_w}{\rho_b}\right)^{0.0293}$	
Okada et al. [62]	$Nu_b = 0.1528 \cdot {Re_b}^{0.66} \cdot {Pr_b}^{0.4}$	

The table can be fully calculated by using Refprop for the physical properties of the fluid and, the comments section of the table.

The values of Pr_b and Re_b are calculated by equations (3.15) and (3.16) respectively, while the value of $\overline{Pr}$ will be calculated further:

$$\overline{Pr} = \frac{\mu_c \cdot \overline{C_p}}{k_c} \tag{3.50}$$

The following figures present the Nusselt Number and the convection heat transfer coefficient for the cold fluid, as a function of its outlet temperature (Figure 3.3 and Figure 3.4) respectively.

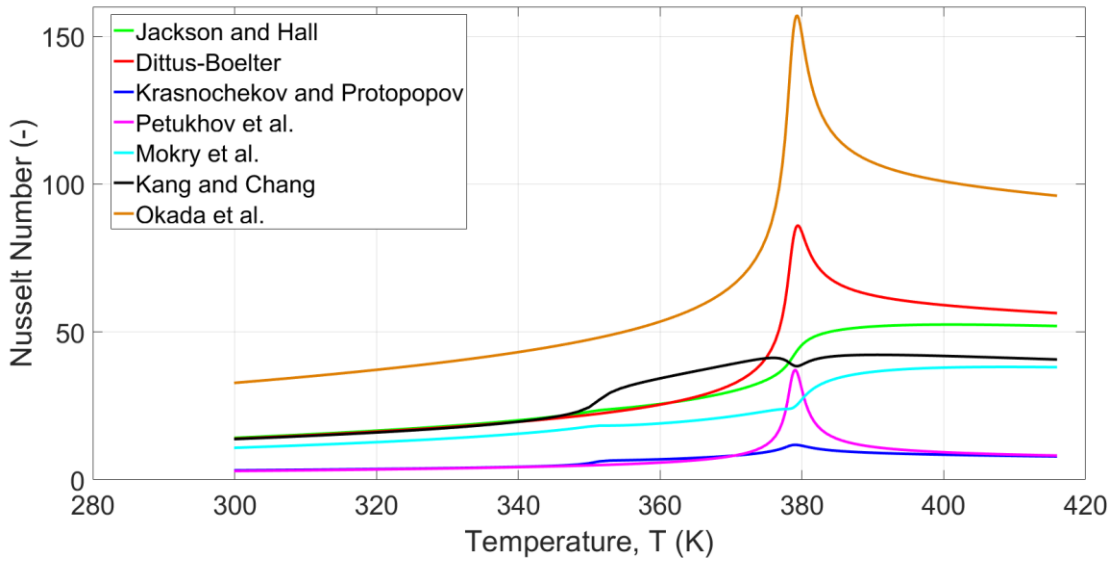

Figure 3.3 Nusselt Number- Temperature Chart for Supercritical Conditions

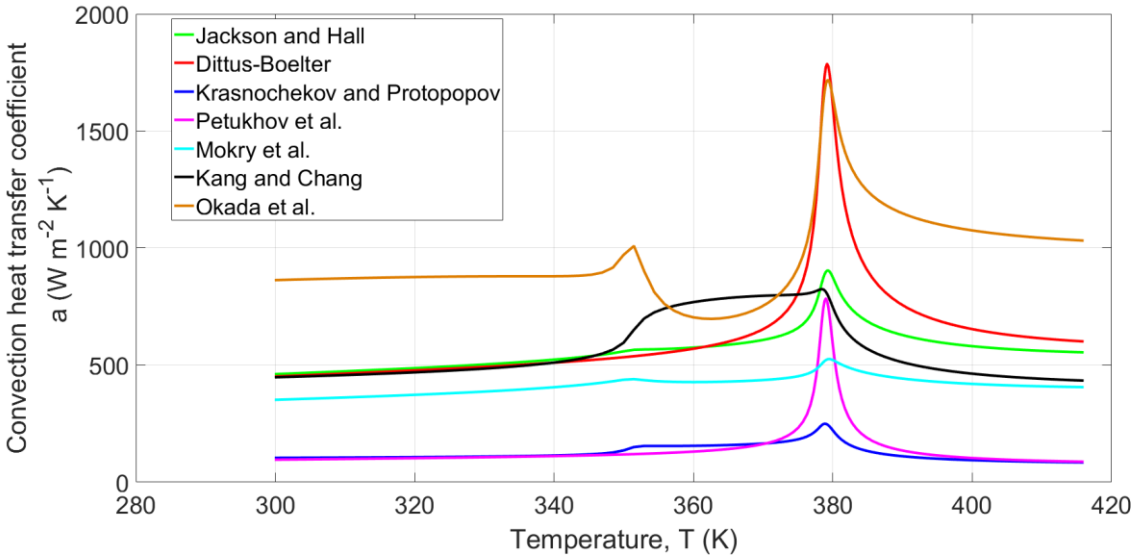

Figure 3.4 Convection Heat Transfer Coefficient- Temperature Chart for Supercritical Conditions

It is also evident for both the Nusselt number and the heat transfer coefficient that some correlations display a sharp peak value. The reason is the influence of the pseudocritical temperature of the fluid that was mentioned in the previous section. The sharp increase of the specific heat capacity at this temperature directly leads to a higher Prandtl number, which in turn vastly increases the Nusselt number. The heat transfer, however, does not follow the same principle in reality and this is exactly the reason why conventional equations cannot be

used for supercritical heat transfer. For this reason, the correlations that can be considered the most appropriate are the ones proposed by Mokry et al. (2010) and by Jackson and Hall (1980), since they attenuate this peak. Hence, the Jackson and Hall correlation will be used as benchmark for further calculations, as it has been thoroughly used in the bibliography of supercritical conditions.

The Nusselt number of the supercritical application will therefore be equal to:

$$Nu_b = 0.023 \cdot {Re_b}^{0.82} \cdot \overline{Pr}^{0.5} \cdot \left(\frac{\rho_w}{\rho_b}\right)^{0.3} \cdot \left(\frac{\overline{C_p}}{C_{p,b}}\right)^n \tag{3.51}$$

$$\overline{C_p} = \frac{h_b - h_w}{T_b - T_w} \tag{3.52}$$

For $T_b < T_{pc} < T_w$ it will be:

$$n = 0.4 + 0.2 \cdot \left(\frac{T_w}{T_{pc}} - 1\right) \tag{3.53}$$

And for $T_{pc} < T_b < 1.2T_{pc}$ and $T_b < T_w$

$$n = 0.4 + 0.2 \cdot \left(\frac{T_w}{T_{pc}} - 1\right)\left(1 - 5\left(\frac{T_b}{T_{pc}} - 1\right)\right) \tag{3.54}$$

The “w” index refers to the wall temperature of the cold fluid that has been calculated by equation (3.8) and the “b” index to the bulk temperature, calculated by equation (3.5).

T_{pc} is the pseudocritical temperature of the working fluid, that was explained in Chapter 2.3 and is calculated by the equations at Table 2-2, for various fluids and operating pressures.

By calculating the Nusselt Number, equation (3.17) will lead to the calculation of the cold fluid’s convection heat transfer coefficient and furthermore, the overall heat transfer coefficient will be calculated through equation (3.22).

For the complete heat transfer at the evaporator it is derived:

$$\dot{q}_{total} = \dot{q}_{in} \tag{3.55}$$

and for the surface required,

$$A_{required} = \frac{\dot{q}_{total}}{\Delta T_{lm} \cdot U_{supercrit}} \tag{3.56}$$

Pressure Drop Calculation:

As previously explained, the hot fluid operates at subcritical pressure and transfers heat at a single phase and thus, the equations presented at Chapter 3.1.2 are adequate to represent its pressure drop realistically.

As was the case with the heat transfer coefficients, the supercritical nature of the working fluid creates the necessity for different pressure drop equations that realistically present the actual pressure losses of the system. Thus, the pressure drop cold fluid will be examined separately and will be examined by different equations.

The following table provides a literature review of various friction factor coefficient correlations (Table 3-4).

Table 3-4 Friction Factor Correlations for Supercritical Conditions

Authors	**Friction Factor**	**Comments**
Fang [63]	$f = 0.25 \cdot \left(\log(\frac{150.39}{Re_b^{0.98865}} - \frac{152.66}{Re_b})\right)^{-2}$	
Yamashita [64]	$f = f_{iso} \cdot \left(\frac{\mu_w}{\mu_b}\right)^{0.72}$	$f_{iso} = (0.79\, ln(Re_b) - 1.64)^{-2}$
Tarasova and Leont'ev [65]	$f = f_{ref} \cdot \left(\frac{\mu_w}{\mu_b}\right)^{0.22}$	$f_{ref} = \frac{0.314}{0.7 - 1.65\, log(Re_b) + (log(Re_b))^2}$
Popov [66]	$f = f_{ref} \cdot \left(\frac{\rho_{film}}{\rho_b}\right)^{0.74}$	
Kutateladze [67]	$f = f_{ref} \cdot \left(\frac{2}{\sqrt{\frac{\bar{T}_{wall,c}}{\bar{T}_c}} + 1}\right)^2$	
Mikheev [68]	$f = f_{ref} \cdot \left(\frac{Pr_{wall}}{Pr_b}\right)^{\frac{1}{3}}$	Pr_{wall} is calculated for the fluid's thermophysical properties at $\bar{T}_{wall,c}$ temperature

The various friction factors as a function of the cold fluid's temperature are presented below (Figure 3.5)

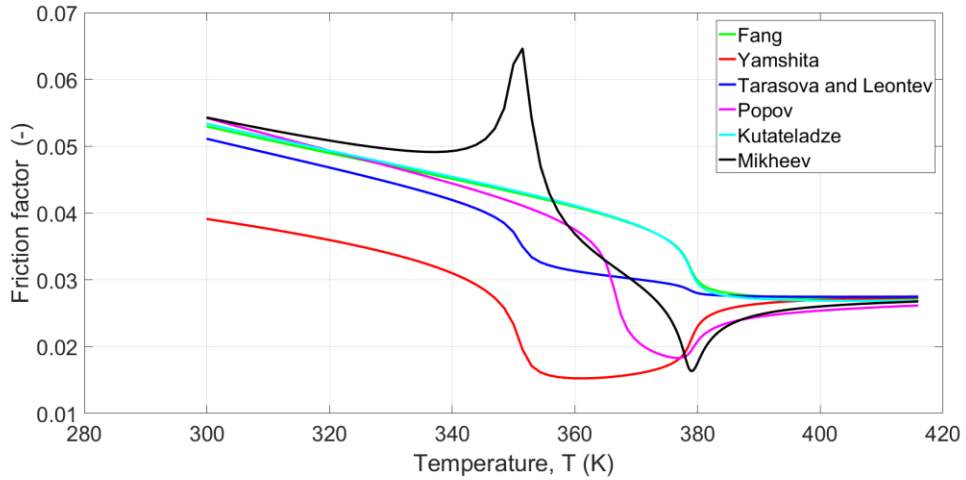

Figure 3.5 Friction factor- Temperature Chart for Supercritical Conditions

From the figure above, it can be derived that some correlations display high sensitivity related to temperature change and therefore are not appropriate for study. The correlations of Fang and Kutateladze present a very similar behavior and thus will be chosen for the study. Specifically, the Fang equation will be used for the heat exchanger calculations.

The Fang friction factor is calculated by the following correlation:

$$f = 0.25 \cdot \left(\log \left(\frac{150.39}{{Re_b}^{0.98865}} - \frac{152.66}{Re_b} \right) \right)^{-2} \tag{3.57}$$

After using this value at equation (3.46), the total pressure drop at the channel can be calculated. Furthermore, by calculating the pressure drop at the port through equation (3.45), correlation (3.40) will present the total pressure drop at the plate heat exchanger.

3.2 Expander

The expander is the installation's component that allows power production and therefore it is closely associated with the system's efficiency. The two main types of expanders are turbomachines and positive displacement type machines. The positive displacement type machines are more suited for a small scale Organic Rankine Cycle, due to the lower flow rates, higher pressure ratios and lower rotational speeds, in comparison with turbomachines [69]. Specifically, a scroll type expander was used for the cycle.

The model of the expander is based on the analysis of Lemort et al [70]. It requires the mass flow of the working fluid, the inlet enthalpy, inlet and outlet pressures and the fluid type as inputs. The inlet conditions of the expander will correspond to the outlet conditions of the evaporator, which are calculated at Chapter 3.1, while the outlet pressure will correspond to the design pressure for a standard temperature at the condenser.

As there is no second fluid involved at the expander, the index "orc" can be neglected, as all conditions refer to the working fluid.

$${P_{exp}}^{in} = {P_{evap}}^{in} - \Delta p_{total,orc} \tag{3.58}$$

$${P_{exp}}^{out} = f(T_{cond}, x = 0) \tag{3.59}$$

$$PR = \frac{{P_{exp}}^{in}}{{P_{exp}}^{out}} \tag{3.60}$$

$${h_{exp}}^{in} = {h_{orc,ev}}^{out} \tag{3.61}$$

The purpose of the model is to calculate the isentropic efficiency of the expander for these conditions, the outlet enthalpy of the working fluid and the power that is produced.

The isentropic efficiency calculation, which will lead to the calculation of the expander's outlet conditions, is based on a fitting equation of experimental data. This data is related to the rotational speed of the expander and its pressure ratio and is provided by Dumont et al. [71].

$$\eta_{is,exp} = f\left(N_{exp}, PR\right) \tag{3.62}$$

Since the isentropic efficiency is a function of both parameters, a three dimensional chart is formed and the efficiency can be calculated for each combination of the two variables. Therefore, having already set the pressure ratio (as shown by equation (3.60)) , the rotational value that leads to the highest value of isentropic efficiency for the given pressure ratio is identified and selected.

Similar to the isentropic efficiency, the data obtained by Dumont et al. correlate the expander's filling factor to its rotational speed. The polynomial approximation for this correlation is presented below:

$$ff = -3.85 \cdot 10^{-12} \cdot {N_{exp}}^3 + 7.198 \cdot 10^{-8} \cdot {N_{exp}}^2 \pm 5.034 \cdot 10^{-4} \cdot N_{exp} + 2.047 \quad (3.63)$$

Having selected the optimal rotational speed, it is clear from equation (3.63) that the expander's filling factor can be calculated. This leads to the calculation of the nominal volumetric displacement of the expander through the following equation:

$$V_{exp,nom} = \frac{60 \cdot \dot{m}}{N_{exp}(rpm) \cdot ff \cdot {\rho_{exp}}^{in}} \quad (3.64)$$

It is necessary to include the expander's thermal losses at the calculations, as they often account to a non-negligible quantity. A value of 5% was selected for the studies and for this reason, the isentropic efficiency of the expander will be equal to:

$$\eta_{is,exp} = \frac{W_{mech}}{W_{is}} = \frac{0.95 \cdot \left({h_{exp}}^{in} - {h_{exp}}^{out}\right)}{\left({h_{exp}}^{in} - {h_{exp,is}}^{out}\right)} \quad (3.65)$$

Having already calculated the value of the isentropic efficiency, the outlet enthalpy conditions can also be determined, after calculating the isentropic enthalpy at the expander's exit. This value can be calculated by using the Refprop software, as it has known pressure and entropy and is presented below:

$${h_{exp,is}}^{out} = f\left({P_{exp}}^{out}, {s_{exp}}^{in}\right) \quad (3.66)$$

Hence, equation (3.66) leads to the calculation of the expander's outlet enthalpy, as:

$${h_{exp}}^{out} = {h_{exp}}^{in} - \frac{\eta_{is,exp} \cdot \left({h_{exp}}^{in} - {h_{exp,is}}^{out}\right)}{0.95} \quad (3.67)$$

The electric power produced will be equal to the mechanical power, multiplied by the motor and generator efficiency.

$$P_{el,exp} = W_{mech} \cdot \eta_{inv} \cdot \eta_{gen} \quad (3.68)$$

The inverter and generator efficiencies will be calculated from data derived by Ziviani et al. [72] and are polynomial approximations, related to the power and rotational speed at the design and at the working point of the expander. The following variables will be introduced:

$$w_i = \frac{W_{mech}}{W_{mech,nom}} \quad (3.69)$$

$$N_i = \frac{N_{exp}}{N_{exp,nom}} \tag{3.70}$$

Furthermore, the torque developed at the shaft of the expander is equal to the mechanical work, divided by the rotational speed. Therefore:

$$\tau = \frac{W_{mech}}{\frac{2\pi N_{exp,nom}}{60}} \tag{3.71}$$

And the ratio for the design and off design point will be:

$$\tau_i = \frac{W_{mech}}{W_{mech,nom}} \frac{N_{exp,nom}}{N_{exp}} = \frac{w_i}{N_i} \tag{3.72}$$

According to the Ziviani polynomials, the efficiencies will be given by the following correlations:

$$\eta_{inv} = \alpha_o + \alpha_1 \cdot \ln N_i + \alpha_2 \cdot (\ln N_i)^2 + \alpha_3 \cdot (\ln N_i)^3 + \alpha_4 \cdot (\ln w_i) + \alpha_5 \cdot (\ln w_i)^2 + \alpha_6 \cdot (\ln w_i)^3 \tag{3.73}$$

$$\eta_{gen} = b_o + b_1 \cdot \ln N_i + b_2 \cdot (\ln N_i)^2 + b_3 \cdot (\ln N_i)^3 + b_4 \cdot (\ln \tau_i) + b_5 \cdot (\ln \tau)^2 + b_6 \cdot (\ln \tau_i)^3 + b_7 \cdot \ln \tau_i \cdot \ln N_i + b_8 \cdot (\ln \tau_i)^2 \cdot \ln N_i + b_9 \cdot \ln \tau_i \cdot (\ln N_i)^2 + b_{10} \cdot (\ln \tau_i)^2 \cdot (\ln N_i)^2 \tag{3.74}$$

The values of the constants are presented at the table below (Table 3-5)

Table 3-5 Inverter and Generator Efficiencies Constants [72]

	0	1	2	3	4	5	6	7	8	9	10
α_i	0.9557	0.02610	0.02423	0.01212	0.04948	0.03314	0.02274	-	-	-	
b_i	0.8937	0.03230	-0.01918	0.01522	0.007329	-0.03171	0.02164	0.01631	0.004376	-0.04120	-0.01627

3.3 Condenser

Heat Transfer Coefficients Calculation

The methodology for the condenser calculation is similar to the one of the evaporator for the subcritical cycle, since condensation takes place below the critical temperature of the working fluid and therefore, a two phase heat transfer occurs for most of condensation. An important difference is that the condensation temperature was set for each fluid, with the specification that the pinch point at the condenser is not lower than 5℃. This assumption simplifies the design, as the "cold" water that absorbs heat from the working fluid can be at a constant temperature, regardless of the fluid.

In contrast to the evaporator calculations, the organic fluid is considered the "hot" fluid for the condenser, as it will reject heat, in order to return to the liquid phase at constant pressure (in reality a pressure drop will occur). For the condenser, plate heat exchangers from Alfa Laval will also be used, as was the case with the evaporator.

The main geometric characteristics of the plates are identical to the ones of the evaporator and can be found at Table 3-1.

As previously stated, the working fluid enters the condenser after leaving the expander, with pressure and enthalpy calculated by equations (3.59) and (3.67) respectively. Condensation takes place under constant temperature and by design, the working fluid will exit the condenser with a subcooling of 5℃, in order to ensure it enters the pump at an exclusively liquid state. Its pressure will be equal to the inlet pressure, diminished by the pressure drop at the condenser.

As was the case at the evaporator, the index "orc" will be used for the working fluid, while for the cooling water the index "wat" will be used.

$$P_{orc,cond}{}^{in} = P_{exp}{}^{out} \tag{3.74}$$

$$P_{orc,cond}{}^{out} = P_{orc,cond}{}^{in} - \Delta p_{orc,cond} \tag{3.75}$$

$$h_{orc,cond}{}^{in} = h_{exp}{}^{out} \tag{3.76}$$

$$T_{subc} = T_{conde} - 5 \tag{3.77}$$

$$h_{orc,cond}{}^{out} = f\left(P_{orc,cond}{}^{out}, T_{subc}\right) \tag{3.78}$$

Water enters the condenser with a known pressure and temperature; therefore, its enthalpy can be calculated as:

$$h_{wat}{}^{in} = f\left(P_{wat}{}^{in}, T_{wat}{}^{in}\right) \tag{3.79}$$

The energy balance equation at the condenser as a total is expressed:

$$\begin{aligned} \dot{q}_{hot} - \dot{q}_{cold} = 0 \Rightarrow \ & \dot{m}_{orc} \cdot \left(h_{orc,cond}{}^{in} - h_{orc,cond}{}^{out}\right) \\ & = \dot{m}_{wat} \cdot \left(h_{wat}{}^{out} - h_{wat}{}^{in}\right) \end{aligned} \tag{3.80}$$

The outlet enthalpy of water is therefore calculated as

$$h_{wat}{}^{out} = h_{wat}{}^{in} + \frac{\dot{m}_{orc} \cdot \left(h_{orc,cond}{}^{in} - h_{orc,cond}{}^{out}\right)}{\dot{m}_{wat}} \tag{3.81}$$

And the heat rejected at the condenser will be:

$$\dot{q}_{cond} = \dot{m}_{orc} \cdot \left(h_{orc,cond}{}^{in} - h_{orc,cond}{}^{out}\right) \tag{3.82}$$

Also the condenser can be divided to 3 parts, just like the evaporator. The working fluid enters the condenser at a superheated state after exiting the expander and therefore, the first part of the condenser will be the de-superheater. The pure condensation that changes the phase of the fluid from gas to liquid occurs at the second part of the condenser and lastly, the subcooler will reduce the fluid's energy content and temperature, as it will reach a subcooled phase.

It is important to note that the heat transfer during de-superheating and subcooling takes place under a single phase of the working fluid (gas and liquid respectively), whereas the fluid change its phase during condensation. For this reason, different heat transfer equations have to be used to properly describe the phenomenon.

In order to calculate the heat transfer coefficients for both fluids it is necessary to assume a mean temperature of each fluid for each finite element (which will be the average of the inlet and outlet temperature at the element), a mean temperature of the plate and also a mean temperature of the wall for both the hot and the cold fluid. The process that will be followed is identical to the evaporator calculations, presented in Chapter 3.1

Therefore the various mean, wall and plate temperatures assumed through equations (3.4)-(3.9) will also be used for the working fluid and the cooling water.

<u>De-superheater:</u>

The enthalpy of the working fluid as it enters the condenser has already been calculated through equation (3.76).

$$h_{orc,des}{}^{in} = h_{exp}{}^{out} \tag{3.83}$$

For the working fluid, its outlet enthalpy from the de-superheater will correspond to its inlet enthalpy at the condensing part, where it will be in saturated steam phase. Hence

$$h_{orc,des}{}^{out} = f\left(P_{orc,cond}, x = 1\right) \tag{3.84}$$

Following the same procedure as for equation (3.81), the following relation for the cold fluid's input can be derived

$$h_{wat}{}^{out} = h_{wat}{}^{in} + \frac{\dot{m}_{orc}}{\dot{m}_{wat}} \cdot \left(h_{orc,des}{}^{out} - h_{orc,des}{}^{in}\right) \tag{3.85}$$

The various heat transfer equations will be identical to the preheater's calculations at the evaporator, as single phase heat transfer occurs and the Donowski equation will be used for the Nusselt number calculation.

The heat transferred at the de-superheater will be equal to

$$\dot{q}_{des} = \dot{m}_{orc} \cdot \left({h_{orc,des}}^{out} - {h_{orc,des}}^{in} \right) \tag{3.86}$$

and the required surface for the preheater:

$$A_{des} = \frac{q_{des}}{\Delta T_{lm,des} \cdot U} \tag{3.87}$$

Condensing Part:

As previously stated, the inlet conditions of the condensing part correspond to the outlet of the de-superheater and the working fluid enters the condensing part as saturated steam and exits as saturated liquid.

$${h_{orc,conde}}^{in} = f\left(P_{evap}, x = 1\right) \tag{3.88}$$

$${h_{orc,conde}}^{out} = f\left(P_{evap}, x = 0\right) \tag{3.89}$$

The cooling fluid calculations will be identical to the evaporator's preheater part, as water remains in liquid phase and thus the equations (3.10)-(3.22) will apply.

The energy balance equations at the condensing part are identical to the ones presented at the de-superheater, but the main difference between them is the phase change of the organic fluid, which creates the need for different equations that refer to heat transfer. For this purpose, the Nusselt number for the working fluid will be calculated by the Thonon correlation, according to which: [73]

$$Nu = 1.564 \cdot 0.347 \cdot \frac{k_b}{D_h} \cdot {Re_{eq}}^{-0.76} \cdot Pr^{\frac{1}{3}} \cdot Re^{0.653} \tag{3.90}$$

The Prandtl and Reynolds numbers are calculated by equations (3.15) and (3.16) respectively.

The Nusselt number will lead to the overall heat transfer coefficient through equation (3.17).

The latent heat transferred at the condensing part is calculated by

$$\dot{q}_{conde} = \dot{m}_{orc} \cdot \left({h_{orc,conde}}^{in} - {h_{orc,conde}}^{out} \right) \tag{3.91}$$

and the required surface of the evaporator

$$A_{conde} = \frac{\dot{q}_{conde}}{\Delta T_{lm,conde} \cdot U} \tag{3.92}$$

Subcooler:

The outlet of the condensing part will correspond to the inlet of the subcooler, as the working fluid will enter it as saturated liquid and the outlet refers to equation (3.78).

$$h_{orc,subc}{}^{in} = h_{orc,conde}{}^{out} \tag{3.93}$$

$$h_{orc,subc}{}^{out} = h_{orc,cond}{}^{out} \tag{3.94}$$

The equations at the subcooler will be identical to the ones of the de-superheater, as single phase heat transfer occurs. Thus, equations (3.10)-(3.22) will be used for the heat transfer and for the surface:

$$\dot{q}_{subc} = \dot{m}_{orc} \cdot \left(h_{orc,subc}{}^{in} - h_{orc,subc}{}^{out}\right) \tag{3.95}$$

and the required surface of the evaporator

$$A_{subc} = \frac{\dot{q}_{subc}}{\Delta T_{lm,subc} \cdot U} \tag{3.96}$$

The total heat exchanger area required for the subcritical cycle will be equal to the sum of the surface of the three parts and therefore

$$A_{tot,req} = A_{des} + A_{conde} + A_{subc} \tag{3.97}$$

Pressure Drop Calculation

The pressure drop of a fluid also presents differences regarding two-phase or single phase heat transfer and thus, similarly to before, the condenser will require different equations to properly assess the working fluid's pressure drop.

For the single-phase heat transfer, the Darcy friction factor will be used for calculations, as it is described through equations (3.41)-(3.45).

Furthermore, pressure drop will occur as described at Chapter 3.1 and equations (3.39)-(3.40).

The total pressure drop at the condenser is calculated:

$$\Delta p_{cond,tot} = \Delta p_{tot(des)} + \Delta p_{tot(conde)} + \Delta p_{tot(subc)} \tag{3.98}$$

As it has been previously mentioned, the working fluid undergoes single phase heat transfer at the de-superheater and the subcooler and therefore the aforementioned equations are applicable. However, during condensation there is phase change and thus, the Darcy coefficient is not appropriate for pressure drop calculation.

For the pressure drop:

$$\Delta p_{ch} = \frac{f \cdot L_p \cdot G_{c,ch}{}^2}{D_h \cdot \rho_{c,L}} \tag{3.99}$$

Where the friction factor f is calculated by the Han correlation [74] and is equal to:

$$f = Ge_3 \cdot {Re_{eq}}^{Ge_4} \tag{3.100}$$

Re_{eq} is calculated by equation (3.27),

$$Ge_3 = 3521.1 \cdot \left(\frac{P_c}{D_h}\right)^{4.17} \cdot \left(\frac{\pi}{2-\beta}\right)^{-7.75} \tag{3.101}$$

$$Ge_4 = 1.024 \cdot \left(\frac{P_c}{D_h}\right)^{0.0925} \cdot \left(\frac{\pi}{2-\beta}\right)^{-1.3} \tag{3.102}$$

P_c the corrugation pitch and β the chevron angle of the plate heat exchanger that can be found at Table 3-1.

Therefore, for the cooling water the Darcy coefficient will be used for all 3 parts of the condenser, while the working fluid will require the Han correlation during condensation. The total pressure drop of the condenser for both fluids will be given by equation (3.40).

3.4 Pump

The last major component of the system is the circulation pump, which increases the fluid's pressure up to the design pressure, while also countering the pressure losses that occur throughout the various components and pipes of the installation.

The pump and data presented are used from Wanner Engineering and refer to the pump model Hydra-Cell G10. For the Organic Rankine Cycle a diaphragm type pump is appropriate, due to the relatively low power consumption, in comparison to a conventional Rankine Cycle.

The model's inputs are the working fluid's mass flow, the inlet enthalpy of the pump, the inlet and outlet pressure and the type of the working fluid.

The pump's inlet corresponds to the outlet of the condenser and therefore its enthalpy will have already been calculated by the condenser's model. Furthermore, the inlet pressure of the pump will be equal to the pressure at the condenser's inlet, reduced by the pressure drop of the working fluid during condensation. Lastly, the outlet pressure of the pump will correspond to the inlet pressure of the evaporator, that has been designed and presented at Chapter 3.1.

Similarly to the expander, due to the lack of a second fluid at the pump, the index "orc" can be neglected and all conditions will refer to the working fluid.

$${h_{pump}}^{in} = {h_{orc,cond}}^{out} \tag{3.103}$$

$${P_{pump}}^{in} = {P_{orc,cond}}^{out} \tag{3.104}$$

$${P_{pump}}^{out} = {P_{evap}}^{in} \tag{3.105}$$

The mechanical work of the pump will be calculated according to the manufacturer's datasheet: [75]

$$W_{mech,pump}\ (kW) = \frac{\dot{V}_{ltm} \cdot \Delta p\ (bar)}{511} + 15 \cdot \frac{N_{pump}(rpm)}{84428} \tag{3.106}$$

Where

$$\Delta p = {P_{pump}}^{out} - {P_{pump}}^{in} \tag{3.107}$$

$$\dot{V}_{ltm}\left(\frac{lt}{m}\right) = \frac{\dot{m}_{orc}}{\rho_{in}} \cdot 60000 \tag{3.108}$$

And

$$\dot{V}_{in}\left(\frac{m^3}{s}\right) = \frac{\dot{m}_{orc}}{\rho_{in}} \tag{3.109}$$

According to the manufacturer's rotational speed- volumetric flowrate chart, the following correlation can be obtained: [75]

$$N_{pump} = 0.048081 \cdot \dot{V}^2 + 49.678 \cdot \dot{V} + 0.14284 \tag{3.110}$$

Having calculated the volumetric flowrate at the inlet of the pump, it is possible through equation (3.110) to determine the pump's rotational speed.

The rotational speed of the pump and the known pressures at the inlet and outlet allow the calculation of the pump's mechanical work through equation (3.106). Having calculated this value, it is then possible to calculate the pump's outlet enthalpy.

Furthermore,

$$W_{mech,pump} = \dot{m}_{orc} \cdot \left({h_{pump}}^{out} - {h_{pump}}^{in}\right) \tag{3.111}$$

And thus

$${h_{pump}}^{out} = {h_{pump}}^{in} + \frac{W_{mech,pump}}{\dot{m}_{orc}} \tag{3.112}$$

The software Refprop allows the calculation of the isentropic enthalpy at the pump's exit, through the following data:

$${h_{pump,is}}^{out} = f\left({P_{pump}}^{out}, {s_{pump}}^{in}\right) \tag{3.113}$$

Hence, the isentropic efficiency of the cycle can also be calculated:

$$\eta_{is,pump} = \frac{{h_{pump,is}}^{out} - {h_{pump}}^{in}}{{h_{pump}}^{out} - {h_{pump}}^{in}} \tag{3.114}$$

Lastly, as was the case with the expander, the electric consumption of the pump will be a function of the inverter and motor efficiency of the pump. However, the more the efficiencies decrease, the more the electricity consumption increases. Therefore, the pump's power consumption is given by the equation:

$$P_{el,pump} = \frac{W_{mech,pump}}{\eta_{inv} \cdot \eta_{motor}} \quad (3.115)$$

For the inverter's and motor's efficiency, the same correlations that were used in the expander analysis will be implemented and are present at Chapter 3.2

Chapter 4. Thermodynamic Performance

4.1 Heat Exchanger Selection

The mass flow and inlet temperature of the thermal fluid at the evaporator and the cooling water at the condenser are kept constant for all working fluids in both subcritical and supercritical conditions and are presented at the table below (Table 4-1).

Table 4-1 Inlet Conditions of Secondary Fluids

	Value
$T_{in,D12}$ (°C)	200
m_{D12} (kg/s)	0.75
$P_{in,D12}$ (bar)	4
$T_{in,wat}$ (°C)	7
m_{wat} (kg/s)	1
P_{wat} (bar)	3

The model that will be used for the selection of the heat exchanger's model and number of plates will follow the exact same calculations previously described and also some limitations referring to the maximum pressure drop of the hot and cold fluid respectively. It is also important to select the smallest possible heat exchanger that allows efficient heat transfer, as the size of the heat exchanger is closely related to its cost. The model is based on the analysis conducted by Roumpedakis (2018) [50].

In order to achieve the desired goal, all the aforementioned calculations will be done for various heat exchanger models that vary in size and when one is found that can achieve the necessary heat transfer and also comply with the limits of the pressure drop set, this heat exchanger will be selected.

Therefore, a variable k will be used that refers to some models of heat exchangers by the company Alfa Laval. Specifically, as the value of k increases, so does the size of the heat exchangers. For each k value, the geometrical characteristics of each heat exchanger are selected and the calculations use these values for each loop. As previously stated, when a heat exchanger that complies with the installation's requirements is found, the simulation stops and the number of the variable k is given, which can be translated to the smallest possible heat exchanger that is appropriate for the installation. It is noted that a further loop, just under the loop of the heat exchanger models is present and refers to the necessary number of plates. Thus, at the end of the simulation the model and the number of plates will be given as an output.

The table below presents the main characteristics of the possible heat exchangers for the installation (Table 4-2).

Table 4-2 Possible Heat Exchangers of the Installation

Model	$D_p\ (mm)$	$L_p\ (mm)$	$L_w\ (mm)$	Nt_{min}	Nt_{max}	$\dot{V}_{max}\ (\frac{m^3}{h})$
CB30	20	250	113	4	150	14
AC70X	20	466	111	4	124	14
AC112	20	519	191	10	300	51
CB200	40	624	324	10	230	128

At the end, the total area of the heat exchanger will be equal to the sum of the iterated parts, or

$$A_{heatex} = \sum_{i=1}^{iter} A_{iter} \tag{4.1}$$

This value applies to the necessary surface area for sufficient heat transfer. This value, therefore, determines the need for the number of plates required, as the real area of a heat exchanger is calculated as such:

$$A_{evap_{real}} = A_l \cdot N_t \tag{4.2}$$

The model establishes three limitations that determine the selection of the heat exchanger:

$$A_{evap_{real}} \geq A_{iter} \tag{4.3}$$

$$\Delta p_{oil} \leq 30\ kPa \tag{4.4}$$

$$\Delta p_{wat} \leq 30\ kPa \tag{4.5}$$

$$\Delta p_{orc} \leq 30\ kPa \tag{4.6}$$

The exact same principle was followed for

It is clear that the pump's outlet conditions should correspond to the evaporator's inlet conditions. Despite the fact that these conditions have already been determined at Chapter 3.1 in order to start solving the cycle, they have to match the pump's outlet conditions, which are related to the system's pressure drop and the pump's isentropic efficiency.

For this reason, a loop will be established that randomly assumes a temperature value at the evaporator's inlet and will solve the ORC, until a new value of the pump's outlet temperature is calculated. The purpose of the loop is to find an evaporator inlet temperature that matches the calculated outlet temperature of the pump.

4.2 Cycle Results

The models presented at Chapter 3 were used for the estimation of the performance of the 6 working fluids described at Chapter 2.1.

An important limitation set for the heat exchangers was the Pinch Point, which presents the lowest temperature difference between the working fluid and the secondary fluid. 5℃ is a common limit in the bibliography and this value was set also for the calculations.

The evaporator's outlet temperature was entered as a function of the desired pinch point, which as previously stated, should not be lower than 5℃. The working fluids, however, display a wide spectrum of critical temperatures and pressures and therefore, a constant pinch point value is not an efficient principle to follow. For fluids that display low critical temperatures, they would require extremely high superheating to closely approach the hot fluid's inlet temperature and the efficiency of the cycle would drop.

For this reason, the outlet temperature of the evaporator was optimized relatively to the electric efficiency of the system, which led in turn to an optimized mass flow for the cycle. For this reason, varying mass flows for the fluids and also for sub and supercritical application are evident.

The current chapter will present the T-s diagrams of each fluid for a subcritical and supercritical cycle, as well as the thermal, electric and exergy efficiency of the system.

The high pressure of the cycle was equal to 90% of the fluid's critical pressure for a subcritical cycle and 110% of the fluid's critical pressure for a supercritical cycle, due to the maximum efficiency of a cycle taking place close to the critical conditions of the fluid. [22]

The condensation temperature, however, could not be kept constant for all the fluids, as due to their varying T-s diagrams, it would lead to extremely high or low pressure ratios, which in turn lead to low system efficiency.

The condensation temperature was optimized for each fluid, but could not be lower than 20℃, as the pinch point at the condenser should not be lower than 5℃.

The thermal and net electric efficiencies of the cycle are given in equations (2.14) and (2.15) respectively.

Where q_{in} is the heat source of the system that is constant and equal to $65\ kW$ and the power of the expander and pump are calculated by equations (3.68) and (3.115) respectively.

Besides the first law efficiency, the model also calculates the exergy efficiency of the system. Exergy is a measure of the energy quality and the exergy efficiency demonstrates the potential for work generation, with a given heat source [76]. The exergy efficiency is defined in the following equation: [77]

$$\eta_{ex} = \frac{Pel_{net}}{Ex_{in}} = \frac{Pel_{net}}{q_{in} \cdot \left(1 - \frac{T_{amb}}{T_{in,D12}}\right)} \tag{4.7}$$

$T_{in,D12}$ is found at Table 4-1 and T_{amb} is the ambient temperature, for which $T_{amb} = 20℃$.

The conditions and thermodynamic performance of each working fluid, under subcritical and supercritical conditions are presented below.

R-134a:

The temperature- entropy diagram of R-134a is presented below (Figure 4.1). The lines that connected the major states of the fluid display linear pressure drop.

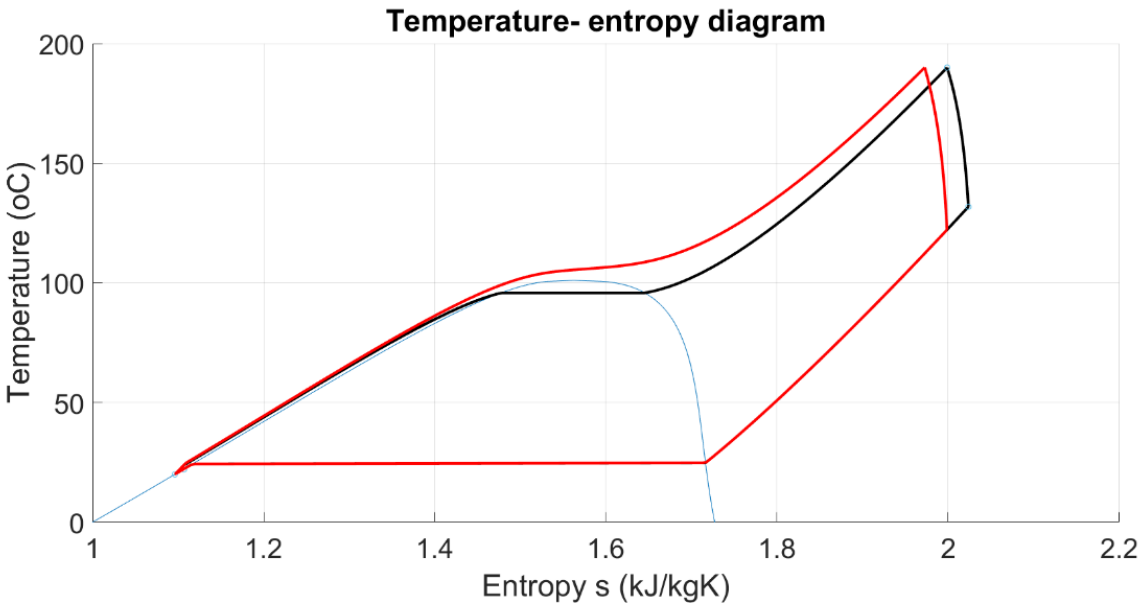

Figure 4.1 T-s diagram of R-134a for subcritical (black) and supercritical (red) cycle

For these cycle conditions, the following results were derived:

Table 4-3 R-134a Cycle Conditions

	Subcritical Cycle	Supercritical Cycle
$m_{orc}\ (kg/s)$	0.195	0.199
$T_{in,evap}$ (°C)	21.76	22.18
$P_{in,evap}\ (bar)$	36.53	44.7
PR	5.48	6.71
T_{cond} (°C)	25	25
η_{th} (%)	11.19	12.31
$\eta_{el,net}$ (%)	9.56	10.52
η_{ex} (%)	25.14	27.66

R-245fa:

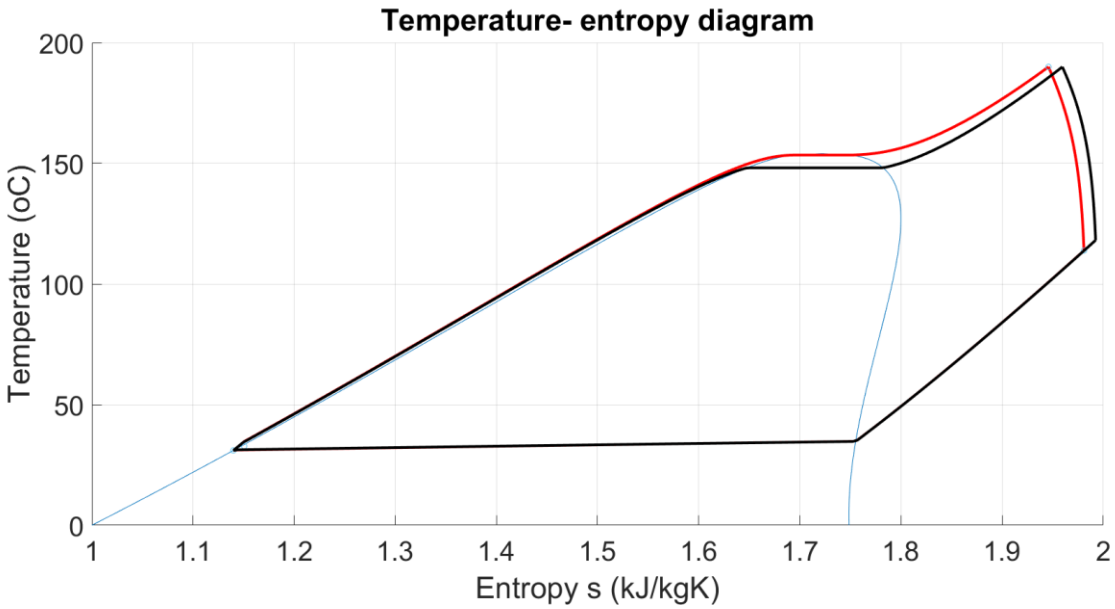

Figure 4.2 T-s diagram of R-245fa for subcritical (black) and critical (red) cycle

For these cycle conditions, the following results were derived:

Table 4-4 R-245fa Cycle Conditions

	Subcritical Cycle	Supercritical Cycle
$m_{orc}\ (kg/s)$	0.203	0.207
$T_{in,evap}$ (°C)	32.20	32.32
$P_{in,evap}\ (bar)$	32.86	36.47
PR	14.97	16.64
T_{cond} (°C)	36	36
η_{th} (%)	13.35	13.47
$\eta_{el,net}$ (%)	11.41	11.51
η_{ex} (%)	30.00	30.26

R-227ea:

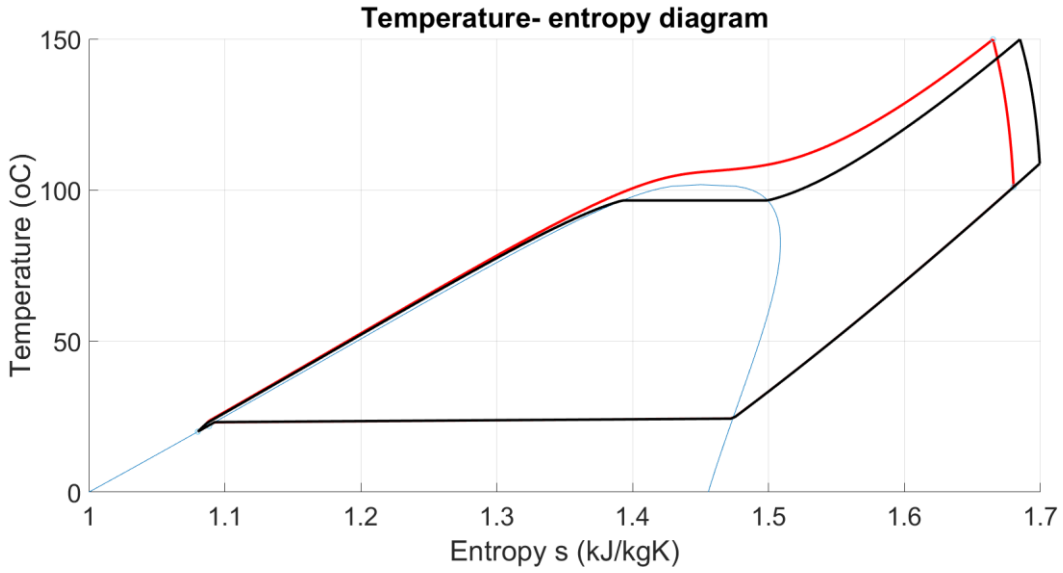

Figure 4.3 T-s diagram of R-227ea for subcritical (black) and supercritical (red) cycle

For these cycle conditions, the following results were derived:

Table 4-5 R-227ea Cycle Conditions

	Subcritical Cycle	Supercritical Cycle
$m_{orc}\ (kg/s)$	0.300	0.308
$T_{in,evap}$ (°C)	21.14	21.39
$P_{in,evap}\ (bar)$	26.33	32.18
PR	5.78	7.07
T_{cond} (°C)	25	25
η_{th} (%)	9.45	10.28
$\eta_{el,net}$ (%)	8.07	8.78
η_{ex} (%)	21.20	23.08

R-1234yf:

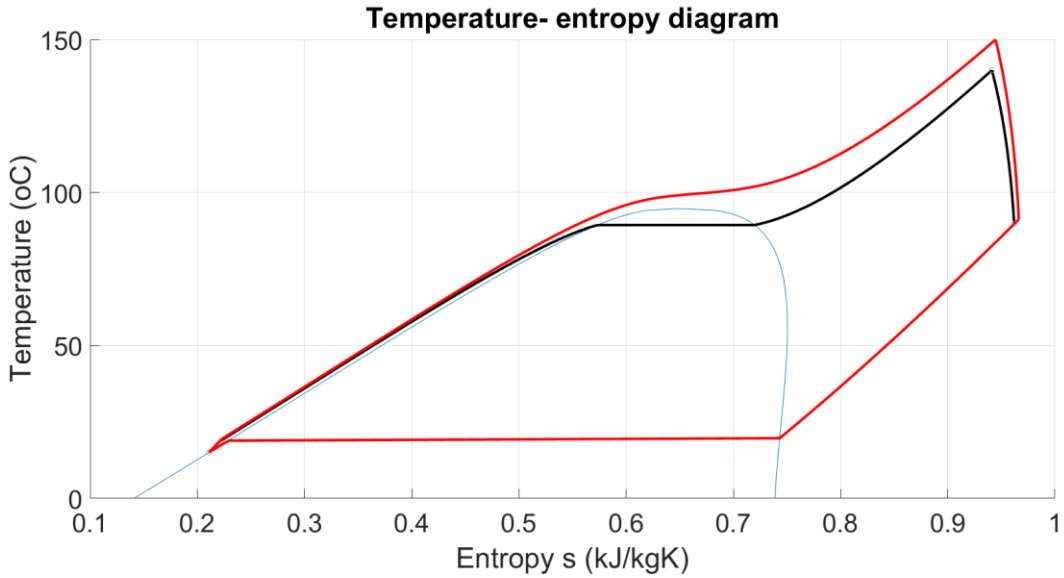

Figure 4.4 T-s diagram of R-1234yf for subcritical (black) and supercritical (red) cycle

For these cycle conditions, the following results were derived:

Table 4-6 R-1234yf Cycle Conditions

	Subcritical Cycle	Supercritical Cycle
$m_{orc}\ (kg/s)$	0.253	0.248
$T_{in,evap}$ (℃)	16.39	16.85
$P_{in,evap}\ (bar)$	30.44	37.20
PR	5.13	6.29
T_{cond} (℃)	20	20
η_{th} (%)	10.21	11.26
$\eta_{el,net}$ (%)	8.72	9.62
η_{ex} (%)	22.93	25.29

R-1234ze:

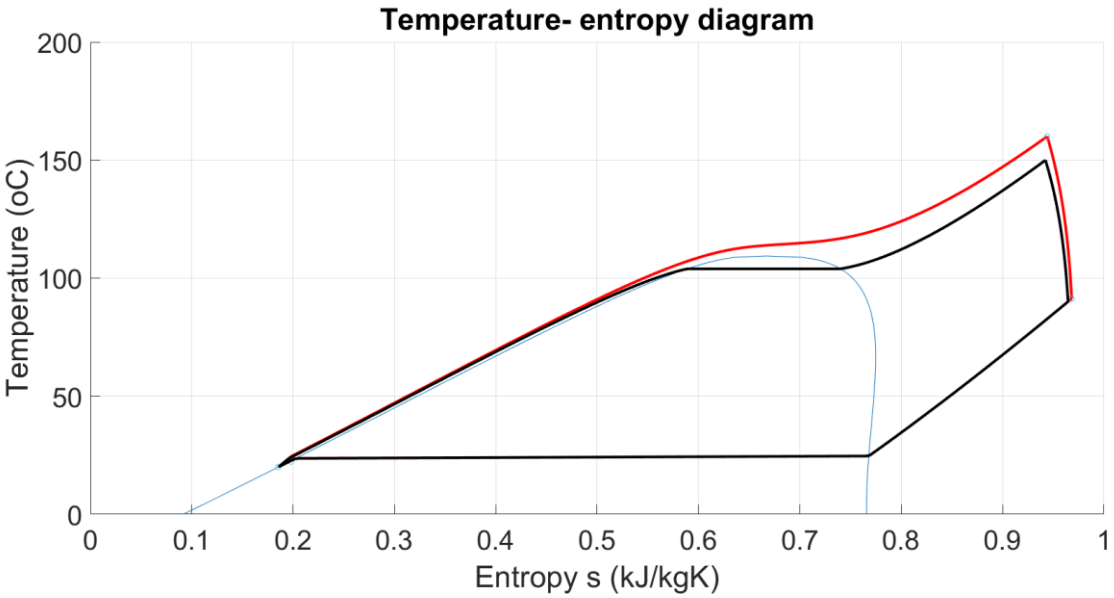

Figure 4.5 T-s diagram of R-1234ze for subcritical (black) and supercritical (red) cycle

For these cycle conditions, the following results were derived:

Table 4-7 R-1234ze Cycle Conditions

	Subcritical Cycle	Supercritical Cycle
$m_{orc}\ (kg/s)$	0.238	0.234
$T_{in,evap}$ (°C)	21.38	21.97
$P_{in,evap}\ (bar)$	32.73	40.00
PR	6.55	8.02
T_{cond} (°C)	25	25
η_{th} (%)	11.49	12.34
$\eta_{el,net}$ (%)	9.82	10.54
η_{ex} (%)	25.80	27.72

R-410A:

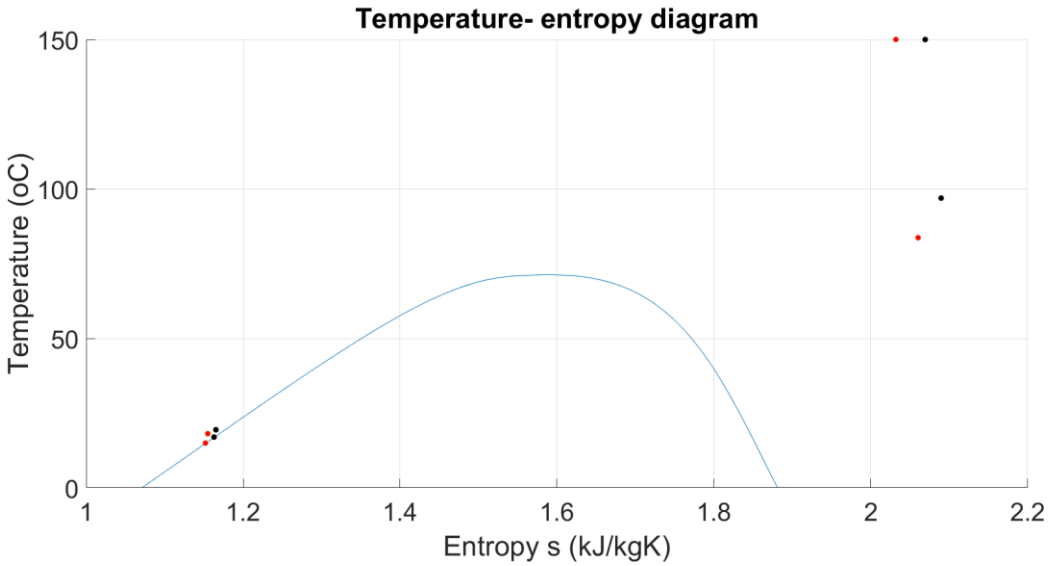

Figure 4.6 T-s diagram of R-410A for subcritical (black) and supercritical (red) cycle

For these cycle conditions, the following results were derived:

Table 4-8 R-410A Cycle Conditions

	Subcritical Cycle	Supercritical Cycle
$m_{orc}\ (kg/s)$	0.208	0.211
$T_{in,evap}$ (°C)	19.14	17.82
$P_{in,evap}\ (bar)$	44.12	53.92
PR	2.88	3.72
T_{cond} (°C)	22	20
η_{th} (%)	8.80	10.00
$\eta_{el,net}$ (%)	7.52	8.54
η_{ex} (%)	19.78	22.44

Various conclusions can be drawn that are related to both the working fluid selection, as well as the comparison between a subcritical and supercritical cycle both with the existing literature, as well as with the preliminary study of an ideal cycle, conducted at 1.4.

It is evident that the results of 1.4 are not identical to the ones of Chapter 4, as some operating conditions were different, such as the mass flow of each fluid. Furthermore, as the initial analysis did not take into consideration the pressure drop that occurs throughout the installation, it is expected that it leads to different results.

Furthermore, in all the scenarios of 1.4, the highest efficiency was achieved by R-245fa, followed by R-1234ze and then R-134a. This was confirmed by the results presented above. Another important factor that influenced the electric efficiency of the cycle was the pressure ratio. Due to the T-s curve of some fluids, such as R-410A, the low pressure of the cycle (at the condenser) is relatively high and therefore the pressure ratio remains low (2.88 for subcritical and 3.72 for supercritical use). As shown in 1.4, the pressure ratio greatly influences that efficiency of a cycle and thus, it is expected that a fluid with a low pressure ratio will display low thermal efficiency. In contrast, the very high pressure ratio of R-245fa led to having the highest thermal efficiency of all fluids, whereas R-1234ze also had the second highest pressure ratio, which led to the second highest thermal efficiency.

The fluids that display the highest efficiency were found to have in principle a high critical temperature. The highest efficiency for both a subcritical and a supercritical cycle was evident for R-245fa, which has the highest critical temperature of all the fluids ($154.01℃$). The second highest efficiency was recorded for R-1234ze, which has the second highest critical temperature, whereas fluids such as R-410A and R-1234yf, that have lower critical temperatures display lower efficiency than the other fluids. Similar conclusion was reached by Mago et al., who studied dry fluids on a Regenerative ORC and noted that the higher the boiling temperature of the organic fluid, the better the thermal efficiency [78].

Another factor that affected the results was the mass flow selected for the cycle. As 1.4 demonstrated, the working fluids presented in principle a greater efficiency for lower mass flows, between $0.15 \text{ and } 0.25\ kg/s$. The mass flow of each working fluid, however, could not always reach the desired optimized value presented at 1.4, as the pressure drop and irreversibility of the cycle provided limitations. For example, very low mass flows lead to very high temperatures and thus demand very large heat exchanger surface. For this reason, an optimized mass flow was selected, which would also lead to viable economic conditions. The results again showed that the fluids that performed greater had typically low mass flows, as was the case mostly with R-134a and R-245fa. On the contrary, the relatively high mass flows of R-227ea and R-1234yf led to lower net electric efficiency. The exceptions to this observation are fluids R-1234ze and R-410A.

Lastly, as shown by equation (4.7), the exergy efficiency of the system is linearly dependent on the net electric power production, or equally to the net electric efficiency of the system. As the heat source is constant in terms of power and temperature, it is clear that the highest exergy efficiency will be achieved when the electric efficiency of the cycle is also the highest.

According to Lakew and Bolland, exergy increases with pressure, as it leads to lower exergy losses at the Heat Exchangers, Pump and Expander [79].

As the literature review has shown, the efficiency of a supercritical cycle tends to be higher than the efficiency of a subcritical, for the same working fluid. The reason is mostly the higher mean temperature of heat addition for supercritical pressure, as well as the better match between the heating curve of the working fluid and the cooling curve of the heat source. In most cases, the electric efficiency of a supercritical cycle was higher by 1 percentage point, with only R-245fa demonstrating a very slight increase (from 11.41 to 11.51%). As Figure 2.3 shows, the effect of the pressure ratio is crucial to the system's efficiency and clearly it is higher for a supercritical cycle.

The biggest increase between the two concepts was evident for R-410A. As explained, for this particular fluid the conditions that were set led to extremely low pressure ratio, which significantly limits the potential of the system for power production. Therefore, by increasing the pressure ratio from 2.88 to 3.72, the ability of the system to produce power is greatly affected. The smallest increase, in terms of percentage, was evident for R-245fa. This fluid displays the exact opposite behavior with R-410A, as its pressure ratio is very high, even for a subcritical cycle. Figure 2.4 shows that the efficiency increases with a lower rate of change as the pressure ratio increases and thus it is expected that the higher the pressure ratio of a cycle, the lower the increase that will be achieved for a supercritical system.

The literature results shown in Table 1-2 demonstrate generally higher efficiency values than the ones of the current study. Most of them, however, are employing higher temperature heat sources, or use different working fluids, which in general display higher efficiency.

A comparable study would be the one conducted by Xu et al. (2013) [21]. The authors found that for a supercritical R-134a, with a maximum temperature 132℃ presented thermal efficiency equal to 13.4%, whereas this study for R-134a led to 12.31%. The pump and expander efficiencies of this study were set by the authors at 85%, which are much higher values than the ones calculated at this study for this working fluid and are presented at Table 5-2. These conditions significantly affect the thermal efficiency and this is a possible explanation for the deviation between the two results.

Another similar study, whose heat source was waste heat was conducted by Uusitalo et al. (2014) [23]. As presented at the Literature review, the study employed water for the high temperature waste heat and R-245fa for the lower temperature charge air of the engine, in comparable temperature with the current study (210℃ instead of 200℃). The evaporating pressure was set at 95% of the critical, instead of the study's high pressure of 90% of the critical and the results obtained for a subcritical cycle were close to the ones of the current study (11.8% instead of 11.41%).

Lastly, a study carried out by Yagli et al. (2016) used R-245fa as a working fluid for an ORC, with an exhaust gas waste heat recovery system [80]. The study included a subcritical and a supercritical cycle and results showed that the supercritical cycle displayed greater thermal and exergy efficiency. The authors found for a supercritical cycle an energy efficiency equal to 15.93%, slightly higher than the value of 13.47% of this study, but also presented a lower

exergy efficiency of 27.76% instead of 30.26%. A possible explanation for the higher thermal efficiency could be the clearly higher isentropic efficiency of both the turbine and the pump (88% and 80% respectively), as well as the size of the plant, which produces 81.52 kW of electric power and it is known that larger systems present higher thermal efficiencies.

Chapter 5. Economics

5.1 Sizing and System Cost

The cost of the system will be calculated by estimating the cost of the various components, as described below:

Cost of control and hardware: [14]

$$c_1 = 800\ €\tag{5.1}$$

Cost of piping[i]:

$$c_2 = 55.3\ €\tag{5.2}$$

Cost of fluid:

$$c_3 = C_{fluid}\left(\frac{€}{lt}\right)\cdot V_{fluid}\ (lt)\tag{5.3}$$

Cost of tank: (Fitting equation by Zilmet USA) [81]:

$$c_4 = f(V_{tank})\tag{5.4}$$

Cost of pump: (Fitting equation for Hydra-Cell G10) [75]

$$c_5 = f(W_{mech,pump})\tag{5.5}$$

Cost of motor: [82]

$$c_6 = 71.7\cdot P_{el,pump}\ (kW)^{0.95}\tag{5.6}$$

Cost of expander: (Fitting equation for Copeland ZR series)

$$c_7 = f\left(P_{el,exp}\ (kW)\right)\tag{5.7}$$

Cost of heat exchangers: [14]

$$c_8 = 190 + 310\cdot A_{evap}\ (m^2)\tag{5.8}$$

$$c_9 = 190 + 310\cdot A_{cond}\ (m^2)\tag{5.9}$$

Cost of labor:

$$c_{10} = \frac{\sum_{i=1}^{9} c_i}{0.7} - \sum_{i=1}^{9} c_i\tag{5.10}$$

Total cost of system:

$$C_{tot} = \sum_{i=1}^{10} c_i\tag{5.11}$$

The cost of each fluid per liter is presented at Table 5-1

Table 5-1 Cost of Refrigerants [83], [84], [85]

Fluid	Cost $(€/lt)$
R-134a[ii]	11.64
R-245fa	43.64
R-227ea	120
R-1234yf	153
R-1234ze	19.95
R-410A	36.76

For the results obtained at Chapter 4, the sizing of the various systems and the total cost for each fluid are presented below:

Table 5-2 System Components for R-134a

	Subcritical Cycle	Supercritical Cycle
Evaporator Model	CB30	AC112
Evaporator Plates	87	106
$A_{evap}\ (m^2)$	2.90	12.40
$\eta_{is,exp}\ (\%)$	76.87	77.78
$P_{el,exp}\ (kW)$	6.94	7.76
Condenser Model	CB30	CB30
Condenser Plates	91	93
$A_{cond}\ (m^2)$	3.03	3.10
$\eta_{is,pump}\ (\%)$	77.93	79.58
$P_{el,pump}\ (kW)$	0.73	0.92
Total Cost (€)	13357	18114

Table 5-3 System Components for R-245fa

	Subcritical Cycle	Supercritical Cycle
Evaporator Model	CB30	CB30
Evaporator Plates	87	87
$A_{evap}\ (m^2)$	2.90	2.90
$\eta_{is,exp}\ (\%)$	74.92	74.02
$P_{el,exp}\ (kW)$	8.14	8.30
Condenser Model	CB30	CB30
Condenser Plates	54	54

$A_{cond}\ (m^2)$	1.80	1.80
$\eta_{is,pump}\ (\%)$	77.93	78.69
$P_{el,pump}\ (kW)$	0.73	0.81
Total Cost (€)	17847	18007

Table 5-4 System Components for R-227ea

	Subcritical Cycle	Supercritical Cycle
Evaporator Model	CB30	AC112
Evaporator Plates	87	112
$A_{evap}\ (m^2)$	2.90	13.10
$\eta_{is,exp}\ (\%)$	76.87	77.89
$P_{el,exp}\ (kW)$	5.96	6.61
Condenser Model	CB30	CB30
Condenser Plates	106	109
$A_{cond}\ (m^2)$	3.53	3.63
$\eta_{is,pump}\ (\%)$	77.82	79.50
$P_{el,pump}\ (kW)$	0.71	0.91
Total Cost (€)	28699	33698

Table 5-5 System Components for R-1234yf

	Subcritical Cycle	Supercritical Cycle
Evaporator Model	CB30	AC112
Evaporator Plates	87	134
$A_{evap}\ (m^2)$	2.90	15.68
$\eta_{is,exp}\ (\%)$	76.38	77.58
$P_{el,exp}\ (kW)$	6.50	7.27
Condenser Model	AC70X	AC70X
Condenser Plates	104	100
$A_{cond}\ (m^2)$	6.34	6.10
$\eta_{is,pump}\ (\%)$	78.91	80.18
$P_{el,pump}\ (kW)$	0.83	1.02
Total Cost (€)	34977	40989

Table 5-6 System Components for R-1234ze

	Subcritical Cycle	Supercritical Cycle
Evaporator Model	CB30	CB200
Evaporator Plates	87	82
$A_{evap}\ (m^2)$	2.90	19.57
$\eta_{is,exp}\ (\%)$	77.72	77.97
$P_{el,exp}\ (kW)$	7.22	7.88
Condenser Model	CB30	CB30
Condenser Plates	120	116
$A_{cond}\ (m^2)$	4.00	3.87
$\eta_{is,pump}\ (\%)$	78.97	80.18
$P_{el,pump}\ (kW)$	0.84	1.03
Total Cost (€)	15205	22957

Table 5-7 System Components for R-410A

	Subcritical Cycle	Supercritical Cycle
Evaporator Model	CB30	AC112
Evaporator Plates	87	35
$A_{evap}\ (m^2)$	2.90	2.14
$\eta_{is,exp}\ (\%)$	77.95	75.58
$P_{el,exp}\ (kW)$	5.71	6.65
Condenser Model	CB30	AC112
Condenser Plates	140	97
$A_{cond}\ (m^2)$	4.67	5.92
$\eta_{is,pump}\ (\%)$	78.85	80.65
$P_{el,pump}\ (kW)$	0.82	1.10
Total Cost (€)	15543	16194

For the calculations, a 50 liter tank was selected and the volume of the fluid was assumed to be 100 liters. As Table 5-1 indicates, the cost of fluids varies significantly and is a very crucial factor that affects the total cost of the system.

This can be proved by the total cost for each system, as shown in Table 5-2 to Table 5-7. The fluids R-227ea and R-1234yf are very expensive and therefore considerably increase the final

cost of the system. For this reason, for both a subcritical and a supercritical cycle, the cost for these two fluids is very high.

Another parameter that has a big impact on the total cost of the system is the one of the heat exchangers. The cost of the system is heavily influenced by the heat exchanger surface, as shown by equations (5.8) and (5.9). For the most working fluids, the supercritical cycle demands much higher evaporator surface, due to the higher pressures and temperatures that are present. This is the main reason for the cost increase between a supercritical and a subcritical cycle.

Another observation from the tables is the superior isentropic efficiency of the expander and the pump for a supercritical cycle. As explained, high pressures lead to lower entropies at the superheated state and thus, more efficient power production can be realized. Despite the pump requiring more electric power to achieve higher pressure increase, its higher isentropic efficiency for a supercritical cycle indicates that the cycle operates better thermodynamically.

The table below presents the cost of the system per kW_{el}, for the various working fluids at their maximum load.

Table 5-8 Cost of system in €/kW_{el}

	Subcritical	**Supercritical**
R-134a	2528.8	3116.5
R-245fa	2831.0	2831.6
R-227ea	6436.7	6946.7
R-1234yf	7260.0	7711.9
R-1234ze	2802.5	3942.2
R-410A	3741.0	3432.1

A case study conducted by Rentizelas, Karellas et al. indicated that the investment cost of an ORC plant is around 2760 euros per kW [86], which is a similar value to the R-134a, R-245fa and R-1234ze system costs. The working fluids that present a significantly higher specific installation cost are not economically viable options.

According to another study that focuses on small scale ORC in WHR applications by Tchanche et al. claimed that the specific installed cost of a 2 kW_{el} system is equal to 5775 per kW, whereas for a 50kW system the cost dropped to 3034 per kW [87]. As Table 5-8 indicates, the installation costs calculated comply with these values, but for the most fluids they are slightly lower.

5.2 Economic Indexes

The current chapter aims to assess the viability and performance of each system, from a financial standpoint. For this reason, three economic indexes will be introduced, which are related to the investment and the cost of energy produced by the Organic Rankine Cycle that is studied. These indexes will be the Net Present Value, Pay Back Period and Levelized Cost of Energy.

The profit generated from the aforementioned system is highly dependent on the country it is used, as well as its working hours throughout the course of the year. For this specific system, the number of working hours is related to maintenance needs, as well as availability of the heat source.

The number of working hours per year is directly related to the annual energy production, whereas the country in place is related to the cost of energy per kWh. As the system produces power and will supply it to the grid, the higher the cost of energy of a country, the more beneficial it is to use the system.

For all the calculations a standard discount rate of return was assumed, equal to 6% and the project's lifetime 25 years.

5.2.1 Net Present Value

The Net Present Value (NPV) of a system calculates the value of all future cash flows over the lifetime of an investment, discounted to the present. It is one most important criteria for assessing an investment and needs to be positive, in order for the investment to be profitable [88].

The formula that calculates the net present value of an investment is presented below: [89]

$$NPV = \sum_{t=0}^{N} \frac{NCF_t}{(1+i)^t} \tag{5.1}$$

Where

t corresponds to each time period

N corresponds to the lifetime of the system in years (for the current study equal to 25 years)

NCF_t corresponds to the net cash flow for year t

i corresponds to the discount rate of return, which is equal to 6%

The net cash flow for year t is equal to:

$$NCF_t = REV_t - OM_t \tag{5.2}$$

Where

REV_t is the revenue from power production for year t

OM_t are the operational and maintenance costs of the system and were assumed equal to 3% of the total investment cost.

It is important to clarify that for year 0, the net cash flow is negative and its absolute value equal to the investment cost. Thus

$$NCF_o = -IC \tag{5.3}$$

The investment cost for each system, combined with the use of a working fluid is presented at Tables 5-2 to-5-7.

As stated regarding operational costs

$$OM_t = 0.03 \cdot IC \tag{5.4}$$

In order to calculate the revenues from power production for one year, the total power that is produced has to be identified.

The study focused in detail on identifying the design point of the system for each working fluid, which would maximize cycle efficiency and therefore power production. In reality, however, the system would not exclusively operate at the design point. For this reason, the cycle will operate for 60% of its annual working hours at the design point and 40% at an off design point, which would yield 75% of its maximum power. Therefore, for the annual energy production:

$$E_{el} = \left(0.6 \cdot P_{el,dp} \cdot +0.4 \cdot \left(0.75 \cdot P_{el,dp}\right)\right) \cdot \frac{hr}{a} \tag{5.5}$$

$$P_{el,dp} = \eta_{el,net} \cdot \dot{q}_{in} \tag{5.6}$$

For the total working hours of the system 3 scenarios will be examined, which aim to demonstrate the minimum necessary number of working hours per year for each system, in order for it to be profitable.

Table 5-9 System Working Hours per Year

	Scenario 1	Scenario 2	Scenario 3
Total working hours per year	1280	2560	5120

The net electric efficiency is presented for each fluid at

Table 4-3 to
Table *4-8* and refers to the design point.
Equation (5.6) calculates the power in kW and thus, equation (5.5) calculates the energy yield in kWh/a.

The revenue from power production will be simply given as

$$REV = E_{el}\left(\frac{kWh}{a}\right) \cdot C_{el}\left(\frac{€}{kWh}\right) \tag{5.7}$$

As stated previously, the cost of electricity differs from country to country. Normally, this value should correspond to the selling price of energy to the electric grid, but this value is influenced by various parameters, such as demand or peak hours and is not an easily accessible value. Therefore, the cost of energy for non- household consumers was assumed, which is significantly lower than cost of electricity for household consumers and presents a more realistic situation, despite not being entirely accurate.

The cost of electricity for all countries of the European Union is presented at the table below (Figure 5.1). [90]

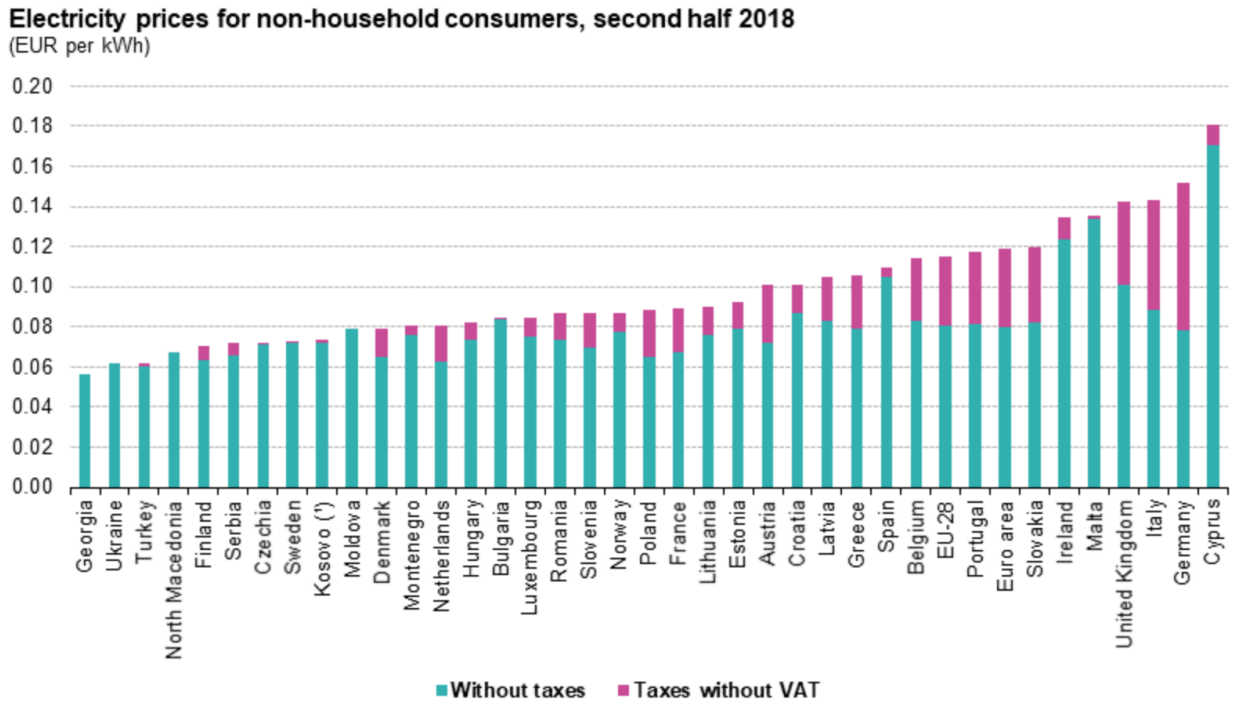

Figure 5.1 Electricity prices in the European Union [90]

The costs that will be examined refer to Germany, Greece and the average price of the European Union and are presented below (Table 5-10).

Table 5-10 Cost of Electricity per kWh

	Germany	Greece	mean EU-28
Cost of electricity ($\frac{€}{kWh}$)	0.155	0.104	0.1149

For each of the 3 scenarios, the Net Present Value of the investment after 25 years is calculated and presented below for each fluid in both a subcritical and a supercritical cycle.

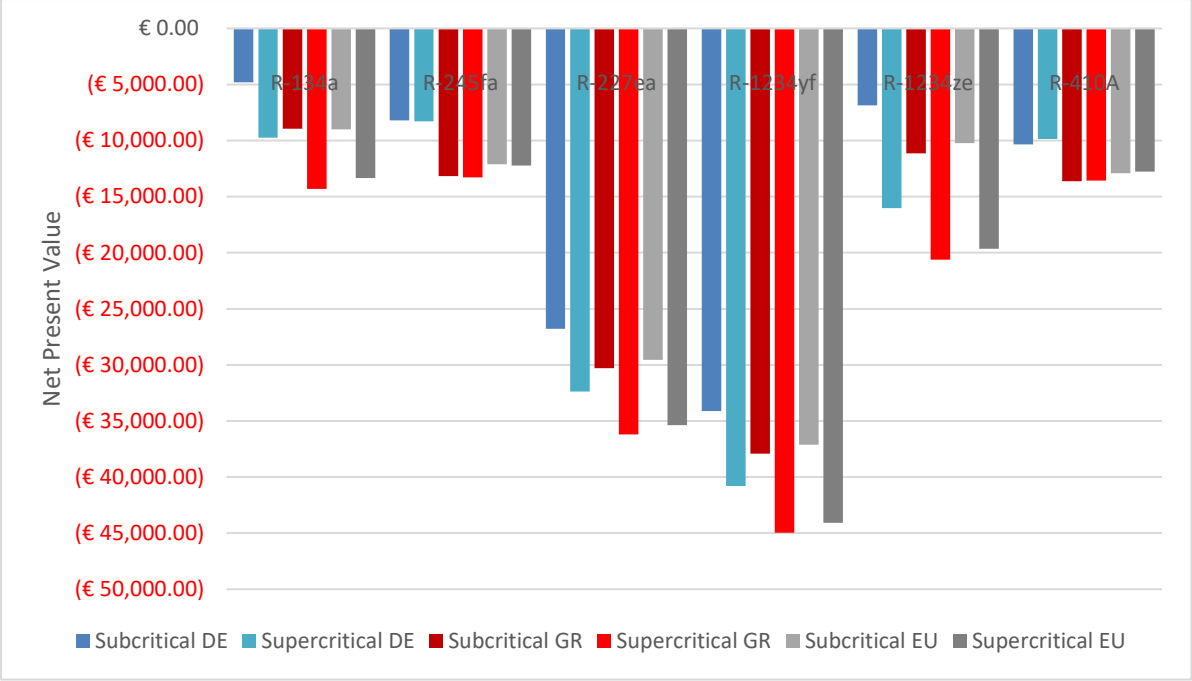

Figure 5.2 Net Present Value of various working fluids for various countries (1280 working hours per year)

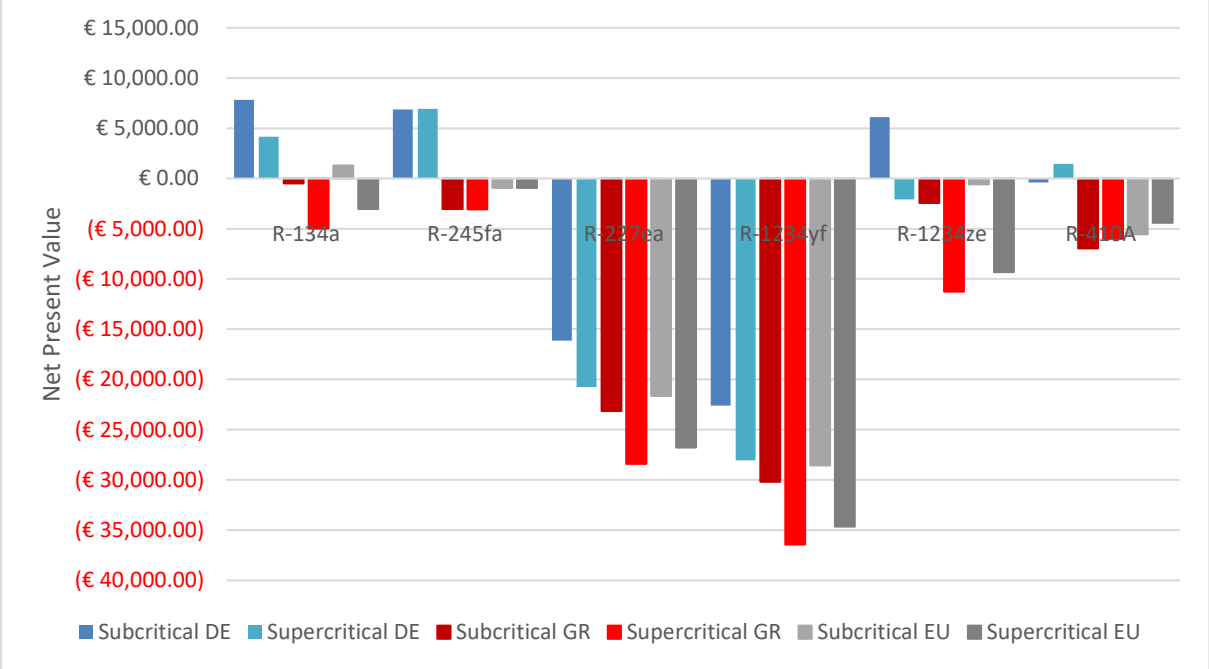

Figure 5.3 Net Present Value of various working fluids for various countries (2560 working hours per year)

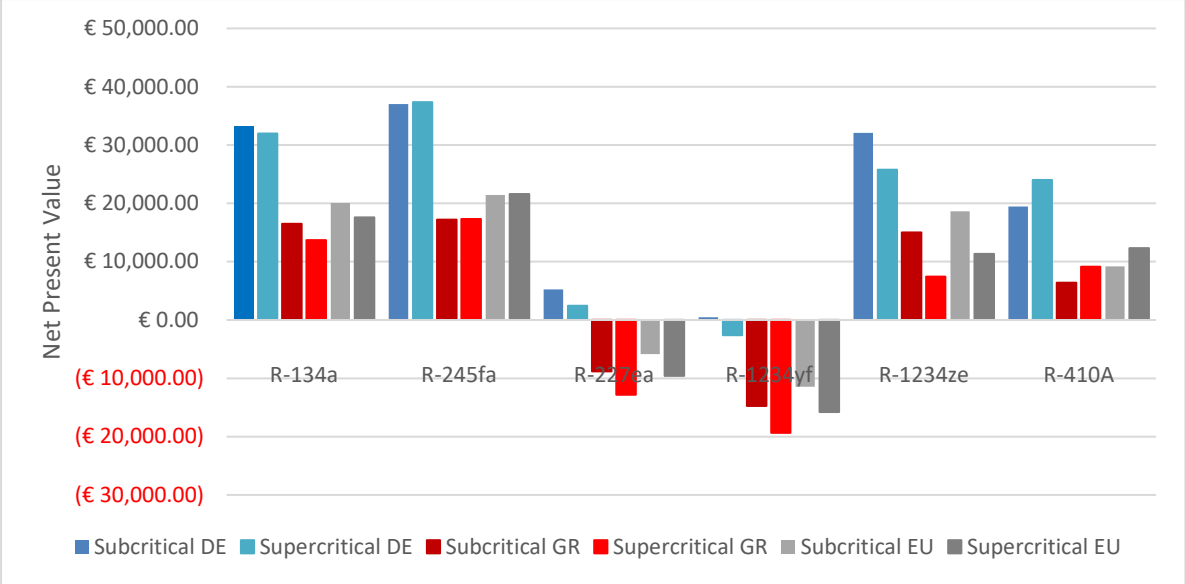

Figure 5.4 Net Present Value of various working fluids for various countries (5120 working hours per year)

From the figures presented above various conclusions can be drawn, regarding the countries examined, working hours per year, as well as the working fluids:

The working hours of the system are a very crucial aspect of the installation, as they directly influence the energy yield and thus the revenue. As it can be seen in Figure 5.2, if the system operates for only 1280 hours per year (less than 15% availability throughout the year) there is no scenario of working fluid or location that provides a positive present value, due to the very low energy yield that can be accomplished in a year.

When the system's working hours are doubled, it can be seen that the location of the system and the working fluids are crucial parameters that determine if the investment will be profitable or not.

As Table 5-10 demonstrates, the cost of energy in Germany is significantly higher compared to Greece or the average of the EU and therefore it greatly influences the revenue that is generated from selling the power to the grid. It is clear from all working fluids that the Net Present Value in 25 years will be much higher in Germany for all working fluids. It can be seen that for this number of hours of operation throughout the year, an investment outside of Germany would lead to a negative Net Present Value and would not be a viable option.

The third scenario is profitable for nearly all working fluids and scenarios, as significant energy yield is achieved. Two fluids, however, (R-227ea and R-1234yf) demonstrate negative values even for this scenario (especially in Greece, due to the low cost of electricity). This is expected, as the cost of the investment per kW is much higher for these two working fluids, roughly 2-3 times higher in comparison with the rest of the fluids. As shown in Table 5-4 and Table 5-5, this is mostly due to the very high investment costs required for systems that operate under these two fluids, without being translated to equally high cycle efficiency.

The highest NPV is evident for the supercritical use of R-245fa, closely followed by subcritical R-245fa and also both states of R-134a.

5.2.2 Payback Period

The payback period refers to the amount of time it takes to recover the cost of an investment. Alternatively, it can be also interpreted as the amount of time required, so that the Net Present Value of an investment is equal to 0 [91]. Specifically, the index that will be calculated will be the discounted payback period, which considers the discount rate of return and provides a more realistic assessment of the breakeven point of the investment.

Similarly to the NPV, it can be expressed as:

$$\sum_{t=0}^{PBP} \frac{NCF_t}{(1+i)^t} = 0 \tag{5.8}$$

All the variables represented at the formula are identical to the ones presented at equation (5.1). The factors that influence the payback period are also the location of the system, the number of working hours and the working fluid.

It is important to note that for various conditions of working hours or working fluids the calculation of the payback period led to extremely high values, which clearly indicate the system is not economically viable. The payback period for these conditions was set constant and equal to 100, in order to demonstrate that it is not attractive from an investment standpoint.

The results for the 3 aforementioned scenarios of working hours are presented at the figures below.

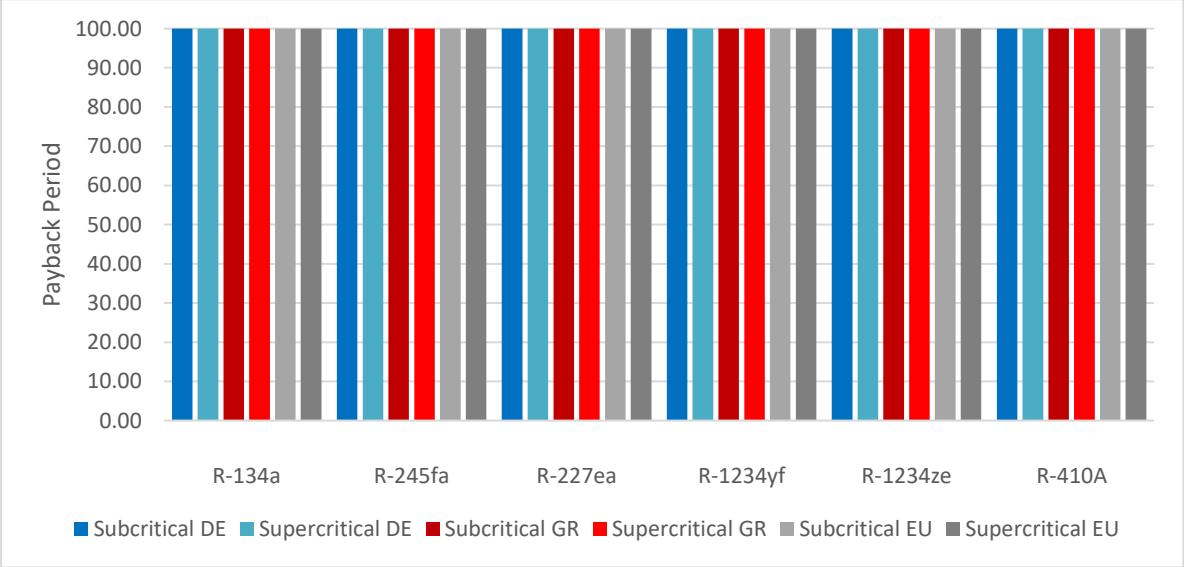

Figure 5.5 Payback period of various working fluids for various countries (1280 working hours per year)

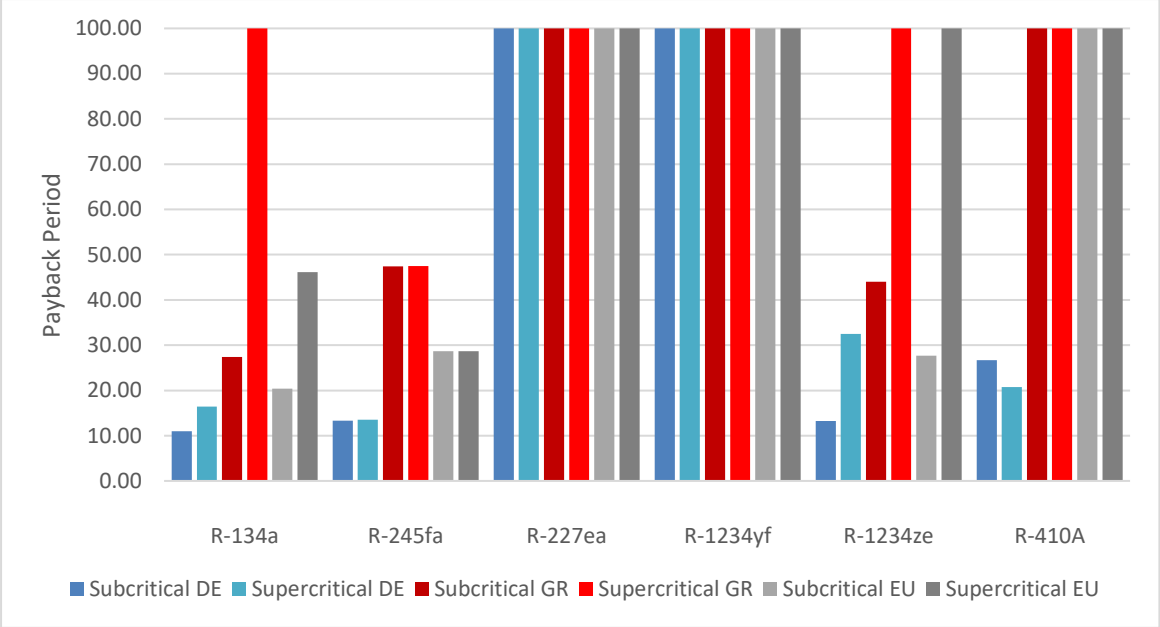

Figure 5.6 Payback period of various working fluids for various countries (2560 working hours per year)

As was the case with the Net Present Value, the figures demonstrate that Scenario 1 (1280 working hours per year) is not economically viable and would require an extremely high number of years for return of investment. For this scenario, all fluids are deemed inappropriate for this use.

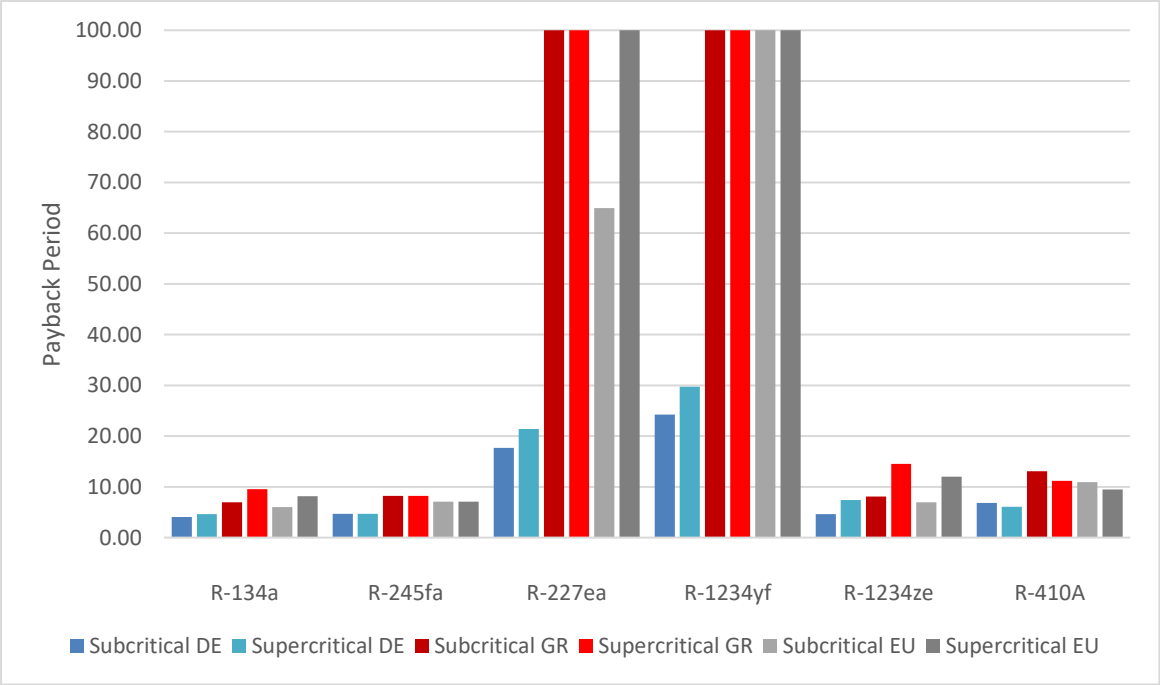

Figure 5.7 Payback period of various working fluids for various countries (5120 working hours per year)

Figure 5.6 clearly shows that the performance of R-227ea and R-1234yf is poor compared to the other fluids, as they would still require 100+ years for payback, while other fluids require as low as 11 years for the same hours of operation in a year.

The last scenario of 5120 working hours per year demonstrates payback periods of 20 years and less for all countries with the use of R-134a, R-245fa, R-1234ze and R-410A and thus their potential for investment is attractive.

An important difference between the payback period and the net present value is related to the subcritical and supercritical systems. For the most part, the Net Present Value at the 25th year indicated was roughly equal for both a subcritical and a supercritical cycle. Figure 5.2 to Figure 5.4, however, show that supercritical systems require in principle a greater number of years in order to pay back the investment costs.

The most probable reason is the higher investment expenditure required for a supercritical system, as demonstrated at Table 5-2 to Table 5-7, coupled with the higher system efficiency that in principle they display. Since the investment cost is in most cases significantly higher, the relatively low difference in efficiency would require many years in order to overcome the Net Present Value of the subcritical cycle. For investments that require 10 and less years for payback, it is understandable that a subcritical cycle is a more attractive option for a limited number of years, but considering the system's lifetime, it is probable that a supercritical cycle can lead to higher Net Present Value.

The lowest payback period is evident for a subcritical cycle of R-134a and specifically in Germany, where as previously stated, the high energy costs directly translate to higher annual income of the system and therefore faster payback. For such a system, the payback period is as low as 4.1 years.

An economic analysis for various ORC configurations for geothermal power plants was carried out by Zare (2015) [92]. Having a heat source of 165℃ and Isobutane as the working fluid, the study showed that a payback period of 3.64 years can be achieved. Compared to the current analysis, the study projected a shorter payback period, despite assuming a 10% interest rate and lower heat source temperature. The expander and pump efficiencies, however, were assumed 85 and 90% respectively, whereas the heat source's mass flow rate was equal to 100 kg/s. Furthermore, the plant operated for 7500 hours per year and therefore it is understandable how such a low value can be possible.

An investigation by Wang et al. (2015) [93] proved the significance of the electricity price for the system's payback period and showed similar results with the current analysis. For R-245fa as a working fluid and a maximum temperature of the cycle equal to 250℃, a Payback Period of 4 years was calculated, when the price of electricity was 18\$/kWh_{el}, roughly equal to the presented price of electricity in Germany.

5.2.3 Levelized Cost of Energy

The Levelized Cost of Energy (LCOE) calculates the lifetime costs of a system, divided by its energy production [94]. The objective of this index is to calculate energy costs based on operational and capital expenditures.

As the lifetime of the system has been set at 25 years, the same number will be used for calculations at the current unit.

The formula that calculates the LCOE of a system is given below: [95]

$$LCOE = \frac{IC \cdot CRF + OM_t}{E_t} \tag{5.9}$$

IC is the investment cost

OM_t the operational cost per year, as calculated in equation (5.4)

E_t is the annual electricity production, given in $\frac{kWh}{a}$

CRF is the Capital Recovery Factor, for which:

$$CRF = \frac{i}{1 - (1 + i)^{-N}} \tag{5.10}$$

N is the lifetime of the system and is equal to 25 years

i is the discount rate of return and is equal to 6%

It is important to note that the LCOE also considers the fuel costs per kWh. For waste heat recovery, however, the cost of the fuel is assumed equal to zero, which is one of the main reasons the final cost per kWh is low.

As the formula indicates, the LCOE is a function of the investment cost, which varies according to the working fluid and also a function of the hours of operation per year. As the energy production is identical, regardless of the cost of energy, the value is not influenced by the country and therefore scenarios regarding Germany, Greece and the average of the European Union don't need to be examined separately. The figures below present the LCOE of the system for the 3 scenarios that are related to hours of operation.

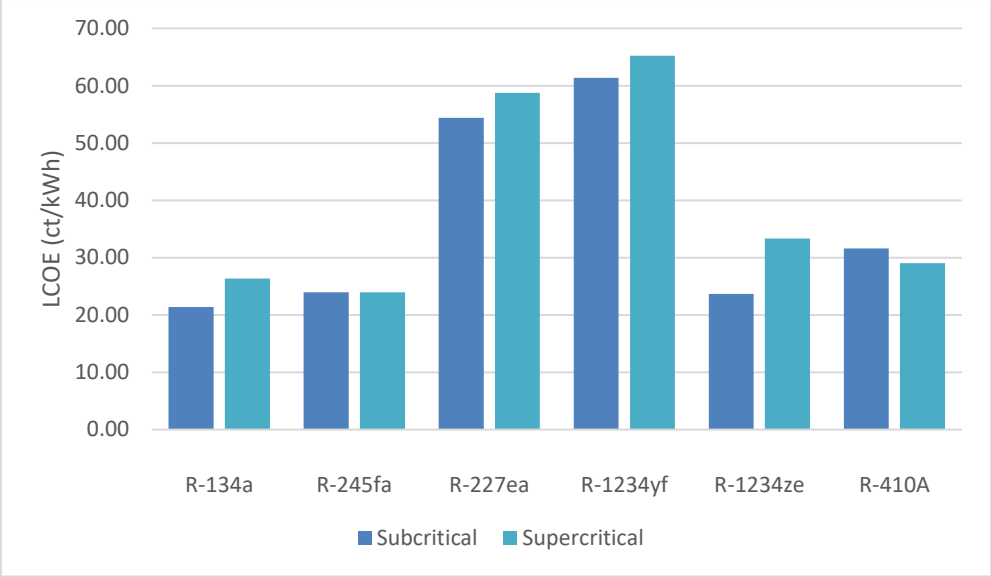

Figure 5.8 LCOE of various working fluids for subcritical and supercritical cycle (1280 working hours per year)

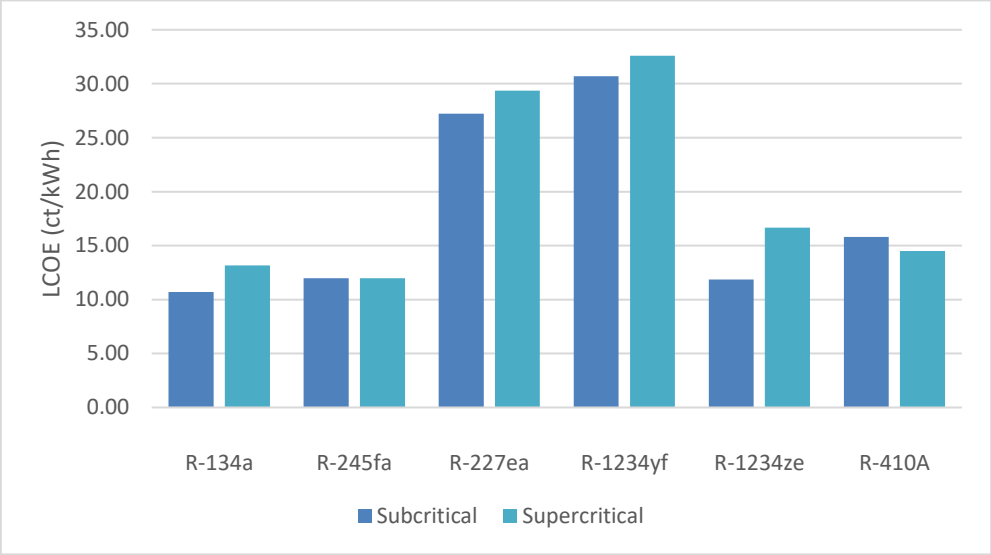

Figure 5.9 LCOE of various working fluids for subcritical and supercritical cycle (2560 working hours per year)

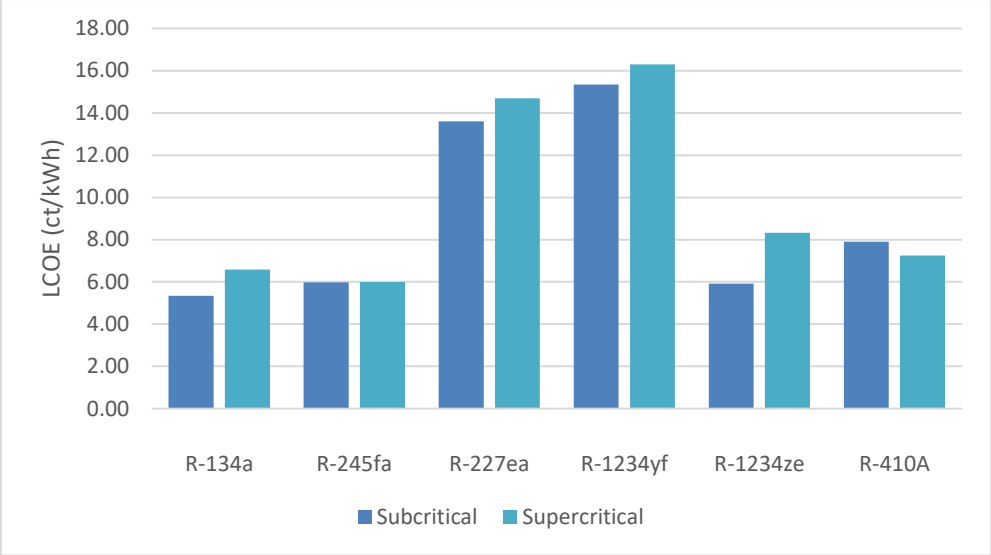

Figure 5.10 LCOE of various working fluids for subcritical and supercritical cycle (5120 working hours per year)

As expected, the 3 figures above have the exact same trend and relation between fluids and subcritical or supercritical system for each. As the formula of the LCOE indicates, when the working hours per year are doubled, the value is divided by two.

As was the case with the other economic indexes, it is clear that R-134a and R-245fa are the most suitable working fluids for the system, as they display very low LCOE values and thus potential for low cost energy production. R-1234ze and R-410A display similar behavior, with R-1234ze being slightly more attractive, especially at subcritical state and as was the case in the previous units, R-227ea and R-1234yf are not economically feasible for operation.

In addition, the supercritical systems present slightly higher costs of energy in most cases, with R-245fa and R-410A being the only exceptions. The lowest cost of energy is evident for a subcritical system that utilizes R-134a and is equal to $5.35\ ct/kWh$.

Walraven et al. [96] reached a similar conclusion for a large scale ORC system, powered by low temperature geothermal brine. Their analysis indicated that for a heat source temperature equal to 150℃ an ORC system can achieve a LCOE of about 55€/MWh, for a system with water as a cooling medium at the condenser.

Barse et al. [97] investigated the efficiency and economics of an ORC system optimally matched with each working fluid. The system's heat source was geothermal brine of 99℃ and the fluids examined all presented high critical temperatures, due to their favorable efficiency, as explained previously. The study's results show that for R-245fa an LCOE of 4.5 ct/kWh is achieved, while also R-134a and R-227ea present values lower than 5 ct/kWh. The analysis refers to an existing large scale geothermal power plant, which tend to reduce the cost of energy according to the economies of scale. On the contrary, the thermal efficiency of the plant is equal to 8%, which is clearly lower than the thermal efficiency presented at Chapter 4.

Kheiri et al. [98] investigated a Waste Heat Recovery System that utilizes a subcritical ORC. The heat source temperature was 150℃ and the working fluids examined were either pure, or zeotropic mixtures. The specific investment costs for the mixtures ranged from roughly 2864 to 3353 $€/kW$, which are slightly higher but comparable to the majority of the working fluids presented at Table 5-8. The lowest value of LCOE presented at the study was evident for pentane and was equal to 6.67 ct/kWh, which is a slightly higher value than the lowest one presented at the current study, but possibly due to the lower temperature of the heat source.

Chapter 6. Conclusion

6.1 Discussion of key findings

In this study, the sizing and the techno-economic optimization of a supercritical ORC has been investigated in comparison to the respective subcritical cycle. Based on the results of the study it is concluded that:

- The components that handle supercritical state flow have to be modeled in a different approach than the respective subcritical components.
- For all considered working fluids, the supercritical cycle results in higher energetic and exergetic efficiencies than the respective subcritical cycle, with the increase in the efficiencies to range from 0.1-2.7%.
- The most improved scenario with respect to the energetic and exergetic efficiencies was R134a, with an increase of 1.1 and 2.5% , respectively.
- The highest energetic and exergetic efficiencies were achieved with R245fa, with 13.5% and 30.3%, respectively.
- As the annual hours of operation of the system increase, the economics of the investment also become more competitive. More specifically, for 2560 hrs/year the NPV is profitable only in Germany. For 5120 hrs/year, almost all considered cases tend to be economically feasible, with the worst scenarios to occur in Greece, owing to the country's cost of electricity.
- The highest NPV is evident for the supercritical use of R-245fa, closely followed by subcritical R-245fa and also both states of R-134a.
- For 5120 hrs/year, R-134a, R-245fa, R-1234ze and R-410A result in payback periods of less than 20 years.
- The lowest cost of energy is evident for a subcritical system that utilizes R-134a and is equal to 5.35 ct/kWh.

6.2 Future work

With regards to the proposed future work, the following topics are proposed:

- A more detailed CFD analysis of the supercritical heat exchanger is proposed to identify the accuracy of the proposed sizing approach and the validity of the used correlations.
- Techno-economic investigation of the supercritical cycle for different heat sources, including biomass, geothermal and solar energy, simulating the off-design performance of the proposed system.
- Exergo-economic analysis of the supercritical cycle with comparison to the supercritical CO_2.
- CFD investigation of a high rotational speed turbine for application in a supercritical cycle.

References

1. Gyftopoulos, E., Beretta, G.P., *Thermodynamics, Foundations and Applications*. 1991. 444-448.
2. Black, W., Hartley, J., *Εφαρμοσμένη Θερμοδυναμική*. 2010. 529-531.
3. Κακαράς, Ε., Καρέλλας, Σ., *Αποκεντρωμένα Θερμικά Συστήματα*. 2015.
4. Reddy, V.S., et al., *An Approach to Analyse Energy and Exergy Analysis of Thermal Power Plants: A Review.* Smart Grid and Renewable Energy, 2010. **Vol.01No.03**: p. 10.
5. Μαθιουδάκης, Κ., *Λειτουργία Αεριοστροβίλων και Ατμοστροβίλων*. 2016.
6. Braimakis, K., et al., *Comparison of Environmentally Friendly Working Fluids for Organic Rankine Cycles: From Numerical to Experimental Techniques*. 2017. p. 377-426.
7. Colonna, P., et al., *Organic Rankine Cycle Power Systems: From the Concept to Current Technology, Applications, and an Outlook to the Future.* Journal of Engineering for Gas Turbines and Power, 2015. **137**(10): p. 100801-100801-19.
8. Quoilin, S., et al., *Techno-economic survey of Organic Rankine Cycle (ORC) systems.* Renewable and Sustainable Energy Reviews, 2013. **22**: p. 168-186.
9. Karellas, S., et al., *Solar Cooling Technologies*. 2018: CRC Press.
10. Zhou, X., et al., *Thermal Investigations into an Organic Rankine Cycle (ORC) System Utilizing Low Grade Waste Heat Sources.* Procedia Engineering, 2017. **205**: p. 4142-4148.
11. Douvartzides, S. and I. Karmalis. *Working fluid selection for the Organic Rankine Cycle (ORC) exhaust heat recovery of an internal combustion engine power plant*. in *IOP Conference Series: Materials Science and Engineering*. 2016. IOP Publishing.
12. Andersen, S.O., et al., *The global search and commercialization of alternatives and substitutes for ozone-depleting substances.* Comptes Rendus Geoscience, 2018. **350**(7): p. 410-424.
13. Hung, T.-C., T. Shai, and S.K. Wang, *A review of organic Rankine cycles (ORCs) for the recovery of low-grade waste heat.* Energy, 1997. **22**(7): p. 661-667.
14. Quoilin, S., et al., *Thermo-economic optimization of waste heat recovery Organic Rankine Cycles.* Applied thermal engineering, 2011. **31**(14-15): p. 2885-2893.
15. Yamaguchi, H., et al., *Solar energy powered Rankine cycle using supercritical CO2.* Applied Thermal Engineering, 2006. **26**(17-18): p. 2345-2354.
16. Schuster, A., S. Karellas, and R. Aumann, *Efficiency optimization potential in supercritical Organic Rankine Cycles.* Energy, 2010. **35**(2): p. 1033-1039.
17. Besarati, S. and D. Goswami, *Supercritical CO2 and other advanced power cycles for concentrating solar thermal (CST) systems*, in *Advances in Concentrating Solar Thermal Research and Technology*. 2017, Elsevier. p. 157-178.
18. Kalra, C., et al. *High-potential working fluids and cycle concepts for next-generation binary organic Rankine cycle for enhanced geothermal systems*. in *37th Workshop on Geothermal Reservoir Engineering, Stanford, CA, Jan*. 2012.
19. Subbiah, S. and R. Natarajan, *Thermodynamic analysis of binary-fluid Rankine cycles for geothermal power plants.* Energy conversion and management, 1988. **28**(1): p. 47-52.
20. Vidhi, R., et al., *Organic fluids in a supercritical rankine cycle for low temperature power generation.* Journal of Energy Resources Technology, 2013. **135**(4): p. 042002.
21. Xu, J. and C. Liu, *Effect of the critical temperature of organic fluids on supercritical pressure Organic Rankine Cycles.* Energy, 2013. **63**: p. 109-122.
22. Pan, L., H. Wang, and W. Shi, *Performance analysis in near-critical conditions of organic Rankine cycle.* Energy, 2012. **37**(1): p. 281-286.

23. Uusitalo, A., et al., *A thermodynamic analysis of waste heat recovery from reciprocating engine power plants by means of organic Rankine cycles.* Applied Thermal Engineering, 2014. **70**(1): p. 33-41.
24. Glover, S., et al., *Simulation of a multiple heat source supercritical ORC (Organic Rankine Cycle) for vehicle waste heat recovery.* Energy, 2015. **93**: p. 1568-1580.
25. Gao, H., et al., *Performance analysis and working fluid selection of a supercritical organic Rankine cycle for low grade waste heat recovery.* Energies, 2012. **5**(9): p. 3233-3247.
26. Boz, B., Diez, A., *Comparative Study of Sub-Critical and Supercritical ORC Applications for Exhaust Waste Heat Recovery.* World Academy of Science, Engineering and Technology, International Journal of Energy and Power Engineering, 2018. **12**(2): p. 119-127.
27. Shu, G., et al., *Performance comparison and working fluid analysis of subcritical and transcritical dual-loop organic Rankine cycle (DORC) used in engine waste heat recovery.* Energy conversion and management, 2013. **74**: p. 35-43.
28. Braimakis, K., et al., *Low grade waste heat recovery with subcritical and supercritical Organic Rankine Cycle based on natural refrigerants and their binary mixtures.* Energy, 2015. **88**: p. 80-92.
29. Chen, H., et al., *A supercritical Rankine cycle using zeotropic mixture working fluids for the conversion of low-grade heat into power.* Energy, 2011. **36**(1): p. 549-555.
30. Maraver, D., et al., *Systematic optimization of subcritical and transcritical organic Rankine cycles (ORCs) constrained by technical parameters in multiple applications.* Applied energy, 2014. **117**: p. 11-29.
31. Astolfi, M., et al., *Binary ORC (organic Rankine cycles) power plants for the exploitation of medium–low temperature geothermal sources–Part A: Thermodynamic optimization.* Energy, 2014. **66**: p. 423-434.
32. Astolfi, M., et al., *Binary ORC (Organic Rankine Cycles) power plants for the exploitation of medium–low temperature geothermal sources–Part B: Techno-economic optimization.* Energy, 2014. **66**: p. 435-446.
33. Shengjun, Z., W. Huaixin, and G. Tao, *Performance comparison and parametric optimization of subcritical Organic Rankine Cycle (ORC) and transcritical power cycle system for low-temperature geothermal power generation.* Applied energy, 2011. **88**(8): p. 2740-2754.
34. Vetter, C., H.-J. Wiemer, and D. Kuhn, *Comparison of sub-and supercritical Organic Rankine Cycles for power generation from low-temperature/low-enthalpy geothermal wells, considering specific net power output and efficiency.* Applied Thermal Engineering, 2013. **51**(1-2): p. 871-879.
35. Wang, J., L. Zhao, and X. Wang, *A comparative study of pure and zeotropic mixtures in low-temperature solar Rankine cycle.* Applied Energy, 2010. **87**(11): p. 3366-3373.
36. Ferrara, F., A. Gimelli, and A. Luongo, *Small-scale concentrated solar power (CSP) plant: ORCs comparison for different organic fluids.* Energy Procedia, 2014. **45**: p. 217-226.
37. Xu, G., et al., *Performance evaluation of a direct vapor generation supercritical ORC system driven by linear Fresnel reflector solar concentrator.* Applied Thermal Engineering, 2015. **80**: p. 196-204.
38. Zhou, C., *Hybridisation of solar and geothermal energy in both subcritical and supercritical Organic Rankine Cycles.* Energy conversion and management, 2014. **81**: p. 72-82.
39. Drescher, U. and D. Brüggemann, *Fluid selection for the Organic Rankine Cycle (ORC) in biomass power and heat plants.* Applied thermal engineering, 2007. **27**(1): p. 223-228.

40. Algieri, A. and P. Morrone, *Comparative energetic analysis of high-temperature subcritical and transcritical Organic Rankine Cycle (ORC). A biomass application in the Sibari district.* Applied Thermal Engineering, 2012. **36**: p. 236-244.
41. McLinden, M., et al., *REFPROP, Thermodynamic and transport properties of refrigerants and refrigerant mixtures.* NIST Standard Reference Database, 1998. **23**.
42. Ashford, P., et al., *Halocarbon Scenarios, Ozone Depletion Potentials, and Global Warming Potentials.*
43. Minor, B. and M. Spatz, *HFO-1234yf low GWP refrigerant update.* 2008.
44. Fedele, L., et al., *Measurements and Correlations of cis-1,3,3,3-Tetrafluoroprop-1-ene (R1234ze(Z)) Saturation Pressure.* International Journal of Thermophysics, 2014. **35**(1): p. 1-12.
45. Zhang, Y.-Q., et al., *Development and experimental study on organic Rankine cycle system with single-screw expander for waste heat recovery from exhaust of diesel engine.* Energy, 2014. **77**: p. 499-508.
46. Lemmon, E.W., M.L. Huber, and M.O. McLinden, *NIST Standard ReferenceDatabase 23: Reference Fluid Thermodynamic and Transport Properties - REFPROP. 9.0.* 2010.
47. Pioro, I. and S. Mokry, *Thermophysical properties at critical and supercritical pressures*, in *Heat Transfer-Theoretical Analysis, Experimental Investigations and Industrial Systems*. 2011, IntechOpen.
48. Automation and Control Institute, T.W., *Compact plate heat exchanger in countercurrent flow arrangement.* 2014, TU Wien.
49. Jogi Nikhil, G. and M. Lawankar Shailendra, *Heat transfer analysis of corrugated plate heat exchanger of different plate geometry: A Review.* Int. J. Emerging Technol. Adv. Eng, 2012. **2**(10): p. 110-115.
50. Roumpedakis, T., *Techo-economic investigations of a solar driven ORC-sorption system for combined cooling, heating and power.* 2018.
51. Donowski, V.D. and S.G. Kandlikar. *Correlating evaporation heat transfer coefficient of refrigerant R-134a in a plate heat exchanger*. in *Engineering Foundation Conference on Pool and Flow Boiling, Anchorage, AK, Apr*. 2000.
52. Yan, Y.-Y., T.-F. Lin, and B.-C. Yang. *Evaporation heat transfer and pressure drop of refrigerant R134a in a plate heat exchanger*. in *ASME 1997 Turbo Asia Conference*. 1997. American Society of Mechanical Engineers.
53. Mota, F.A., M.A. Ravagnani, and E. Carvalho, *Optimal design of plate heat exchangers.* Applied Thermal Engineering, 2014. **63**(1): p. 33-39.
54. Martin, H., *A theoretical approach to predict the performance of chevron-type plate heat exchangers.* Chemical Engineering and Processing: Process Intensification, 1996. **35**(4): p. 301-310.
55. Hsieh, Y.Y. and T.F. Lin, *Evaporation Heat Transfer and Pressure Drop of Refrigerant R-410A Flow in a Vertical Plate Heat Exchanger.* Journal of Heat Transfer, 2003. **125**(5): p. 852-857.
56. *Alfa Laval AC112*. Brazed Plate Heat Exchangers 2016; Available from: https://www.alfalaval.com/globalassets/documents/microsites/heating-and-cooling-hub/pd-leaflets/ac112_product-leaflet.pdf.
57. Jackson, J., *Fluid flow and convective heat transfer to fluids at supercritical pressure.* Nuclear Engineering and Design, 2013. **264**: p. 24-40.
58. Dittus, F. and L. Boelter, *Heat transfer in automobile radiators of the tubular type.* International Communications in Heat and Mass Transfer, 1985. **12**(1): p. 3-22.
59. Harmen, et al. *Theoretical investigation of heat transfer correlations for supercritical organic fluids*. in *AIP Conference Proceedings*. 2018. AIP Publishing.
60. Petukhov, B., *Heat transfer and friction in turbulent pipe flow with variable physical properties*, in *Advances in heat transfer*. 1970, Elsevier. p. 503-564.

61. Kang, K.-H. and S.-H. Chang, *Experimental study on the heat transfer characteristics during the pressure transients under supercritical pressures.* International Journal of Heat and Mass Transfer, 2009. **52**(21-22): p. 4946-4955.
62. Yazıcıoğlu, A.G., et al., *4.2 Heat Exchangers.* 2018.
63. Fang, X., Y. Xu, and Z. Zhou, *New correlations of single-phase friction factor for turbulent pipe flow and evaluation of existing single-phase friction factor correlations.* Nuclear Engineering and Design, 2011. **241**(3): p. 897-902.
64. Yamashita, T., et al., *Heat transfer and pressure drop of a supercritical pressure fluid flowing in a tube of small diameter.* Memoirs of the Faculty of Engineering, Kyushu University, 2003. **63**(4): p. 227-244.
65. Tarasova, N. and A. Leontév, *Hydraulic resistance during flow of water in heated pipes at supercritical pressures*. 1968, MAIK NAUKA/INTERPERIODICA C/O PLENUM/CONSULTANTS BUREAU 233 SPRING ST, NEW …. p. 721-&.
66. Popov, V. *Theoretical calculation of heat transfer and friction resistance for supercritical carbon dioxide*. in *Proceedings of the 2nd All-Soviet Union Conference on Heat and Mass Transfer, Minsk, Belarus*. 1964.
67. Fang, X., et al., *Pressure drop and friction factor correlations of supercritical flow*. Nuclear Engineering and Design, 2012. **242**: p. 323-330.
68. Mikheev, M. and I. Mikheeva, *Fundamentals of Heat Transfer [in Russian], l~ nergiya*. 1973, Moscow.
69. Persson, J., *Performance mapping vs design parameters for screw compressors and other displacement compressor types.* VDI Berichte, 1990. **859**.
70. Lemort, V., S. Declaye, and S. Quoilin, *Experimental characterization of a hermetic scroll expander for use in a micro-scale Rankine cycle.* Proceedings of the Institution of Mechanical Engineers, Part A: Journal of Power and Energy, 2012. **226**(1): p. 126-136.
71. Dumont, O., R. Dickes, and V. Lemort, *Experimental investigation of four volumetric expanders.* Energy Procedia, 2017. **129**: p. 859-866.
72. Ziviani, D., et al., *Characterizing the performance of a single-screw expander in a small-scale organic Rankine cycle for waste heat recovery.* Applied Energy, 2016. **181**: p. 155-170.
73. Thonon, B. and A. Bontemps, *Condensation of pure and mixture of hydrocarbons in a compact heat exchanger: experiments and modelling.* Heat transfer engineering, 2002. **23**(6): p. 3-17.
74. Han, D.-H., K.-J. Lee, and Y.-H. Kim, *The characteristics of condensation in brazed plate heat exchangers with different chevron angles.* JOURNAL-KOREAN PHYSICAL SOCIETY, 2003. **43**(1): p. 66-73.
75. Engineers, M.S., *Wanner Hydra-Cell G10 Series.* 2015(2).
76. da Silva, J.A., et al., *Exergy evaluation and ORC use as an alternative for efficiency improvement in a CI-engine power plant.* Sustainable Energy Technologies and Assessments, 2018. **30**: p. 216-223.
77. Darvish, K., et al., *Selection of optimum working fluid for Organic Rankine Cycles by exergy and exergy-economic analyses.* Sustainability, 2015. **7**(11): p. 15362-15383.
78. Mago, P.J., et al., *An examination of regenerative organic Rankine cycles using dry fluids.* Applied thermal engineering, 2008. **28**(8-9): p. 998-1007.
79. Lakew, A.A. and O. Bolland, *Working fluids for low-temperature heat source.* Applied Thermal Engineering, 2010. **30**(10): p. 1262-1268.
80. Yağlı, H., et al., *Parametric optimization and exergetic analysis comparison of subcritical and supercritical organic Rankine cycle (ORC) for biogas fuelled combined heat and power (CHP) engine exhaust gas waste heat.* Energy, 2016. **111**: p. 923-932.

81. *Zilmet Expansion Tanks*. 2016; Available from: http://zilmetusa.com/upload/5-Documents/list-price-guide---solar-2016.pdf.
82. Boyaghchi, F.A. and P. Heidarnejad, *Thermoeconomic assessment and multi objective optimization of a solar micro CCHP based on Organic Rankine Cycle for domestic application.* Energy conversion and Management, 2015. **97**: p. 224-234.
83. *Refrigerant R-410A*. 2019; Available from: https://elgracool.pl/product-eng-569-Refrigerant-R410A-R-410A.html.
84. *R-1234YF Refrigerant*. 2019; Available from: http://www.eurorefrigerant.com/r1234yf-refrigerant-gas-cylinders-honeywell/121-r1234yf-r1234-honeywell-1kg-refillable-cylinder.html.
85. *Possible Bans for Aerosols and Foams*, E. Commission, Editor. 2013, SKM Enviros.
86. Rentizelas, A., et al., *Comparative techno-economic analysis of ORC and gasification for bioenergy applications.* Energy Conversion and Management, 2009. **50**(3): p. 674-681.
87. Tchanche, B.F., et al. *Economic feasibility study of a small scale organic rankine cycle system in waste heat recovery application*. in *ASME 2010 10th Biennial Conference on Engineering Systems Design and Analysis*. 2010. American Society of Mechanical Engineers.
88. Arnaboldi, M., G. Azzone, and M. Giorgino, *Performance measurement and management for engineers*. 2014: Academic Press.
89. Žižlavský, O., *Net present value approach: method for economic assessment of innovation projects.* Procedia-Social and Behavioral Sciences, 2014. **156**: p. 506-512.
90. Eurostat, *Electricity prices for non-household consumers, second half 2018*. 2018, European Commission.
91. Bhandari, S.B., *Discounted payback period-some extensions.* Journal of Business and Behavioral Sciences, 2009. **21**(1): p. 28-38.
92. Zare, V., *A comparative exergoeconomic analysis of different ORC configurations for binary geothermal power plants.* Energy conversion and management, 2015. **105**: p. 127-138.
93. Wang, X.-Q., et al., *Payback period estimation and parameter optimization of subcritical organic Rankine cycle system for waste heat recovery.* Energy, 2015. **88**: p. 734-745.
94. Ueckerdt, F., et al., *System LCOE: What are the costs of variable renewables?* Energy, 2013. **63**: p. 61-75.
95. *Simple Levelized Cost of Energy (LCOE) Calculator Documentation*. Energy Analysis 2010.
96. Walraven, D., B. Laenen, and W. D'haeseleer, *Minimizing the levelized cost of electricity production from low-temperature geothermal heat sources with ORCs: water or air cooled?* Applied Energy, 2015. **142**: p. 144-153.
97. Barse, K.A. and M.D. Mann, *Maximizing ORC performance with optimal match of working fluid with system design.* Applied Thermal Engineering, 2016. **100**: p. 11-19.
98. Kheiri, A., M. Feidt, and S. Pelloux-Prayer, *Thermodynamic and economic optimizations of a waste heat to power plant driven by a subcritical ORC (Organic Rankine Cycle) using pure or zeotropic working fluid.* Energy, 2014. **78**: p. 622-638.

[i] As bought by NTUA, Laboratory of Steam Boilers and Thermal Plants, January 2019

[ii] Prices for R-134a, R-245fa, R-227ea are based on actual purchases from NTUA